JPL NO. 9950-594

Report No. DOE/JPL 954833-81/4
Distribution Category UC-63b

BOEING ENGINEERING & CONSTRUCTION
the BOEING ENERGY AND ENVIRONMENT DIVISION

WIND LOADS ON FLAT PLATE PHOTOVOLTAIC ARRAY FIELDS (NONSTEADY WINDS)

JPL CONTRACT NO. 954833

LOW COST SOLAR ARRAY PROJECT
ENGINEERING AREA

Phase IV Final Report

August 1981

Ronald D. Miller
Donald K. Zimmerman

The JPL Low Cost Solar Array Project is sponsored by the U.S.Department of Energy and forms part of the Solar Photovoltaic Conversion Program to initiate a major effort toward the development of low-cost solar arrays. This work was performed for the Jet Propulsion Laboratory, California Institute of Technology by agreement between NASA and DOE.

Prepared for
Jet Propulsion Laboratory
4800 Oak Grove Drive
Pasadena, California 91103

By the
Boeing Engineering and Construction Company
(A Division of The Boeing Company)
Seattle, Washington 98124

WIND LOADS ON
FLAT PLATE PHOTOVOLTAIC ARRAY FIELDS
(NONSTEADY WINDS)

JPL Contract No. 954833

Low Cost Solar Array Project
Engineering Area

Phase IV Final Report

August, 1981

Ronald D. Miller
Donald K. Zimmerman

"The JPL Low Cost Solar Array Project is sponsored by the U.S. Department of Energy and forms part of the Solar Photovoltaic Conversion Program to initiate a major effort toward the development of low-cost solar arrays. This work was performed for the Jet Propulsion Laboratory, California Institute of Technology by agreement between NASA and DOE."

Prepared for

Jet Propulsion Laboratory
4800 Oak Grove Drive
Pasadena, California 91103

By the

Boeing Engineering and Construction Company
(A Division of The Boeing Company)
Seattle, Washington

Acknowledgements

Management and engineering on this project was provided by the Solar Systems organization of the Boeing Engineering and Construction Company (a Division of The Boeing Company). Dr. Ronald Ross, Mr. Robert Weaver, and Mr. Donald Moore Manager and technical monitors , respectively, in the Engineering area of the Low Cost Solar Array Project, Jet Propulsion Laboratory, California Institute of Technology, contributed many helpful suggestions during the program. Mr. Weaver served as technical monitor for the aerodynamics investigation and Mr. Moore for the structural response analysis. Mr. Abraham Wilson, also of JPL, detailed the JPL array structural design used in this analysis. The wind tunnel test was performed by the Fluid Dynamics Laboratory staff of Colorado State University, Fort Collins, Colorado. The responsible Manager for the testing was Dr. Jack E. Cermak, the Project Director was Dr. Jon A. Peterka, and Principal Investigators were N. Hosoya and Dr. Mike Poreh.

Table of Contents

Figures

Tables

1.0 SUMMARY

This report presents the results of a combined experimental (wind tunnel test results) and theoretical analysis utilizing random harmonic analysis techniques to predict the dynamic response and the structural dynamic loads of flat plate photovoltaic arrays due to wind turbulence. Guidelines for use in predicting the turbulent portion of the wind loading on future similar arrays using the results of this study are presented.

The dynamic response and the loads dynamic magnification factor of the two array configurations (a four post array and a two post array) are similar. Figures 1-1 and 1-2 are typical magnification factors for the two array configurations located in identical positions within the array field. The figures show the magnification factors at a mid chord and outer chord location on the array illustrated and at four points on the chord. The wind tunnel test experimental rms pressure coefficient that the magnification factors are based on is also shown on each figure. In general, the largest response and dynamic magnification factor occur at a mid chord location on an array and near the trailing edge. A technique employing these magnification factors and the wind tunnel test rms fluctuating pressure coefficients to calculate design pressure loads due to wind turbulence is presented in Figure 1-3.

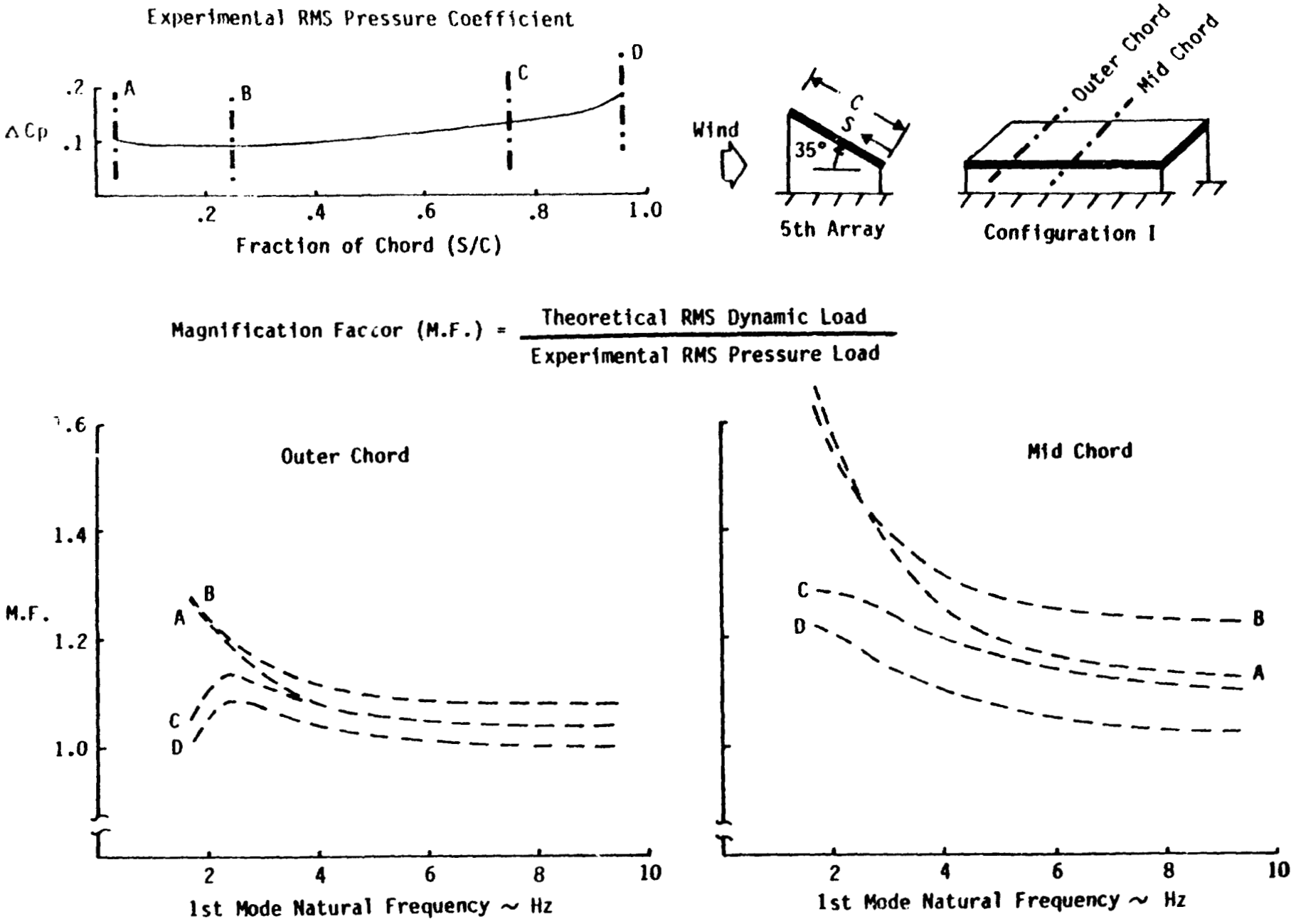

Figure 1-1. Configuration I - Dynamic Analysis Results for 5th Array with an Array Field

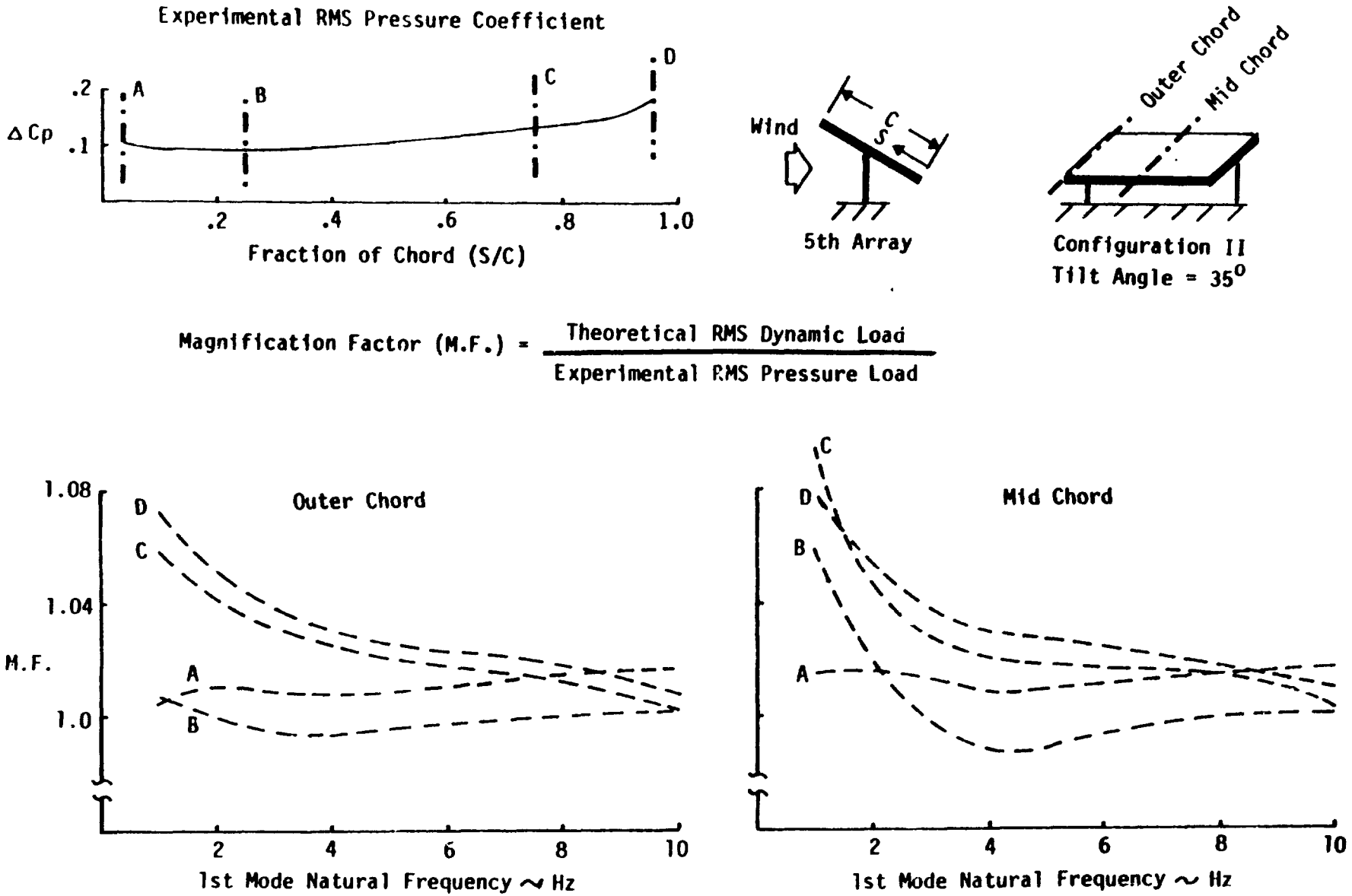

Figure 1-2. Configuration II - Dynamic Analysis Results for 5th Array within an Array Field

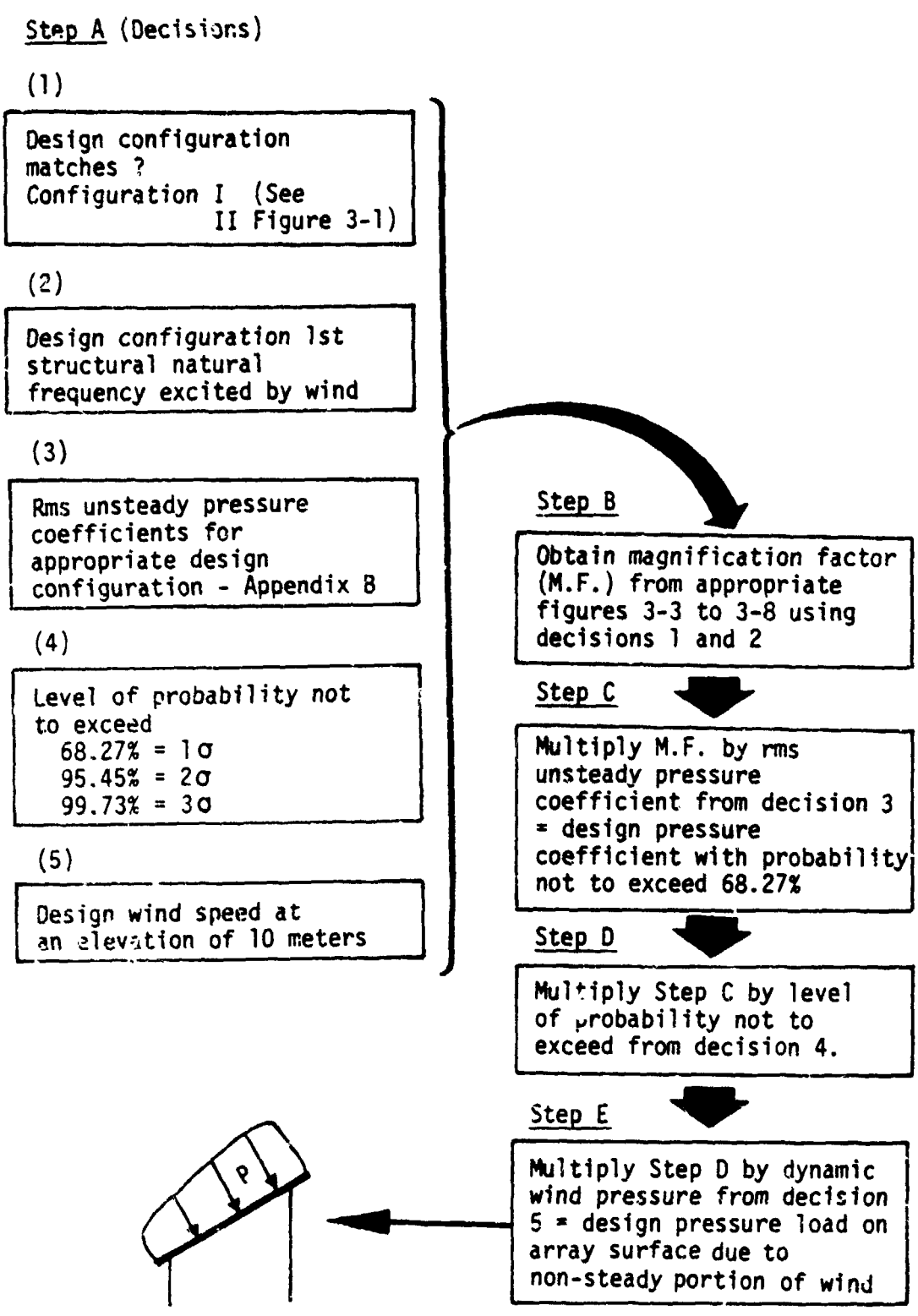

Figure 3. Flow Chart to Calculate Array Design Wind Loads due to the Non-Steady Portion of the Wind

2.0 INTRODUCTION

This report summarizes a combined theoretical experimental analysis of the structural dynamic loading on long, flat plate photovoltaic arrays resulting from exposure to the non-steady portion of the wind environment. This report is an extension to the analyses reported in DOE/JPL 954833-79/2 and -81/3. The study was performed under contract number 954833 to the Jet Propulsion Laboratory as part of the Engineering Area Task of the Low Cost Solar Array (LSA) Project. This project is being managed by JPL for the Department of Energy, Division of Solar Technology.

2.1 Objectives

The cost associated with the design and construction of solar photovoltaic arrays to produce electric energy from sunlight is an important factor in the acceptance and use of solar energy. The load due to wind on an array and on its support structure strongly influences the design and ultimately the cost of the photovoltaic panels, panel and array support structure and foundation of the array. It is, therefore, essential to determine the true maximum wind load that the array will experience during its lifetime in order to minimize the structure costs. The objective of this study was to establish wind load guidelines on flat plate photovoltaic arrays for that portion of the wind environment that is considered non-steady (turbulence).

2.2 Discussion and Background

Three factors affect the amount of wind loading on a body: the flow field in which the body is placed, the aerodynamic characteristics of the body itself, and the dynamic response of the body due to the wind loading. Although the structural loads resulting from this latter factor are not totally composed of aerodynamic forces (they also include inertia forces), these structural loads do result from the wind loading, or more precisely, the fluctuations in wind loading.

The flow field of the type that would be found around arrays in an array field has three aspects: 1) the steady state flow before it encounters any obstacles, 2) atmospheric gusts, and 3) turbulence. The steady state flow

is characterized by of a shear layer adjacent to the ground whose shearing effects decrease with elevation above the ground until a uniform flow is attained. Gusting is the result of velocity variations and changes in the direction of the prevailing wind due to atmospheric instabilities. Turbulence may be caused by several factors. Gusting can cause turbulence when adjacent volumes of air are moving at different velocities, thus producing a shearing effect. Terrain roughness causes turbulence because of shearing effects. An obstacle in the path of the flow can also create turbulence by upsetting the flow and causing eddies and vortices to form. In addition, the shape of the body will affect the characteristics of the turbulence. Turbulent flow is highly complex, with varying frequencies and intensities occurring in a random manner.

The effect on the array forces due to the flow field is a function of the airflow characteristics and the resulting pressure distribution over the array. When the flow is turbulent, the pressure distribution and, consequently, the forces exerted on the array are nonuniform in frequency and intensity. These forces may cause vibrations in the structure resulting in additional structural dynamic forces on the array. Since turbulence varies in frequency and intensity, the resulting loading will also vary as a function of the frequency and intensity.

2.3 Study Requirements

The requirements of this study involve analysis and test. They are:

1. Wind tunnel test and data reduction in the form of auto and cross spectrums.
2. Theoretical structural dynamic modeling of arrays.
3. Dynamic analysis results.
4. Establishment of design guidelines for estimating unsteady wind loads on photovoltaic arrays.

The following is a summary of the statement of work for Phase IV.

1. Array Vibration Characteristics
   i) A structural finite element computer model will be developed in sufficient detail to adequately define the structure for use in the calculation of structural mode shapes of a photovoltaic array. The tilt angle of the array will match one of the tilt angles of the arrays used in the Phase III study (reported in reference 1).

   ii) Structural vibration characteristics of the array will be calculated to produce mode shapes and generalized mass and stiffness data for the array model developed in i).

2. Array Structural Dynamic Load
   i) The generalized mass and stiffness data and the vibration mode shapes will be combined with the steady state aerodynamics from one array field configuration chosen from the Phase III test data to generate the structural dynamic equations of motion.
   ii) The Phase III wind tunnel pressure time history data will be analyzed for the array configuration chosen in 2 (i) to yield auto- and cross-spectral density functions and will be used in calculating the generalized forcing functions for the equations of motion.

3. Structural Dynamic Loads

   Structural dynamic responses and loads for the arrays will be calculated from the equations of motion and load equations developed in 2. The resulting aerodynamic forces from the dynamic analysis will be compared to the steady state aerodynamic forces to indicate the level of increase to be expected from the dynamic forces.

2.4 Report Organization

The remainder of this report presents the results of the dynamic analysis and its formulation. Section 3.0 presents the basic technical approach, details the results and discusses the pertinent findings. Conclusions are presented in Section 4.0. The use of the results as design guidelines are presented for wind turbulence in Section 5.0. New Technology and References are outlined in

Sections 6.0 and 7.0 respectively. Appendix A presents the analysis procedure; Appendix B, the wind tunnel measured rms delta pressure coefficients; and Appendix C, the Colorado State University test report for the test and test data reduction pertinent to the dynamic analysis.

3.0 TECHNICAL APPROACH, RESULTS AND DISCUSSION

Because the pressure fluctuation on the arrays caused by the wind turbulence is random in nature, random harmonic analysis techniques can be applied to determine the dynamic response of the arrays. The technical approach was to develop theoretical mathematical models of arrays and solve for the response of the arrays using wind tunnel measured pressure fluctuations on the arrays as the forcing function. Pressure measurements were recorded simultaneously at several locations on rigid arrays during a wind tunnel test conducted at Colorado State University. These pressure data were then reduced to yield auto and cross spectra at and between each pressure tap. The test procedures and results of the wind tunnel test is presented in Appendix C.

The structural dynamic response of an array is dependent on the structural characteristics of the array as well as the forcing function. For this study, two typical arrays (Figure 3-1) were modeled theoretically utilizing the modal approach; the mode shapes are shown in Appendix A. The first configuration was a four post array designed by JPL (see Ref. 5 for the detailed design configuration) and the second configuration was a two post array (support posts at the center of each end of the array). The theoretical equations for the dynamic response of the arrays were calculated and included the equation of motion and pressure load equations on the arrays. The theoretical procedure is detailed in Appendix A. The fluctuating wind induced pressure forcing functions (auto and cross spectra*) on these arrays were simulated from the wind tunnel test for the wind conditions on the first array of an array field exposed to the wind, the first array protected by a fence, and the fifth array within an array field. The wind was considered to be head-on to the arrays.

The wind tunnel test results consisting of auto and cross spectra of the array pressure coefficients are of significant importance to the dynamic response of the arrays. Figure 3-2 shows a typical normalized cross spectrum for the 5th array located in an array field with a tilt angle of 35° and a 90 mph wind. Of importance in the cross spectrum is that the phase angle in all cases were

---

*The cross-spectrum relates pressure versus frequency at two different points (i and j); the auto-spectrum is similar except at a single point (i=j). These terms are used in the analysis as shown in Appendix A. A detailed technical description of the auto and cross spectrum can be found in References 3 and 4.

Configuration I

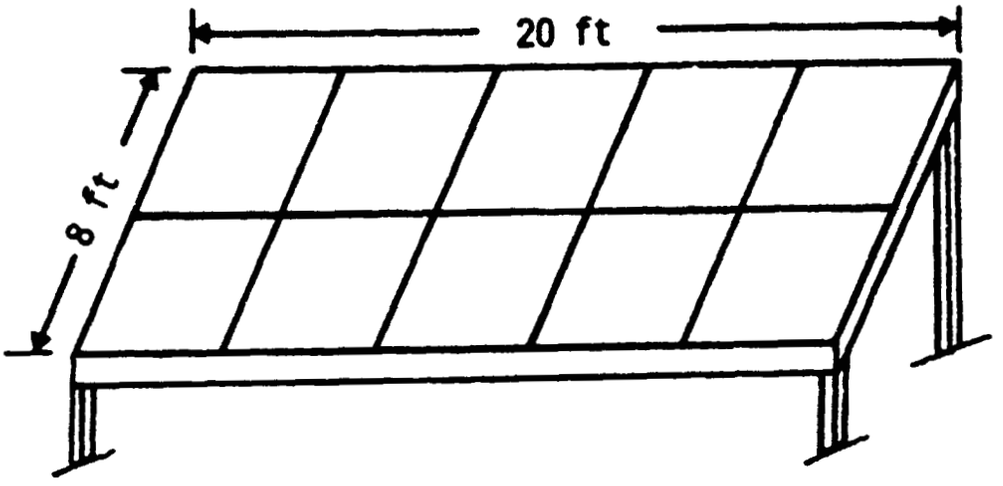

Weight = 977 lbs
First Plate Bending Mode = 10 Hz

Configuration II

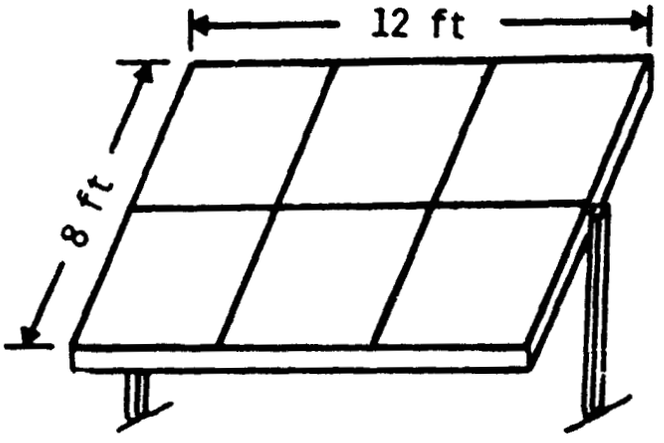

Weight = 933 lbs
Pitch Mode = 3 Hz
First Plate Bending Mode = 10 Hz

Figure 3-1. Array Configuration Characteristics

zero. That is, the pressure at each pressure tap is in phase with each other pressure tap on the array. The importance of this feature is that only symmetric modes of vibration about the center line of the array can be excited by the wind turbulence. Another important aspect of the spectra is that for a ninety mph wind the power in the wind as indicated by the array pressure coefficient spectra becomes insignificant (<1% of maximum) at frequencies greater than 5 Hz.

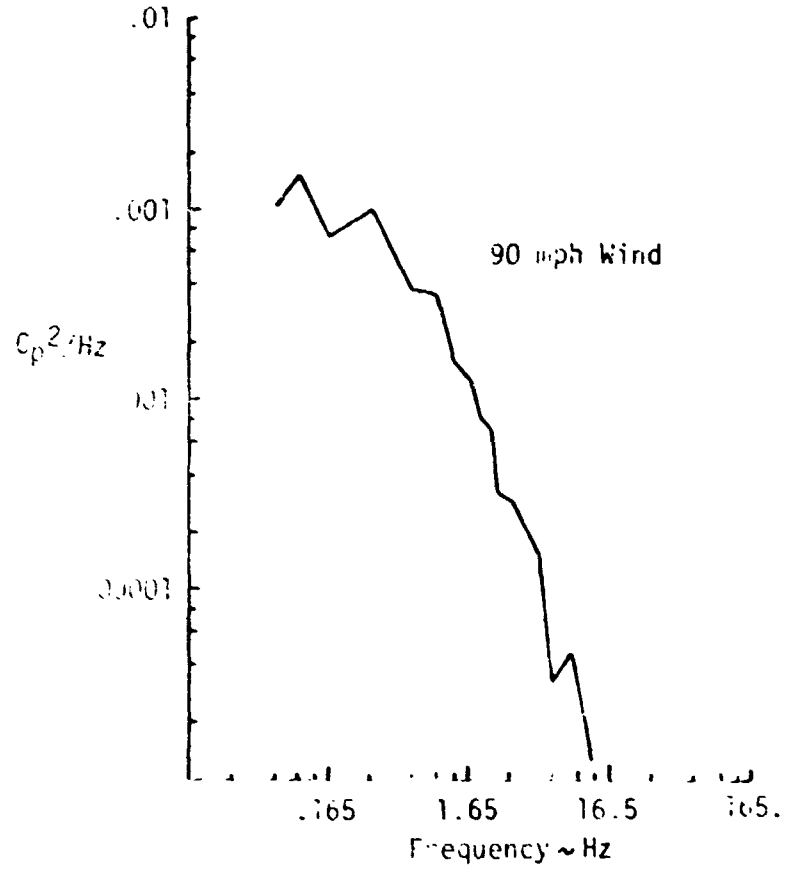

Figure 3-2. Typical Cross Spectrum between Pressure Taps on an Array in a 90 mph Wind

Utilizing random harmonic analysis techniques and the properties of auto and cross spectrums, a structural dynamic analysis was performed for the two array configurations. The results presented as magnification factors defined as the theoretical RMS dynamic load divided by the experimental RMS pressure load is shown in figures 3-3 to 3-5 for configuration I and figures 3-6 to 3-8 for

configuration II. Figures 3-3 to 3-5 show the effect of location of configuration I arrays in an array field (1st array without a fence, 1st array protected by a fence, and 5th array within an array field, respectively). Each figure also shows the effect of the first modal structural frequency on the magnification factor and the effect of location on the array (mid chord and outer chord locations). In general, the largest magnification factors are located near the trailing edge of the array (downwind edge) and at the mid chord location. The magnification factor decreases with an increase in the first mode structural frequency. For the condition where the first mode frequency is between one and two cycles/sec, the magnification factors change rapidly. This is caused by the combination of the very flexible structures (as indicated by the low natural frequency) and the aerodynamics interacting to reduce the stability of the structure. At frequencies above 3 Hz, the structure becomes stiff enough so that the interaction with the aerodynamics does not present a problem. The magnification factors for the 5th array and the 1st array protected by a fence tend to be slightly larger than the 1st array that is unprotected. This is expected since the fence and the upwind arrays will increase the level of turbulence in the wind compared to the wind flowing over the 1st array.

The results for configuration II arrays (figures 3-6 to 3-8) are similar but of reduced magnitude compared to the results for configuration I arrays. The reduced magnitude is a result of the larger weight per unit surface area that is required for static load considerations by configuration II compared to configuration I. As a result of the higher weight, less dynamic response occurs for the same 1st mode structural frequency. Also, the magnification factors for the outer chord and the mid chord locations are very similar in shape and magnitude for configuration II.

In general, the structural configuration (weight, stiffness and shape) will affect the dynamic response of the structure. The larger the weight and stiffness, the less the dynamic response for a given forcing function. The weight and stiffness of the array considered as configuration I was about as light and flexible as possible and yet maintain structural integrity for the static loads. The nominal first structural natural frequency of this array that would be excited by the wind was just slight below 10 Hz. For both

configurations, the structure whose 1st wind excited structural frequency is below 5 Hz is sufficiently flexible that it is questionable whether it could withstand the static loads with sufficient confidence to be a viable structure. Because for configuration I to have a lowest natural frequency of 5 Hz requires the structure to be approximately 4 times as heavy or 4 times as flexible as the nominal structural configuration, the results for the configuration with a 5 Hz frequency should be very conservative. If 5 Hz is considered as the lower limit for a variable structure, the maximum magnification factor for configuration I is 1.3 and configuration II is 1.08.

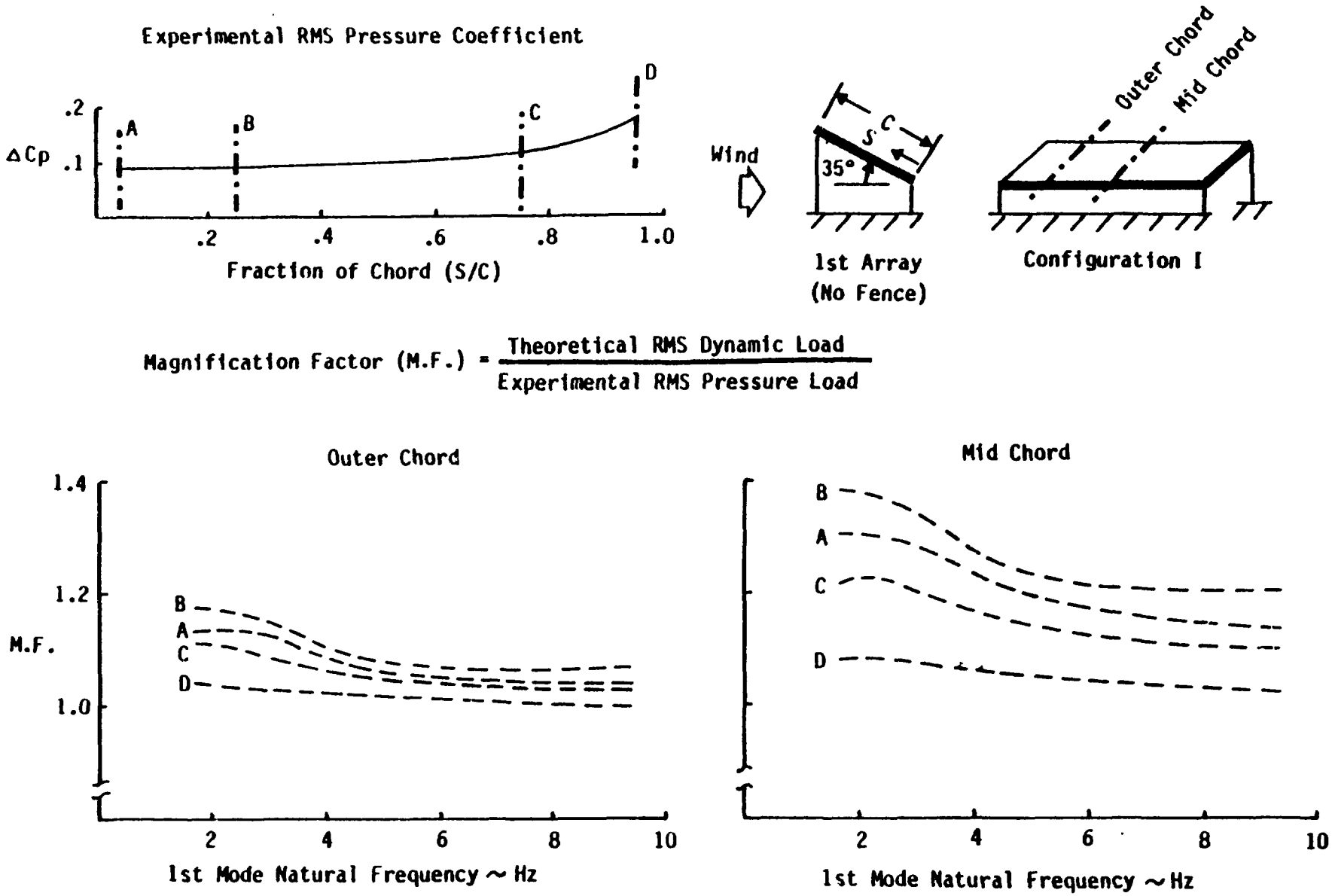

Figure 3-3. Configuration I - Dynamic Analysis Results for 1st Array Unprotected from the Wind

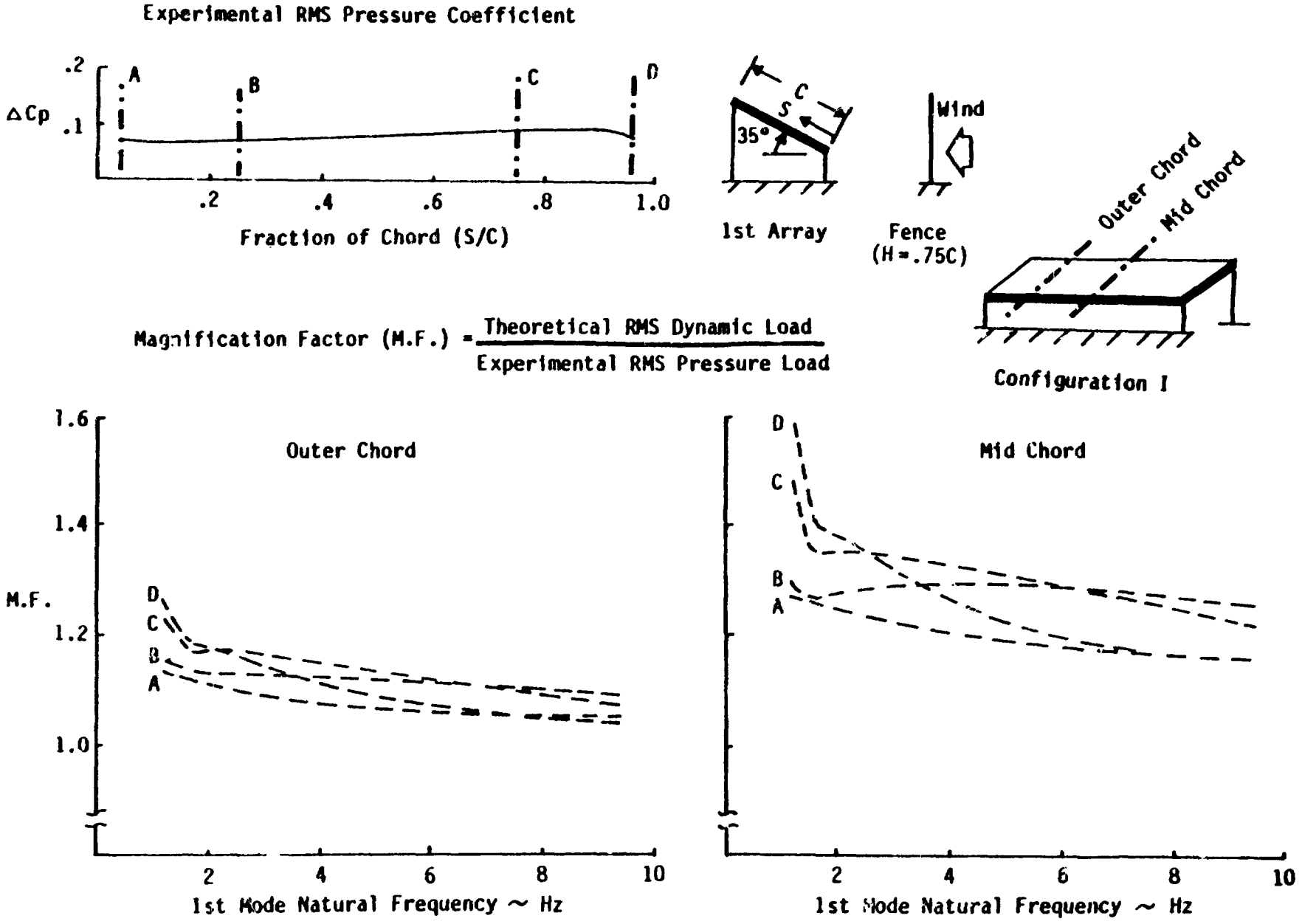

Figure 3-4. Configuration I - Dynamic Analysis Results for 1st Array Protected from the Wind by a Fence

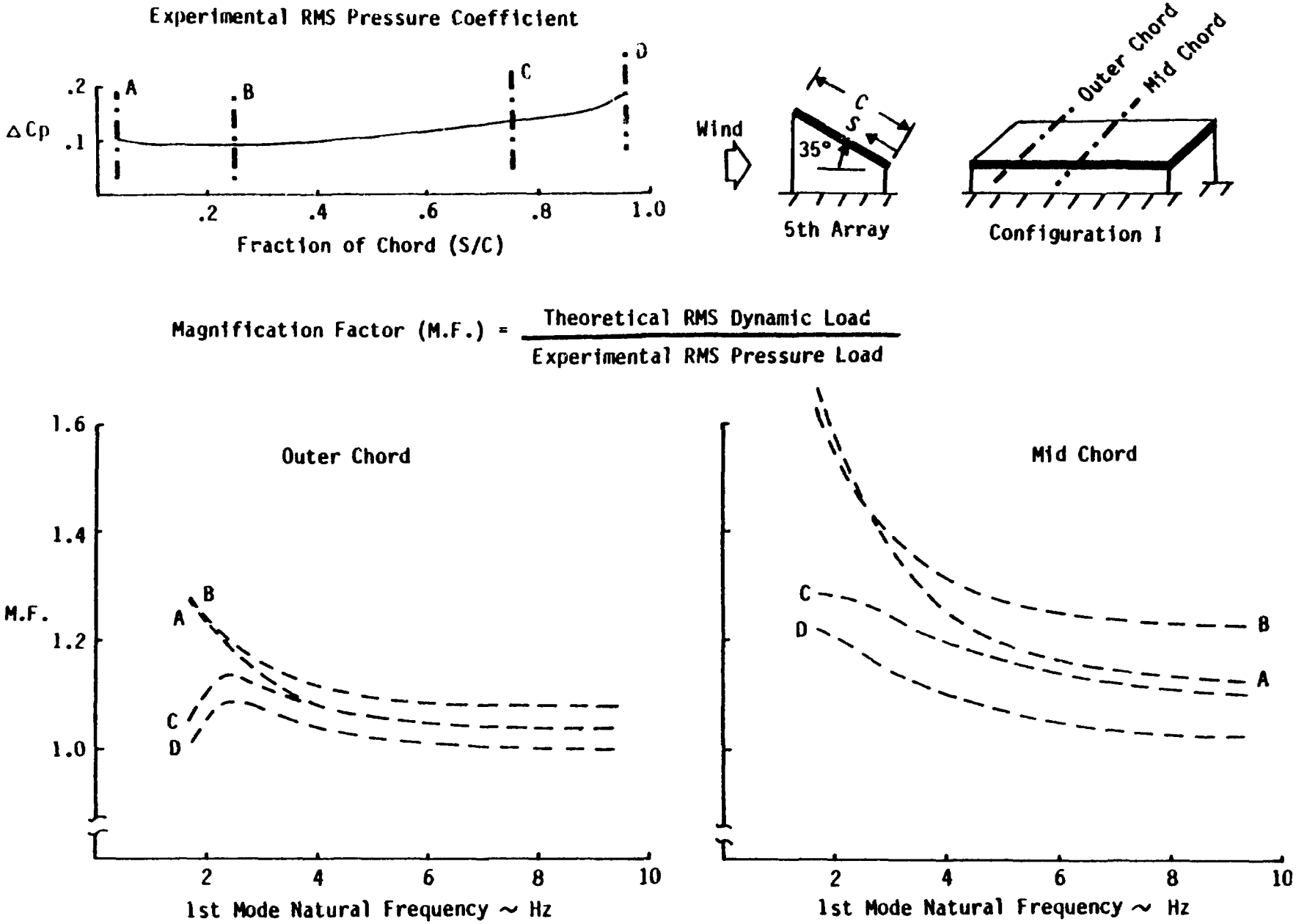

Figure 3-5. Configuration I - Dynamic Analysis Results for 5th Array within an Array Field

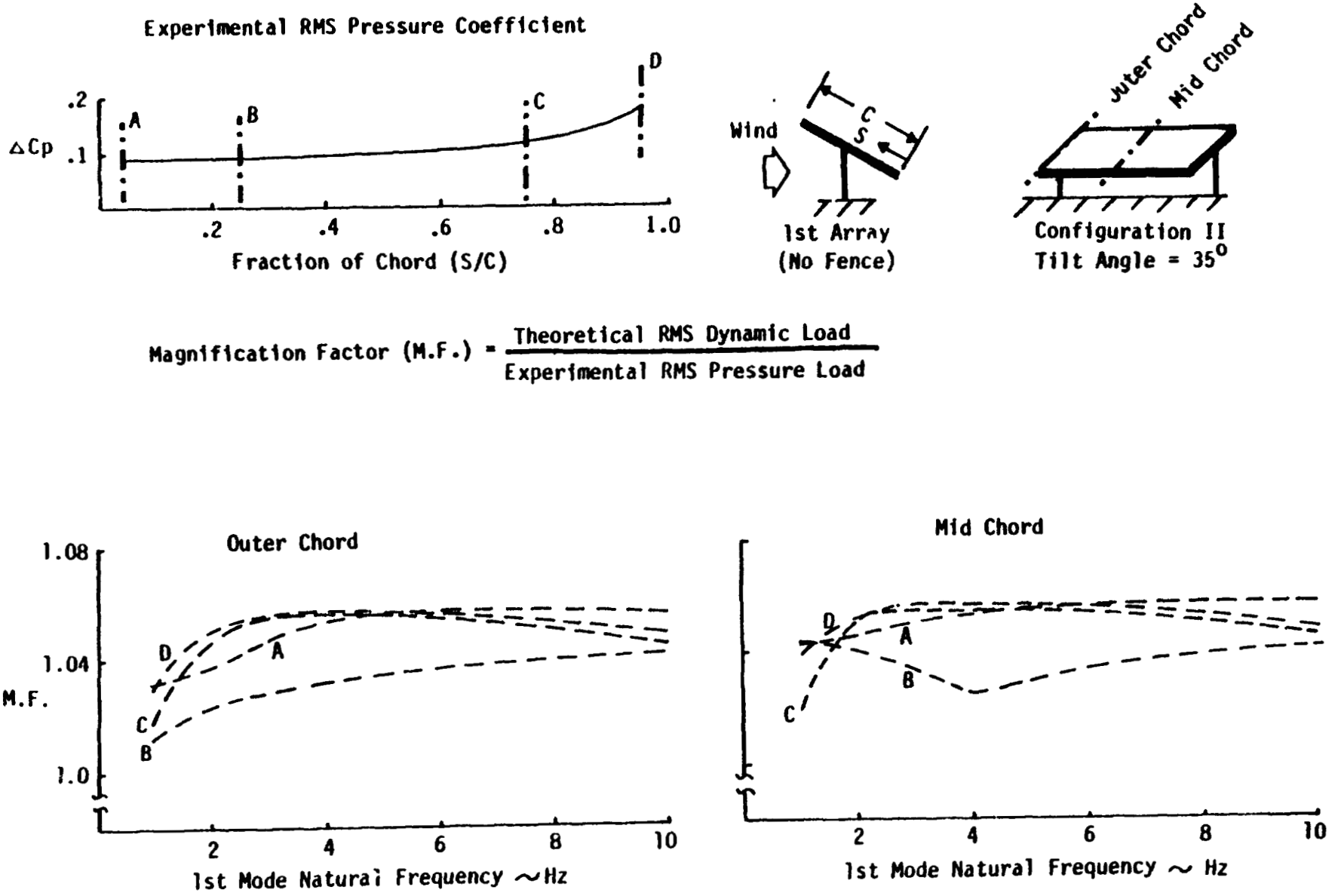

Figure 3-6. Configuration II - Dynamic Analysis Results for 1st Array Unprotected from the Wind

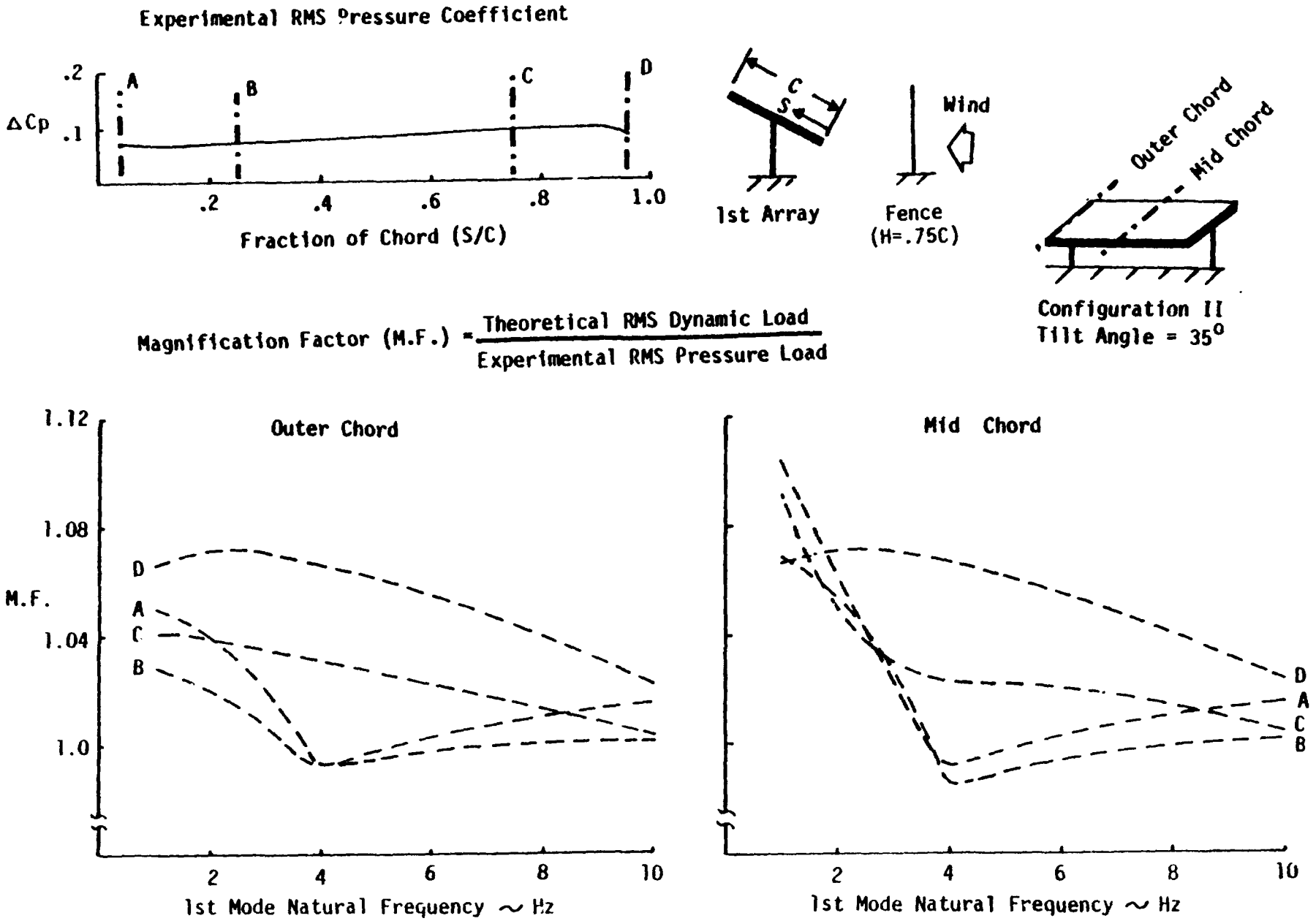

Figure 3-7. Configuration II - Dynamic Analysis Results for 1st Array Protected from the Wind by a Fence

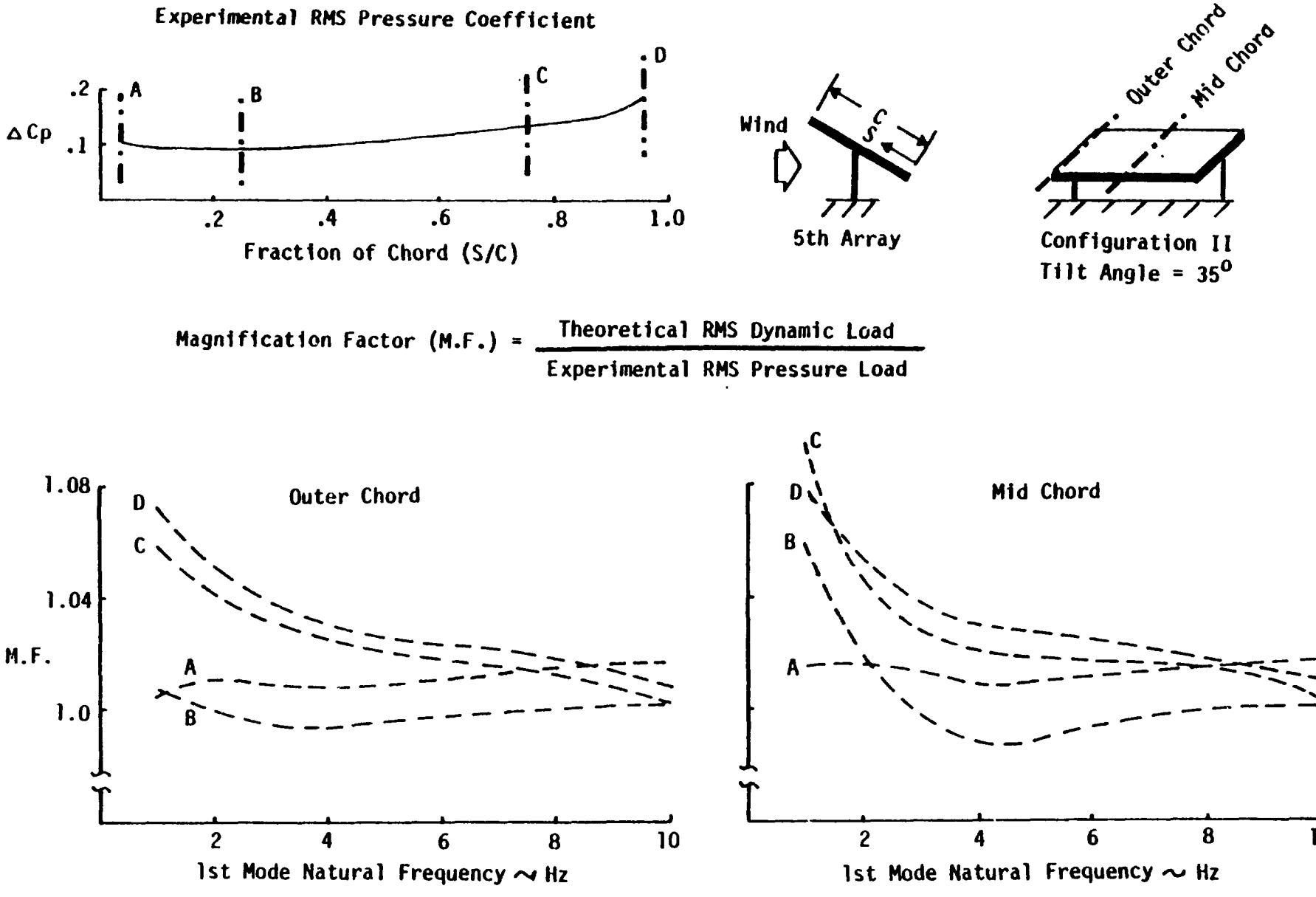

Figure 3-8. Configuration II - Dynamic Analysis Results for 5th Array within an Array Field

4.0 CONCLUSIONS

Although the structural configuration affects the dynamic response due to wind turbulence, the general trends of the two configurations studied are similar. The mid chord location on an array has the largest response and the largest magnification factors on both configurations. The outer chord magnification factor of configuration I is considerably lower than the mid chord factor because of the corner constraints, whereas for configuration II, the outer chord magnification factor is only slightly reduced compared to the mid chord. The largest dynamic response occurs near the downwind edge of the array and decreases as the 1st structural modal frequency increases. Thus, to minimize the dynamic loads due to turbulence requires the maximum practical stiffness for the structure. A dynamic magnification factor of 1.3 appears to be a conservative factor for any type of flat plate photovoltaic array structure.

It should be noted that for the types of structures used in this analysis, if the 1st wind excited structural frequency is below 5 Hz the structure is sufficiently flexible that it is questionable whether it could withstand the static loads with sufficient confidence to be a viable structure. For configuration I to have a lowest natural frequency of 5 Hz requires the structure to be approximately 4 times as heavy or 4 times as flexible as the nominal structural configuration, thus, the results for the configuration with a 5 Hz frequency should be very conservative. If 5 Hz is considered as the lower limit for a variable structure, the maximum magnification factor for configuration I is 1.3 and configuration II is 1.08.

5.0 ARRAY DESIGN GUIDELINES FOR WIND TURBULENCE

Based on the results of the boundary layer wind tunnel test and the results of this dynamic analysis, the following design guidelines are given for determining wind loading on photovoltaic flat plate arrays for the turbulent portion of the wind. These guidelines are valid for arrays at least 2 chord lengths from the edge and for a wind velocity profile that approximates a 1/7 power law. However, because of the edge constraints of the arrays in a dynamic sense, and because of the conservatism in this analysis, the wind designs loads calculated using these guidelines would probably be also adequate for the side edge arrays.

Figure 5-1 presents guidelines to calculate design pressure loads on array surfaces due to the non-steady portion of the wind. (The design guidelines for the steady state portion of the wind that needs to be combined with the turbulent portion for the total design load was documented in reference 1.) This procedure requires a number of decisions which includes; 1) the choice of configuration I or II must be representative of the design under consideration; 2) the choice of the rms unsteady pressure coefficients for the appropriate design array tilt angle and array location from the wind tunnel results presented in Appendix B; 3) the level of probability not to exceed a given level (i.e., 1σ = 68.27%, 2σ = 95.45%, 3σ = 99.73%); 4) the design configuration first structural natural frequency that can be excited by the wind turbulence; 5) the design free stream wind speed. The appropriate magnification factors from figure 3-3 to 3-8 multiplied by the rms unsteady pressure coefficient chosen from Appendix B is the design rms pressure coefficient for wind turbulence with a 68.3% probability of not exceeding. For a higher probability such as 95.5%, this design rms pressure coefficient would be multiplied by 2.0. The following is an example applying this procedure.

Assume that the design is similar to configuration I, has a tilt angle of 35° and the first structural frequency normal to the array is 5 Hz. For any interior arrays, the rms unsteady pressure coefficient for this condition extracted from Appendix B is reshown in figure 5-2. The magnification factor (M.F.) for 5 Hz at the mid span location (figure 3-5) and these M.F. multiplied by the rms ΔCp from figure 5-1 is shown in table 6.1 as a function of chord position. Assuming that a level of probability not to exceed 95.5%

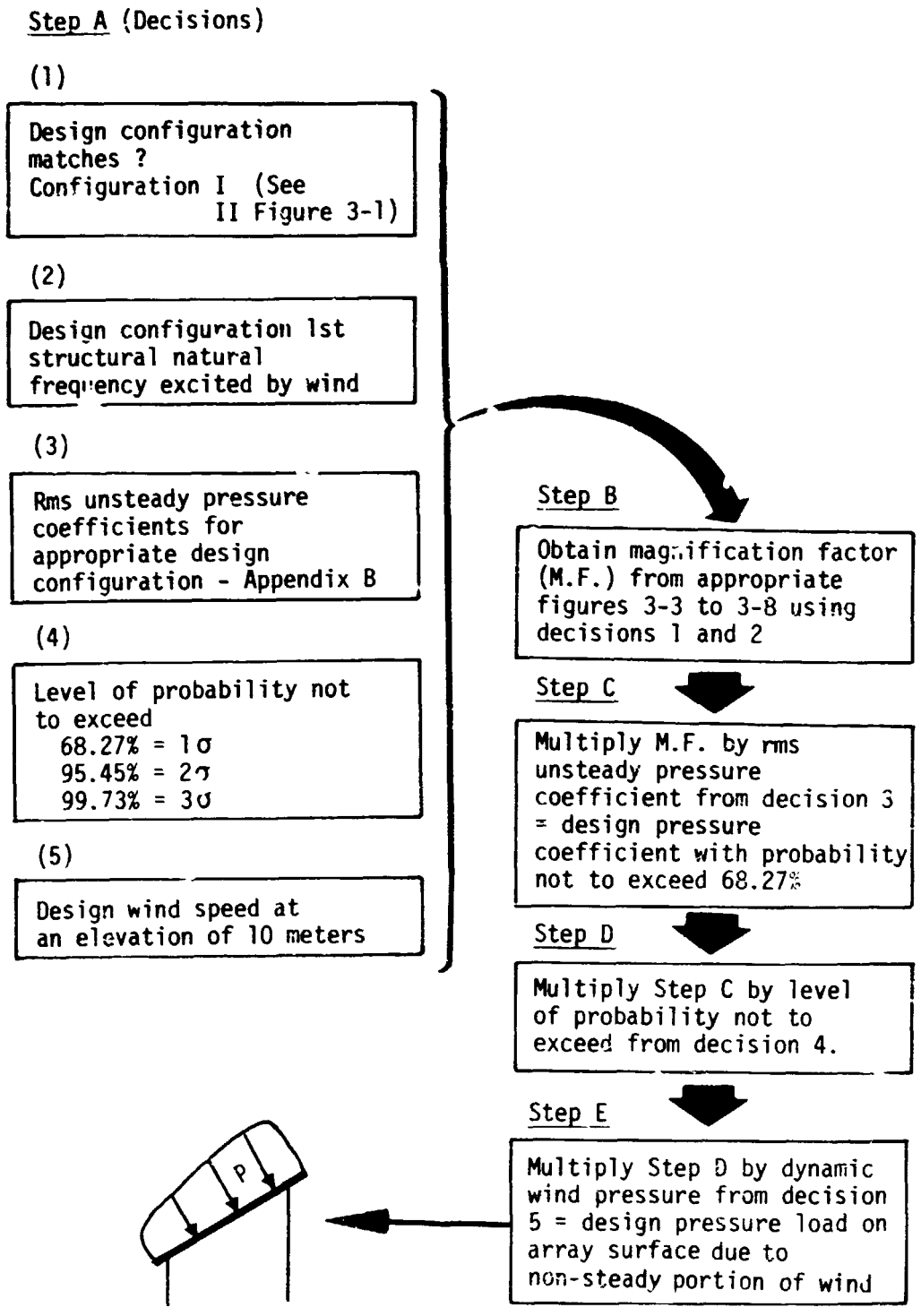

Figure 5-1. Flow Chart to Calculate Array Pressures due to the Non-Steady Portion of Wind

of the design load due to turbulence is required, the rms ΔCp times the M.F. is increased by a factor of 2. The design delta pressure coefficient for the turbulent portion of the wind is shown in table 5-1 and in figure 5-3. The pressure due to a 90 mph wind is also shown in table 5-1 and figure 5-3.

The design load for the front array (either protected or unprotected by a fence) is calculated in the same manner using the appropriate rms delta pressure coefficient and magnification factors. This procedure can be simpified by utilizing the highest M.F. (M.F. = 1.3 for modal frequencies > 5 Hz) for all conditions. This would eliminate the need to determine the design configuration natural frequency as well as not requiring the determination of the M.F. along the chord from figures 3-3 to 3-8.

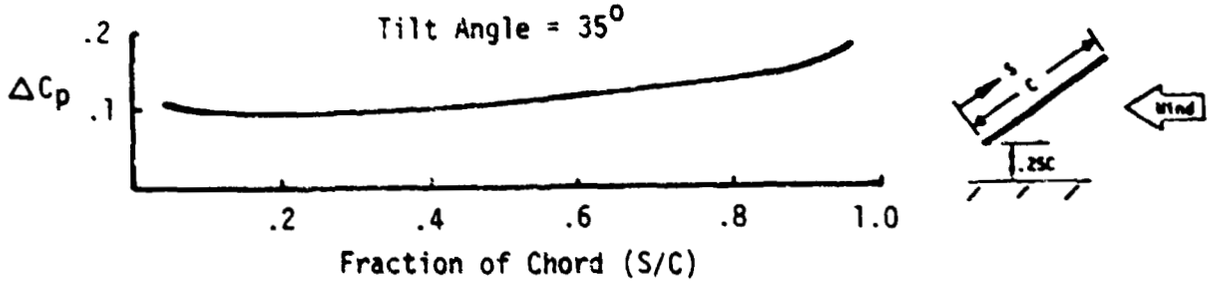

Figure 5-2. Wind Tunnel Test RMS Pressure Coefficients on the 5th Array in an Array Field

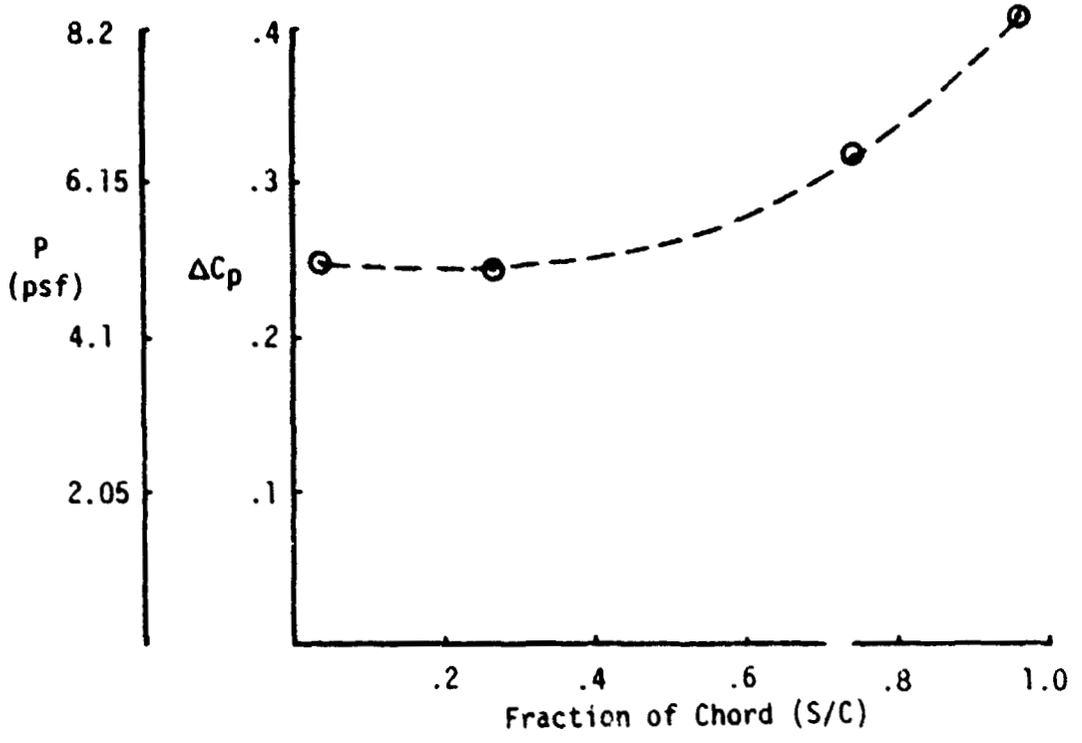

Figure 5-3. Example Design Wind Loads on Interior Arrays in an Array Field Using the Design Guidelines

Table 5-1. Results for an Interior Array Using the Design Guidelines

Steps see Figure 5-1		S/C			
		.96(T.E)	.74	.26	.04(L.E)
Step A	Rms ΔCp (see Figure 5-2)	.104	.095	.133	.189
Step A	q (psf) (90 mph wind)	20.5	—	—	—
Step B	M.F. (see Figure 3-5)	1.19	1.27	1.17	1.07
Step C	(M.F.) (rms ΔCp)	.1238	.1207	.1556	.2022
Step D	Design ΔC_p (2σ) (M.F.) (rms ΔCp)	.2475	.2413	.3112	.4045
Step E	Design Pressures (psf)	5.07	4.95	6.38	8.29

T.E. = Trailing Edge

L.E. - Leading Edge

6.0 NEW TECHNOLOGY

No reportable items of new technology have been identified by Boeing during the contract of this work.

7.0 REFERENCES

1. "Wind Loads on Flat Plate Photovoltaic Array Fields", DOE/JPL - No. 954833-81/3, Boeing Engineering and Construction Company, April, 1981.

2. Miller, R. D.; and Graham, M. L.: "Random Harmonic Analysis Program, L221 (TEV156) Volume I; Engineering and Usage". NASA CR-2857, 1979.

3. Bendat, J. S. and Piersol, A. G.: "Random Data: Analysis and Measurement Procedures", (1971), John Wiley and Sons, Inc.

4. Crandall, S. H., "Random Vibrations", (1958), MIT and John Wiley and Sons, Inc.

5. Wilson, A.H.: "Low Cost Solar Array Structure Development," DOE/JPL - 1012-53, Jet Propulsion Laboratory, Pasadena, California, June 15, 1981.

Appendix A - Analysis Procedure

A mathematical model of the photovoltaic array included the important structural, mass and aerodynamic characteristics necessary to simulate the dynamic response of the array to the turbulence generated by the upwind arrays and that contained in the free stream wind.

The structural model included the elastic characteristics of the complete array. A finite element program NASTRAN was used to model the structure and to calculate modes of vibration. The mode shapes for the two configurations that can be excited by aerodynamic turbulence are shown in Figure A-1. Generalized aerodynamic forces representing the aerodynamics on the array were computed using the steady state pressure distributions measured in Phase III (reference 1) and combined with the modes of vibration to produce the following equations of motion for use in a Boeing developed Random Harmonics analysis computer program (reference 2).

$$[M_1]\{q\} + [M_3]\{\ddot{q}\} + [M_4]\{q\} + [M_5]\{\dot{q}\} = [C]\{\Delta p\}$$

$[M_1]$ generalized structural stiffness and structural damping matrix
$[M_3]$ generalized mass matrix
$[M_4]$ aerodynamic stiffness matrix
$[M_5]$ aerodynamic damping matrix
$\{q\}$ vector of generalized coordinates
$[C]$ matrix of generalized forces associated with unit pressures at each of the excitation points
$\{\Delta p\}$ vector of excitation pressures

A corresponding set of load equations using the force summation method was developed in the form

$$\{L\} = [\bar{M}_1]\{q\} + [\bar{M}_3]\{\ddot{q}\} + [\bar{M}_4]\{q\} + [\bar{M}_5]\{\dot{q}\} + [\bar{C}]\{\Delta p\}$$

Where $\{L\}$ is the load vector and the $[\bar{M}_i]$ matrices are as defined for the response equations, except that they represent generalized load coefficients.

The auto and cross power spectral densities of the pressures measured in the wind tunnel was used to excite the array mathematical model. The loads output spectrum was calculated utilizing the following equation:

$$L(\omega) = \sum_{i=1}^{N} \sum_{j=1}^{N} X_i(\omega)\, X_j^*(\omega)\, \phi_{ij}(\omega)$$

where

$X_i(\omega)$	transfer function for system response to excitation i
$*$	denotes conjugate
ϕ_{ij}	i = j auto power spectral density for pressure i
	i ≠ j cross power spectral density between pressures i and j

Integration of the output spectrum produces the rms load response

$$\bar{L} = \left(\int_0^{\infty} L(\omega)\, d\omega \right)^{1/2}$$

Because the pressure taps on the wind tunnel model in the Phase III study were located on only one spanwise station, other spanwise stations were assumed to have an identical auto- and cross-spectrum chordwise and a correlation function of unity spanwise. The assumption of the same chordwise spectrum at each spanwise station is a valid assumption since the process is random. However, the assumption of a correlation function of unity between spanwise pressure taps is conservative.

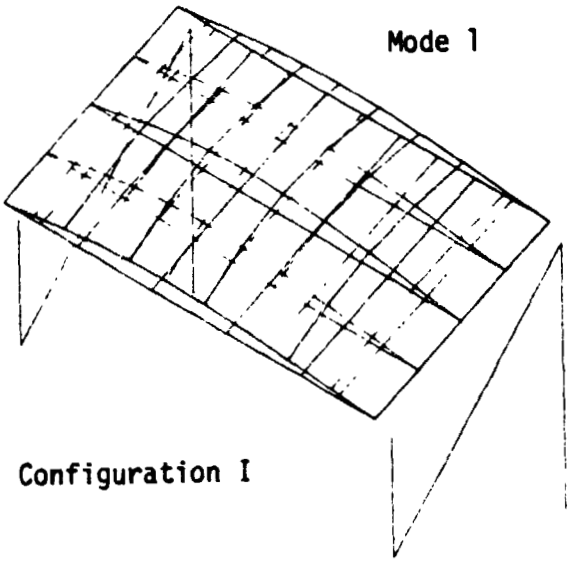

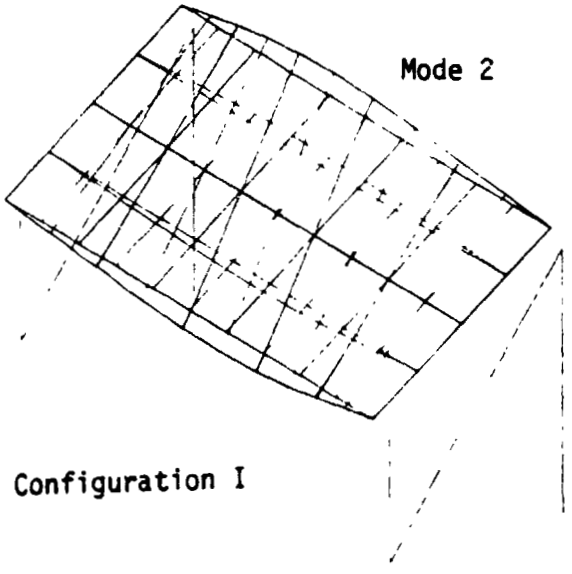

Frequency Ratio: Mode 2/Mode 1 = 1.6

Figure A-1. Array Mode Shapes

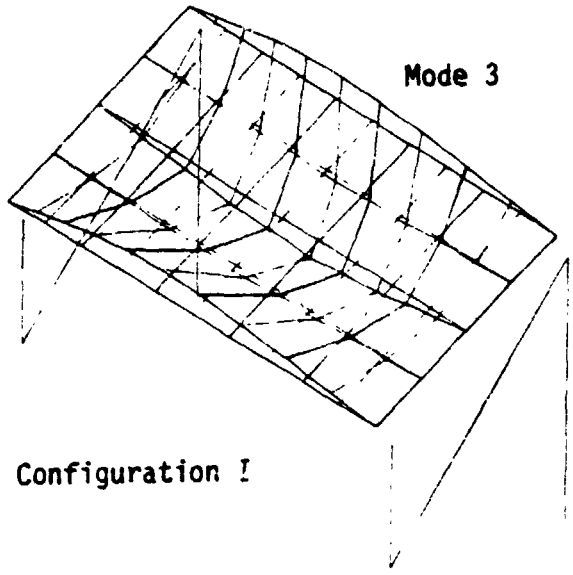

Frequency Ratio: Mode 3/Mode 1 = 3.3

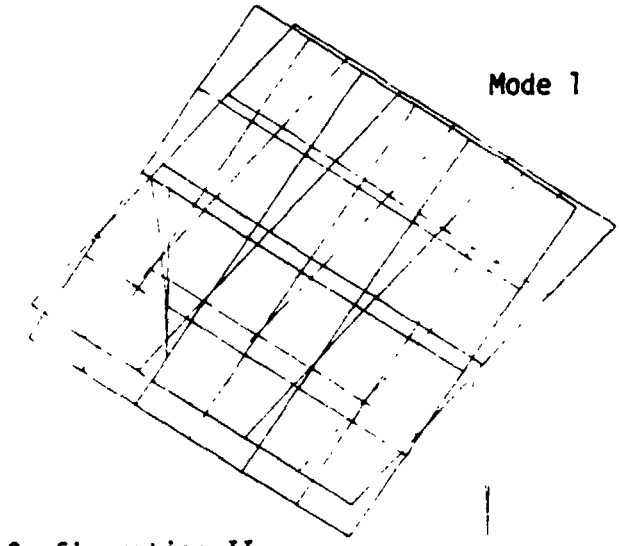

Figure A-1. Array Mode Shapes (Continued)

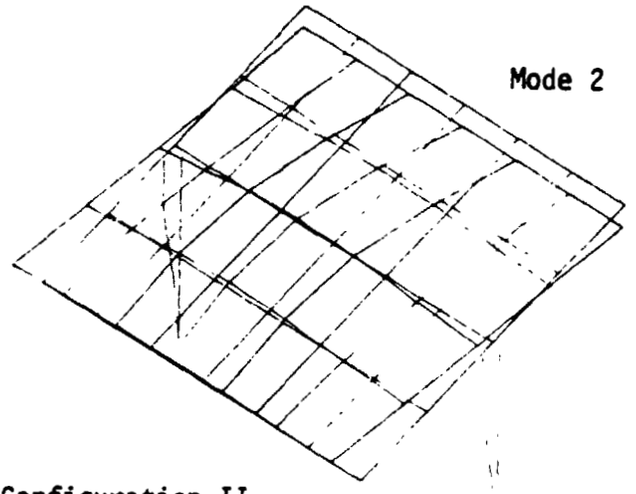

Configuration II

Frequency Ratio: Mode 2/Mode 1 = 3.6

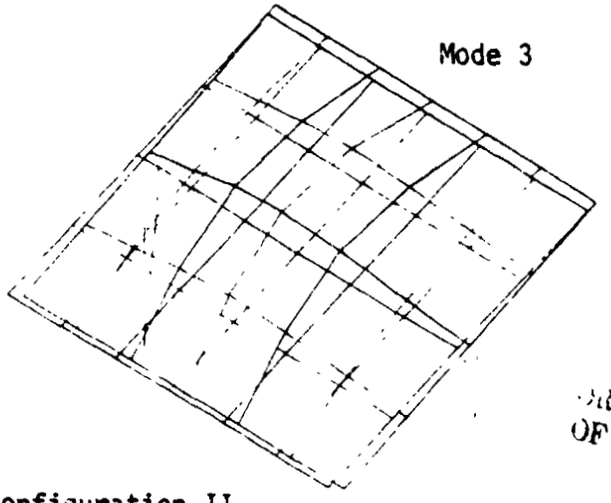

Configuration II

Frequency Ratio: Mode 3/ Mode 1 = 5.0

Figure A-1. Array Mode Shapes (Concluded)

Appendix B

Wind Tunnel Test RMS Unsteady Delta Pressure Coefficients

RMS pressure coefficients shown in Figures B-1 to B-3 of the fluctuating pressures were obtained from the wind tunnel test results reported in reference 1. These coefficients were obtained for three tilt angles (20°, 35° and 60°), and for the first array of an array field unprotected and protected by a fence, the fifth array within an array field, and for wind directions from the front and rear. The pressure coefficients were calculated based on a wind reference velocity at 10 meters and a 1/7 power law wind velocity profile.

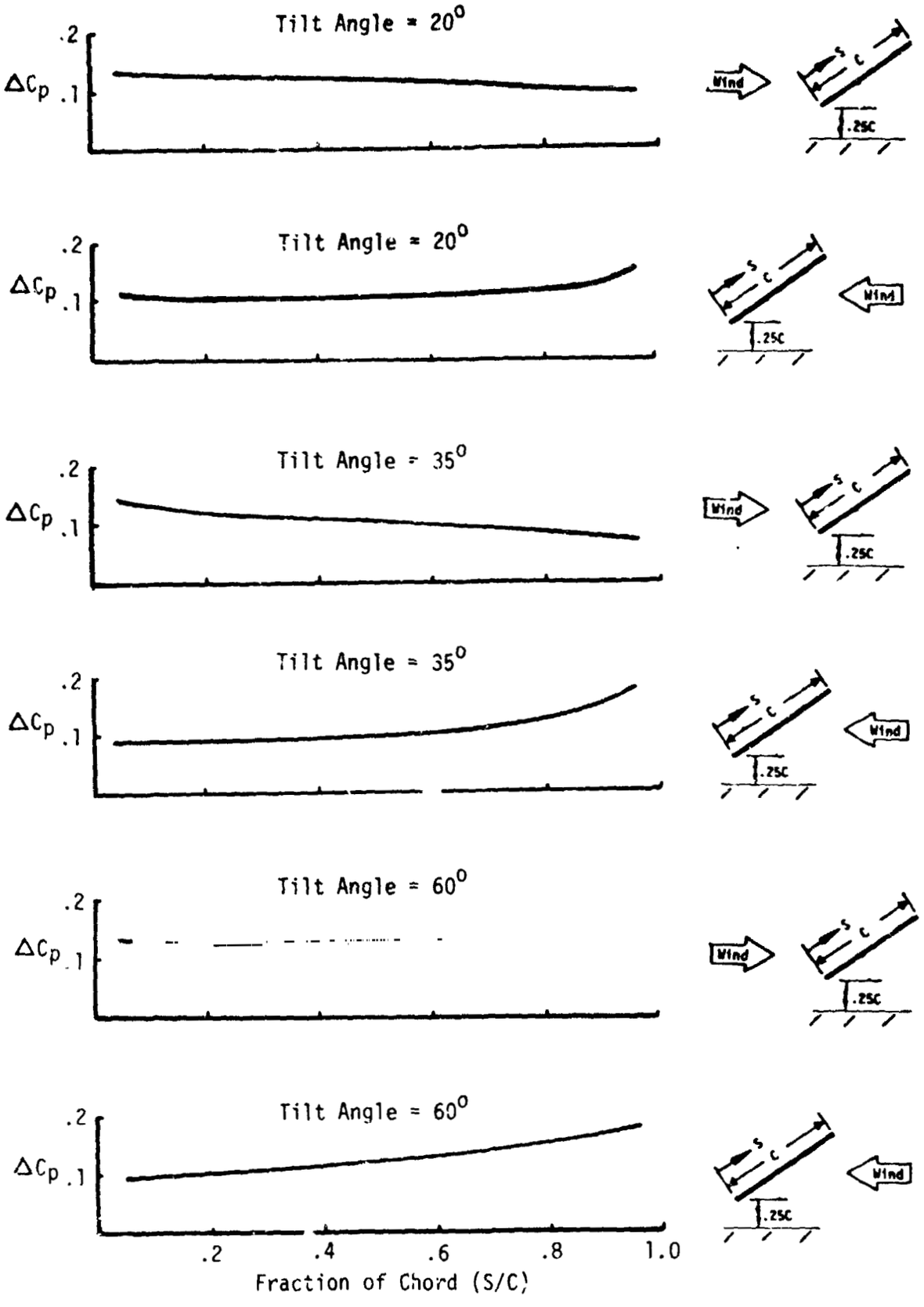

Figure B-1. RMS Pressure Coefficients on the First Array of an Unprotected Array Field

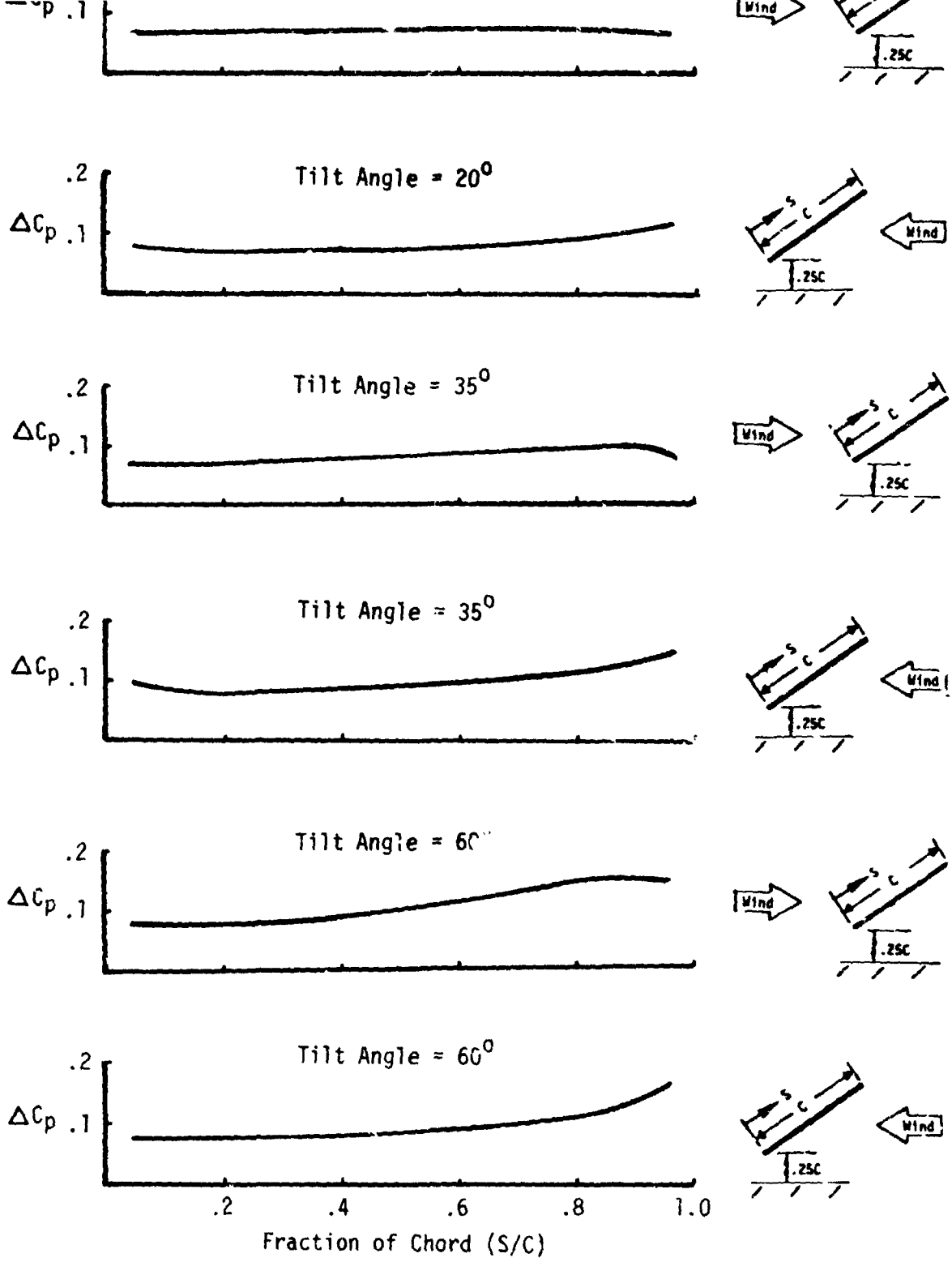

Figure B-2. RMS Pressure Coefficients on th First Array of an Array Field Protected by a Fence

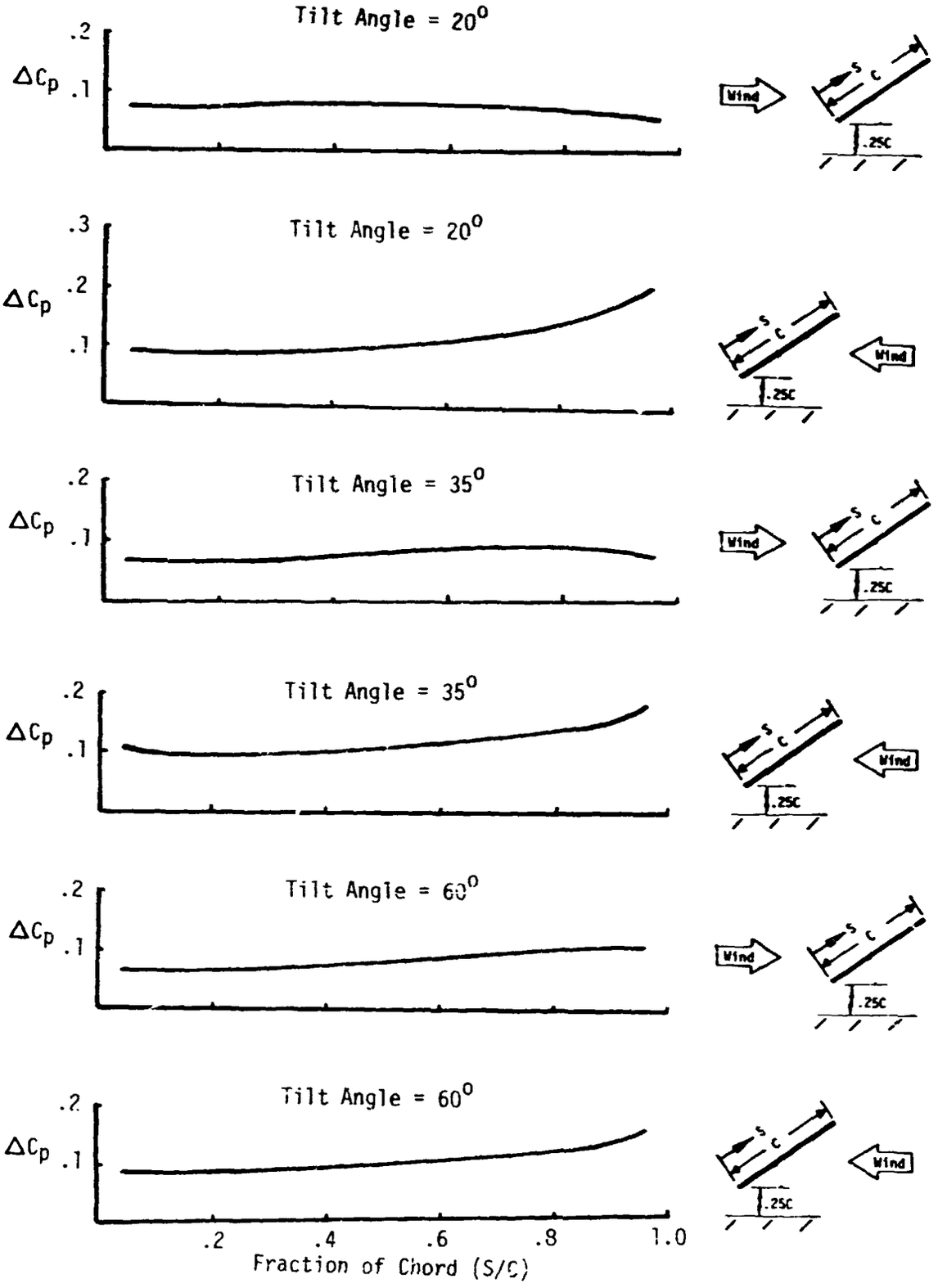

Figure B-3. RMS Pressure Coefficients on the Fifth Array within an Array Field

APPENDIX C

WIND LOADS ON FLAT PLATE PHOTOVOLTAIC ARRAY FIELDS (Spectra Analysis)

PHASE IV - FINAL REPORT

WIND TUNNEL TEST REPORT

Prepared for Jet Propulsion Laboratory
under Contract 954833

Boeing Engineering and Construction Company
(A Division of The Boeing Company)
Seattle, Washington 98124

WIND PRESSURES AND FORCES ON FLAT-PLATE PHOTOVOLTAIC SOLAR ARRAYS-- CROSS-SPECTRAL ANALYSIS

by

N. Hosoya,* J. A. Peterka,**
and J. E. Cermak***

for

Boeing Engineering and Construction Company
P.O. Box 3707
Seattle, Washington 98124

Fluid Dynamics and Diffusion Laboratory
Civil Engineering Department
Colorado State University
Fort Collins, Colorado 80523
Project S-36022

June 1981

*Graduate Research Assistant
**Associate Professor
***Professor-in-Charge, Fluid Mechanics
and Wind Engineering Program

CER80-81NH-JAP-JEC57

TABLE OF CONTENTS

LIST OF FIGURES

LIST OF TABLES

LIST OF SYMBOLS

Symbol	Definition
c	chord length of solar array (4 in model, 8 ft full-scale)
C_M	pitching moment coefficient
C_N	normal force coefficient
C_p	instantaneous pressure coefficient
C'_p	fluctuation of pressure coefficient
$C_{p_{mean}}$	mean pressure coefficient
$C_{p_{rms}}$	root-mean-square of pressure coefficient
e	eccentricity of center of pressure from mid-chord
FN	normal force per unit area
H_f	fence height
M	pitching moment per unit area about center of chord
N	frequency
N*	normalized frequency = $\frac{N \cdot c}{U_{ref}}$
P	local pressure on collector
ΔP	pressure difference across collector
q_{ref}	reference dynamic pressure at 10 m full-scale
$R_{ij}(\tau)$	correlation function
U_{ref}	reference wind velocity (approx. 43 fps model) at 10 m height
x_f	fence distance
α	angle of attack
τ	time lag
$\Phi_{ij}(N)$	power spectral function
$\Phi^*_{ij}(N^*)$	normalized power spectral function

PREFACE

Simultaneous pressure measurements on flat plate photovoltaic solar arrays were conducted in a simulated atmospheric boundary layer characterized by a 1/7th power law mean velocity distribution. This report describes random properties of fluctuating local pressures on solar arrays by cross-spectral analysis. The random properties to be analyzed include the auto- and cross-spectra for fluctuating pressures for several typical array configurations.

The essential experimental configurations, including facilities, wind-tunnel models, instrumentation and the flow simulation technique, have been described in a preceding report [5] "Wind Pressures and Forces on Flat-Plate Photovoltaic Solar Arrays," Colorado State University Report CER80-81NH-JAP-MP-JEC13. The simultaneous pressure measurements presented in this supplementary report required some additional arrangements for instrumentation and data acquisition. These arrangements will be described in Sections 1 and 2 of this report.

1.0 PRESSURE TAPS AND ARRAY CONFIGURATIONS

1.1 Pressure Taps

The simultaneous pressure measurements were obtained at four pressure taps along the chord on the upstream surface and four pressure taps on the downstream surface of the solar array. These pressure taps tested were taps 1, 4, 7 and 10 on the upstream surface, and taps 11, 14, 17 and 20 on the downstream surface. The location of each pressure tap is shown in Figure 1 which duplicates Figure 10 of the preceding report.

1.2 Array Configurations

All array configurations tested for this phase of the study are listed in Table 1. Array locations are shown in Figure 2 which duplicates Figure 11 in the preceding report. Several typical array configurations are chosen to be presented and discussed in this report. For this study, the ground clearance and spacing of solar arrays were 0.25 c and 2.0 c respectively, and were not varied. The wind direction was 0° for all array configurations. The definitions of these test parameters are seen in Figure 2.

2.0 DATA ACQUISITION

The mean wind velocity outside the simulated turbulent boundary layer in the Meteorological Wind Tunnel, shown in Figure 1 of the main report, was approximately 50 fps as was used for the preceding tests (giving a $U_{ref} \simeq 43$ fps). The outputs from the 8 pressure transducers were recorded simultaneously on digital magnetic tape for 35 seconds at 500 samples per second using a data acquisition system based on a Hewlett-Packard System 1000 minicomputer. The data were then analyzed by the same computer. Pressure, normal force and pitching moment

coefficients presented in this report were referenced to the mean dynamic pressure at 10 m elevation in the prototype. The power spectral densities of local peak pressures were evaluated with these pressure coefficients.

2.1 Pressure and Normal Force Coefficients

Pressure and normal force coefficients are respectively defined in Sections 3.2 and 3.3 of the preceding report. The same definitions apply to this report:

$$C_p = \frac{P}{q_{ref}} \quad , \quad \Delta C_p = \frac{\Delta P}{q_{ref}}$$

$$C_N = \frac{1}{c} \int_0^c \Delta C_p(s) ds \tag{1}$$

2.2 Pitching Moment Coefficients

Pitching moment coefficients, C_M, about the mid-chord of the solar array are defined by

$$C_M = \frac{M}{q_{ref} \cdot c} \tag{2}$$

where M is the calculated pitching moment per unit surface area about the mid-chord of the array, q_{ref} is the reference dynamic pressure of approaching flow at 10 m full-scale, and c is the chord length of the array. In order to calculate M, the eccentricity of the center of pressure, e, was obtained numerically by a curve fitting to the pressure distribution using linear interpolation schemes along the chord of the array. Thus

$$M^* = FN \cdot e \tag{3}$$

where FN is the normal force.

*pitching moment lifting windward edge up is defined to be positive.

2.3 Spectral Analysis

2.3.1 Matrix Arrangement

A set of cross-power spectral densities of local pressure fluctuations on the solar array were calculated. For simplicity of notation, the pressure tap numbers 1,4,7,10,11,14,17 and 20 can be renamed as 1,2,3,...,8 in order. Any pressure tap number used in this report will be, hereafter, referred to as the renamed one.

Matrices for the correlation and power spectral densities are written as follows.

$$\left[R_{ij}(\tau)\right] = \begin{cases} \text{auto-correlation} & \text{, if } i = j \\ \text{cross-correlation} & \text{, if } i \neq j \end{cases}$$

$$\left[\Phi_{ij}(N)\right] = \begin{cases} \text{auto-spectrum} & \text{, if } i = j \\ \text{cross-spectrum} & \text{, if } i \neq j \end{cases}$$

where τ is time lag, N is frequency, and i,j refer to the pressure tap numbers.

2.3.2 Correlation Functions

For this analysis, auto- and cross-correlation functions are defined by

$$R_{ij}(\tau) = \lim_{T\to\infty} \frac{1}{T} \int_0^T \left[C_{p_i}(t) - C_{p_{mean_i}}\right]\left[C_{p_j}(t+\tau) - C_{p_{mean_j}}\right] d\tau \qquad (4)$$

where $C_{p_k}(t)$ and $C_{P_{mean_k}}$ are instantaneous and time-averaged values of pressure coefficient with respect to tap number k. Defining a fluctuating component of pressure coefficient, $C'_{p_k}(t)$, as

$$C'_{p_k}(t) = C_{p_k}(t) - C_{p_{mean_k}} \qquad (5)$$

the auto-correlation function, at $\tau = 0$, becomes for one tap

$$R_{ii}(0) = \overline{C'_{p_i}(t)\, C'_{p_i}(t)} = C^2_{p_{rms_i}} \tag{6}$$

in which an overbar denotes a time averaging.

2.3.3 Power Spectral Density Functions

Power spectral density functions are defined by

$$\Phi_{ij}(N) = 4 \int_0^\infty R_{ij}(\tau)\, \exp(-j2\pi N\tau)\, d\tau \tag{7}$$

where j appearing in the exponential function refers to $j^2 = -1$.

The integral property of the auto-spectral function requires

$$\int_0^\infty \Phi_{ii}(N)\, dN = R_{ii}(0) = C^2_{p_{rms_i}} \tag{8}$$

Because of this property, the power spectral density can be normalized by

$$\Phi^*_{ij}(N) = \frac{|\Phi_{ij}(N)|}{C_{p_{rms_i}} \cdot C_{p_{rms_j}}} \quad \text{with units} \left[\frac{1}{Hz}\right] \tag{9}$$

It is also common practice to normalize the frequency N by

$$N^* = \frac{Nc}{U_{ref}} \tag{10}$$

where U_{ref} is the reference wind velocity.

The cross-spectral analysis was performed digitally by a Fourier Transform subroutine using standard techniques such as those in references [1] and [3]. Transforms were performed on 8 time segments, each 2048 samples in length, for each pressure record (recorded at

500 samples per second). Transforms were combined to form cross-spectra and appropriate averaging across data points in frequency and time segments was performed to reduce normalized standard error of the spectrum. Because of memory limitations, the cross-spectra were only calculated to a maximum frequency of 125 Hz ($N^* \doteq 1.0$). This frequency retained virtually all the energy in the fluctuating pressures. Normalized standard error of the cross-spectra reached a maximum of 11 percent at the lower frequencies.

3.0 RESULTS AND DISCUSSIONS

3.1 Pressure and Normal Force Coefficients

Examples of time traces of normal force and pitching moment coefficients are shown in Figure 3 obtained with the first solar array at $\alpha = 35°$, without fence. The time-averaged mean and rms pressure coefficients are tabulated in Table 2 for six typical array configurations, including Runs 21331, 21344, 21346, 21352 and 21368. These values agree well with those found in the preceding report [5].

3.2 Power Spectral Analysis

The auto-spectra for each pressure tap are shown in Figures 4 through 9 for the six cases listed in Table 2. Comparing the auto-spectra for the individual pressure taps and for both surfaces of the solar array, the power spectra show that the energy is shifted to higher frequencies for the first array with fence and the fifth array, consistent with the smaller scales of turbulence expected behind the fence and within the array field. The rear side of the first array also shows this effect. The area under the auto-spectra over the available frequency range is compared to the measured variance in fluctuating pressure in Table 3. Figures 4 through 9 clearly show that the energy content in the power

spectra is concentrated at $N^* < 0.1$. At $N^* \simeq 0.3$, a spike in the power spectra is seen for both the upstream and downstream surfaces. This spike in the power spectra is due to vibration of the wind-tunnel model. Moreover, for some cases, another spike at $N^* \simeq 0.4$ was obtained which is a second mode of vibration of the model. No attempt was made to model the full-scale structural stiffness or damping so that these response spikes do not indicate full-scale response.

Both the real and imaginary parts of the auto- and the cross-spectra were calculated. Only the real part is shown in Figures 4 through 9. The imaginary part was essentially zero for all cases. The implication of this finding is that the phase angles of the various frequencies are uncorrelated. This is a typical result in velocity or pressure fluctuations in turbulent boundary layer flows.

Figures 10 through 15 show cross-spectral plots for all combinations of taps for each of the six cases listed in Table 2. Cross-spectra for each array were grouped on plots so that similarly-shaped curves would appear on the same plot. The plots reveal the same increase in energy at higher frequencies for arrays behind the fence and within the array field as was observed for the auto-spectra. Also, the model natural frequency of vibration shows in the plots.

4.0 CONCLUSIONS

On the basis of the data presented in previous sections, the following conclusions can be drawn.

1. Auto-spectra of local pressure fluctuations characteristically fall rapidly with increasing frequency.

2. Auto-spectra show higher energy at the higher frequencies where the pressure tap is within the array field or behind a wind fence.

3. Cross-spectra showed properties similar to those in 1 and 2 above.

4. Cross-spectra between taps in separated zones were quite similar.

5. The imaginary parts of both auto- and cross-spectra were essentially zero.

REFERENCES

1. Akins, R. E. and J. A. Peterka, "Computation of Power Spectral Densities and Correlations Using Digital FFT Techniques," (1975), Colorado State University Report CER75-76REA-JAP13, Fort Collins.

2. Bearman, P. W., "Wind Loads on Structures in Turbulent Flow," (1971), Proc. Modern Design of Wind Sensitive Structures, Paper 4, pp. 57-64.

3. Bendat, J. S. and A. G. Piersol, "Random Data: Analysis and Measurement Procedures," (1971), John Wiley and Sons Inc.

4. Cermak, J. E., "Aerodynamics of Buildings," (1976), Annual Review of Fluid Mechanics, Vol. 8, pp. 75-106.

5. Hosoya, N., J. A. Peterka, M. Poreh, and J. E. Cermak, "Wind Forces and Pressures on Flat-Plate Photovoltaic Solar Arrays," (1980), Fluid Mechanics and Wind Engineering Program, Colorado State University Report CER80-81NH-JAP-MP-JEC13, Fort Collins, September.

FIGURES

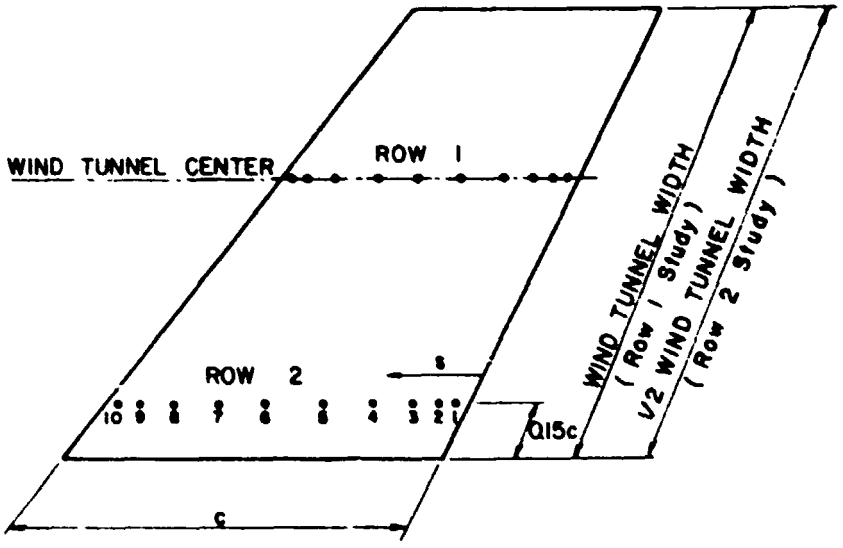

TAP LOCATIONS - FRACTION OF CHORD s/c

	1	2	3	4	5	6	7	8	9	10
UPSTREAM SURFACE	0.052	0.102	0.172	0.272	0.432	0.592	0.752	0.852	0.922	0.972
DOWNSTREAM SURFACE	0.028	0.078	0.148	0.248	0.408	0.568	0.728	0.828	0.898	0.948

Figure 1. Position of Pressure Taps on Instrumented Model

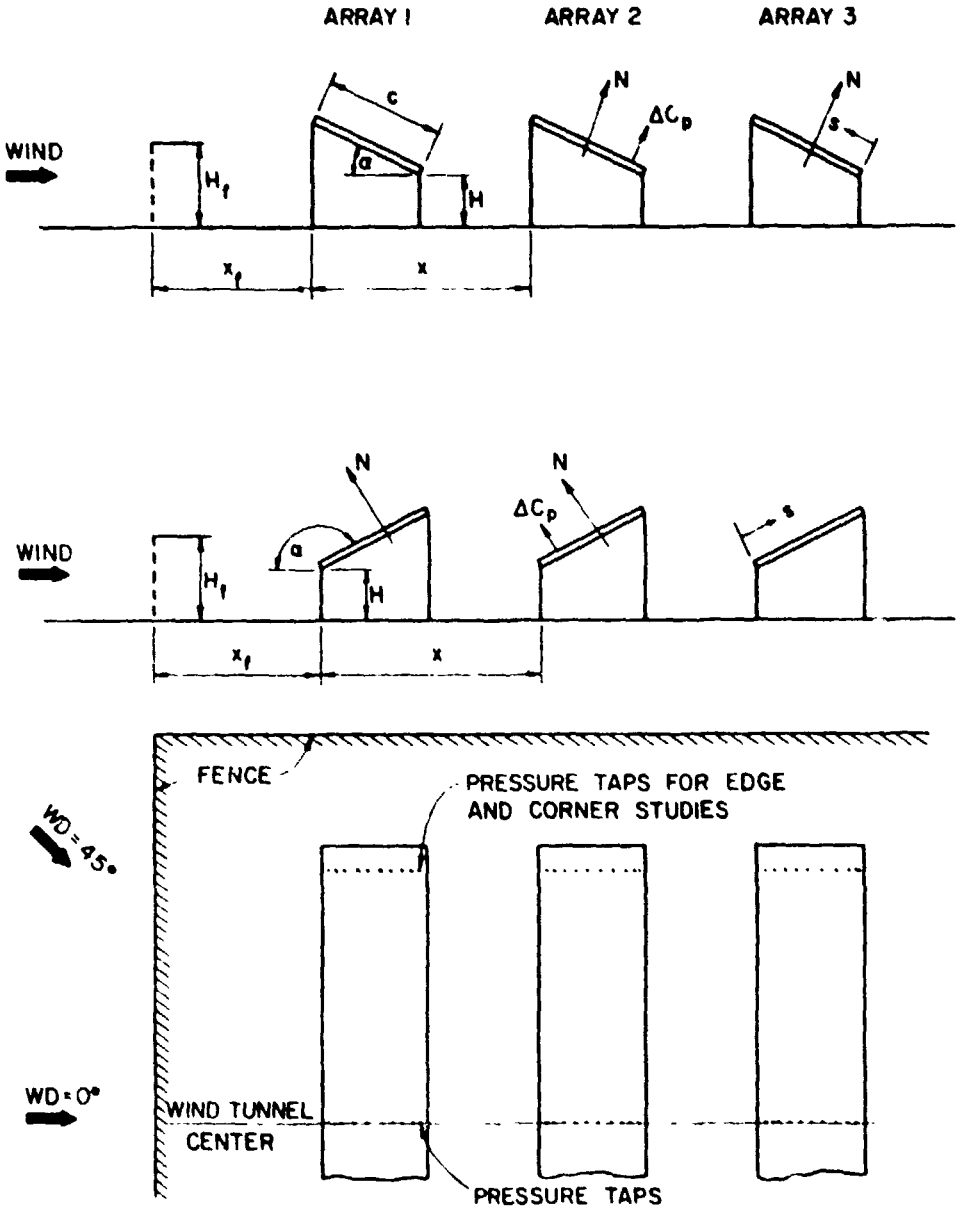

Figure 2. Schematic Description of Array Field

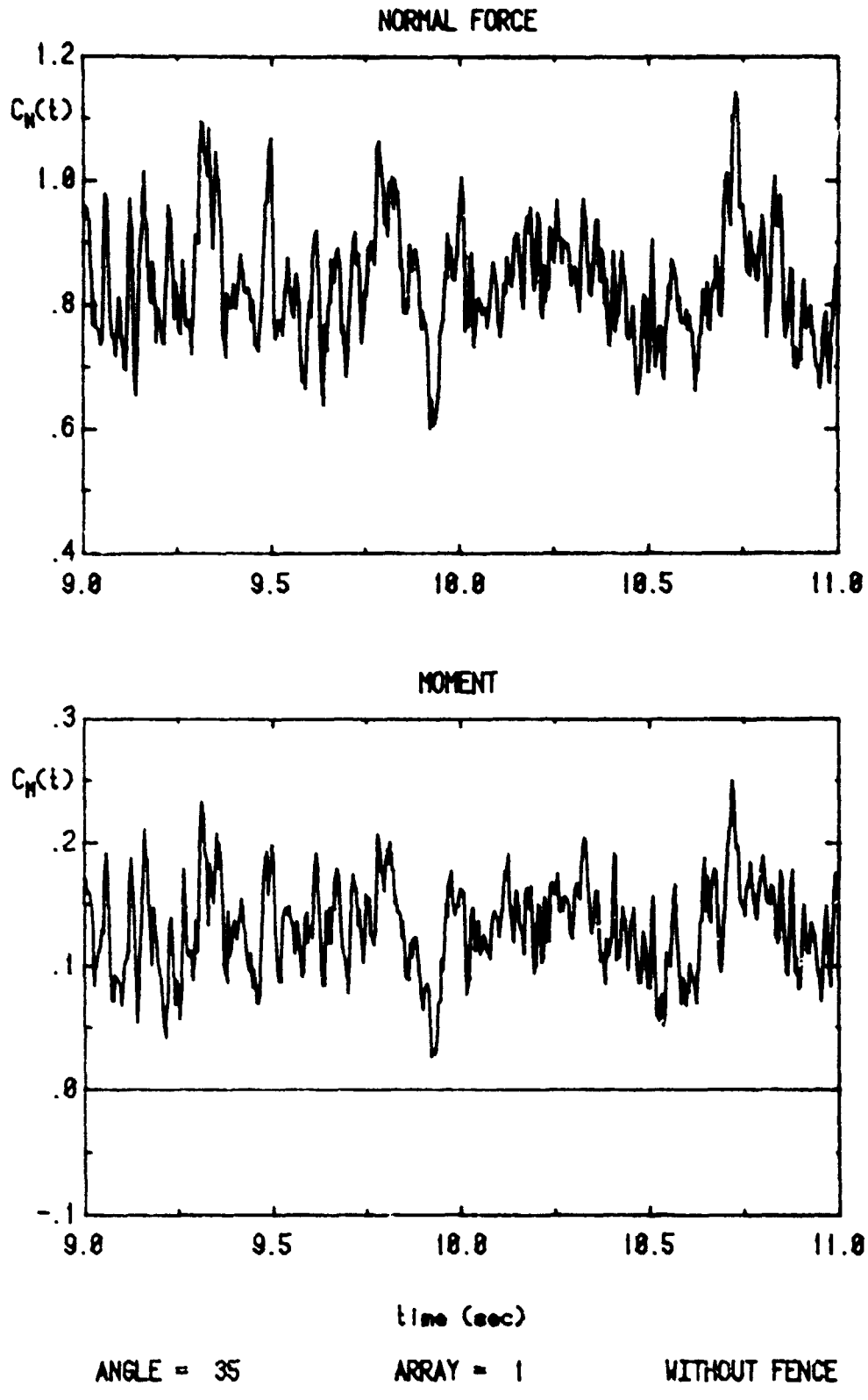

Figure 3. Time Trace of the Normal Force and Pitching Moment Coefficients

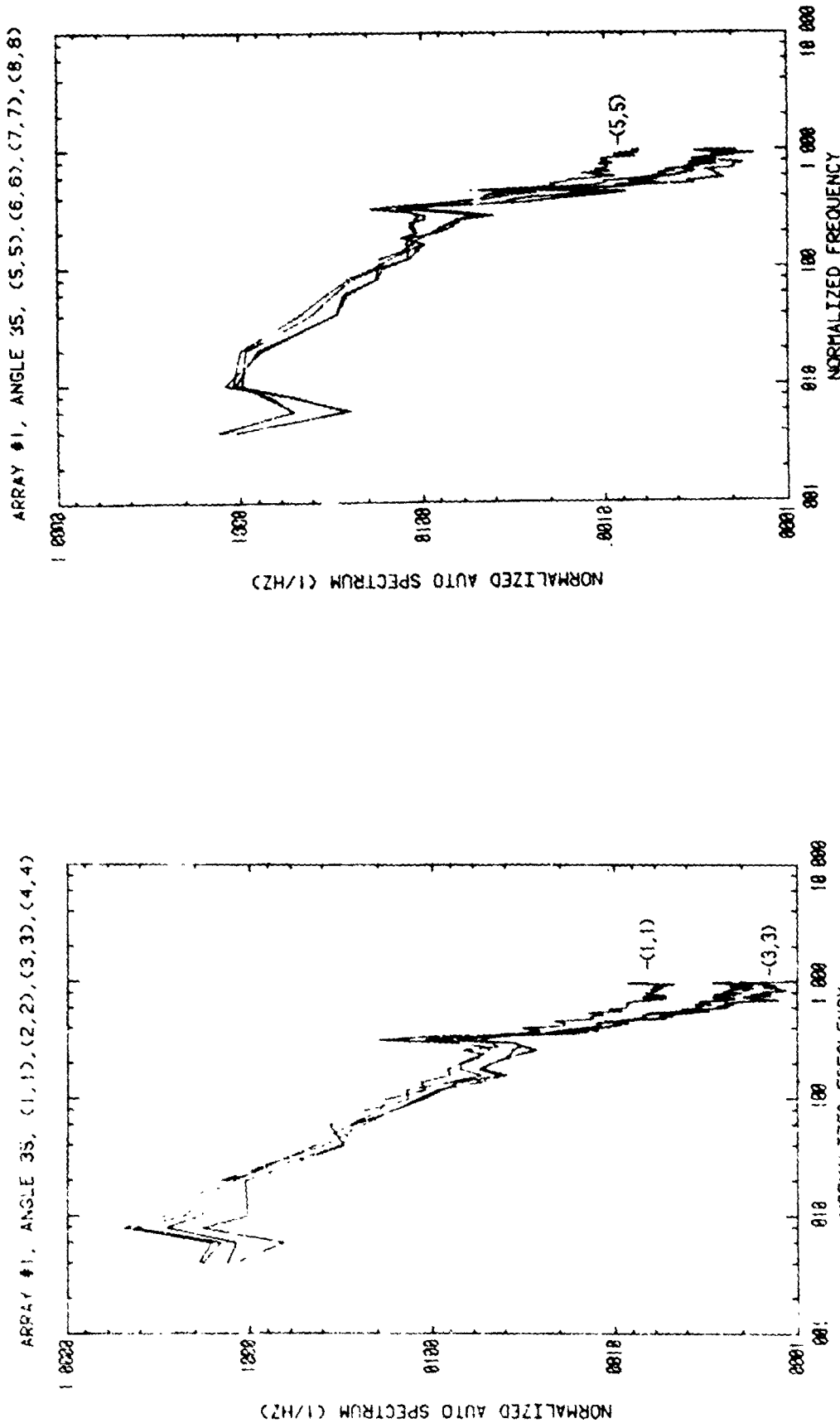

Figure 4. Auto-Spectra for First Array at $\alpha = 35°$, without Fence

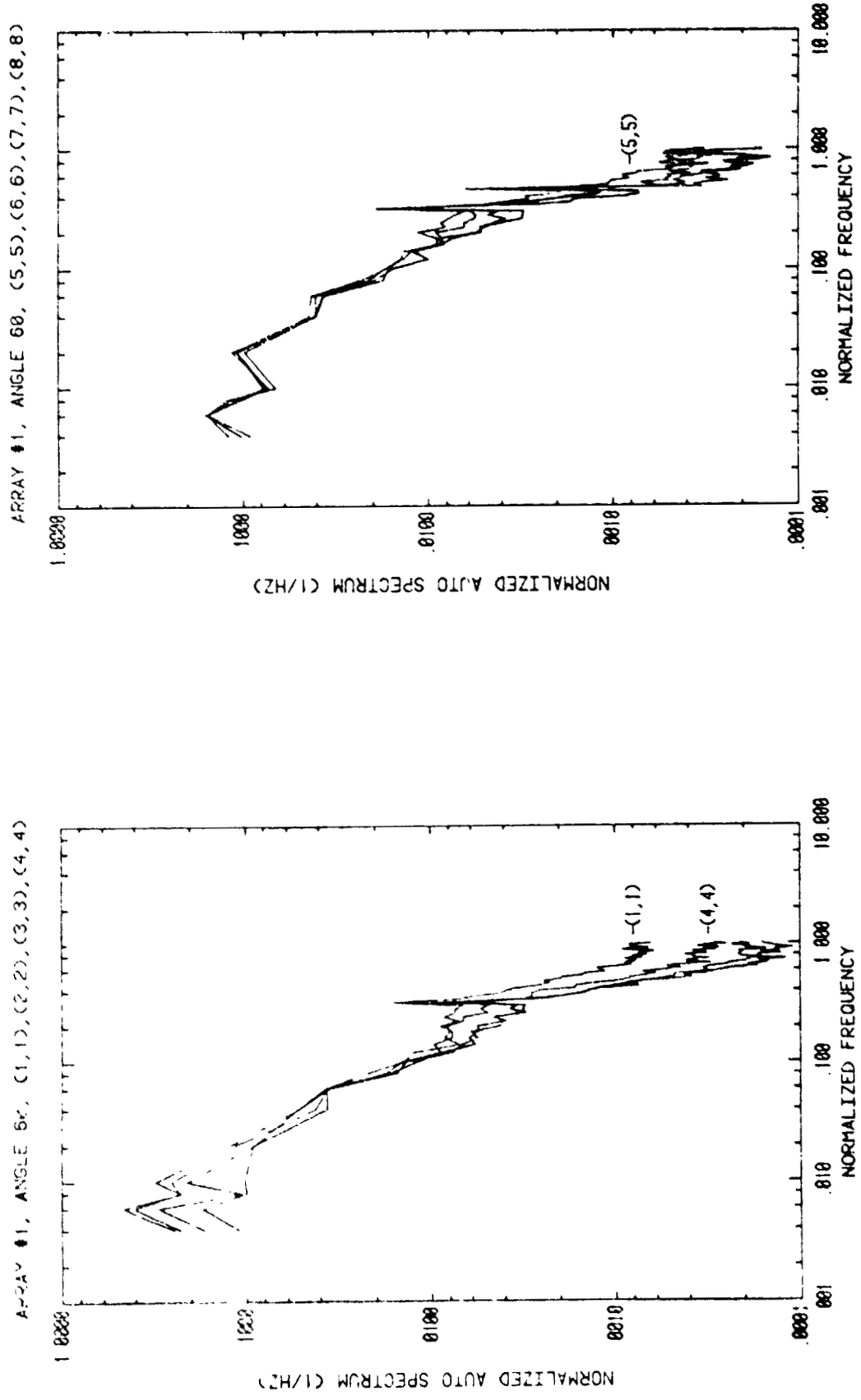

Figure 5. Auto-Spectra for First Array at $\alpha = 60°$, without Fence

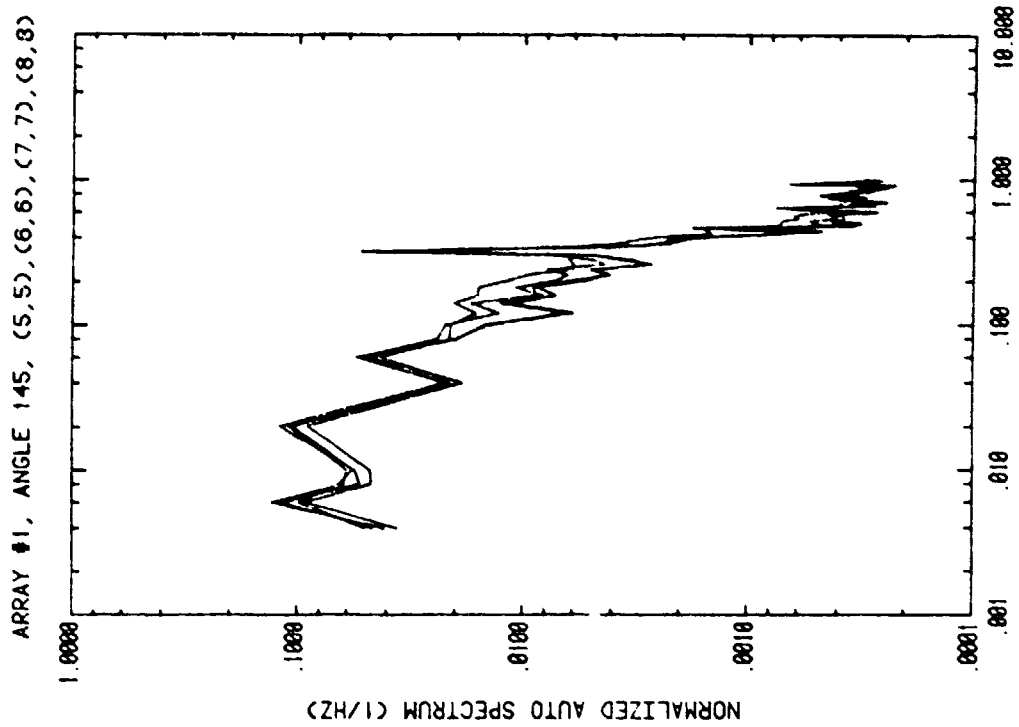

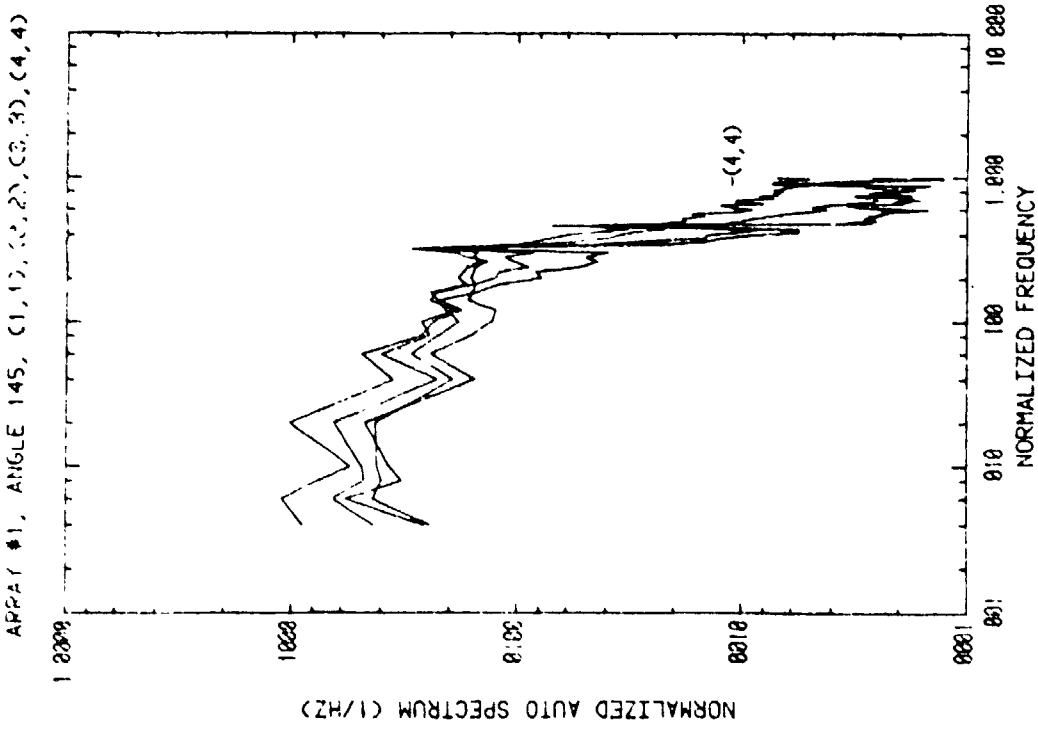

Figure 6. Auto-Spectra for First Array at α = 145°, with Fence

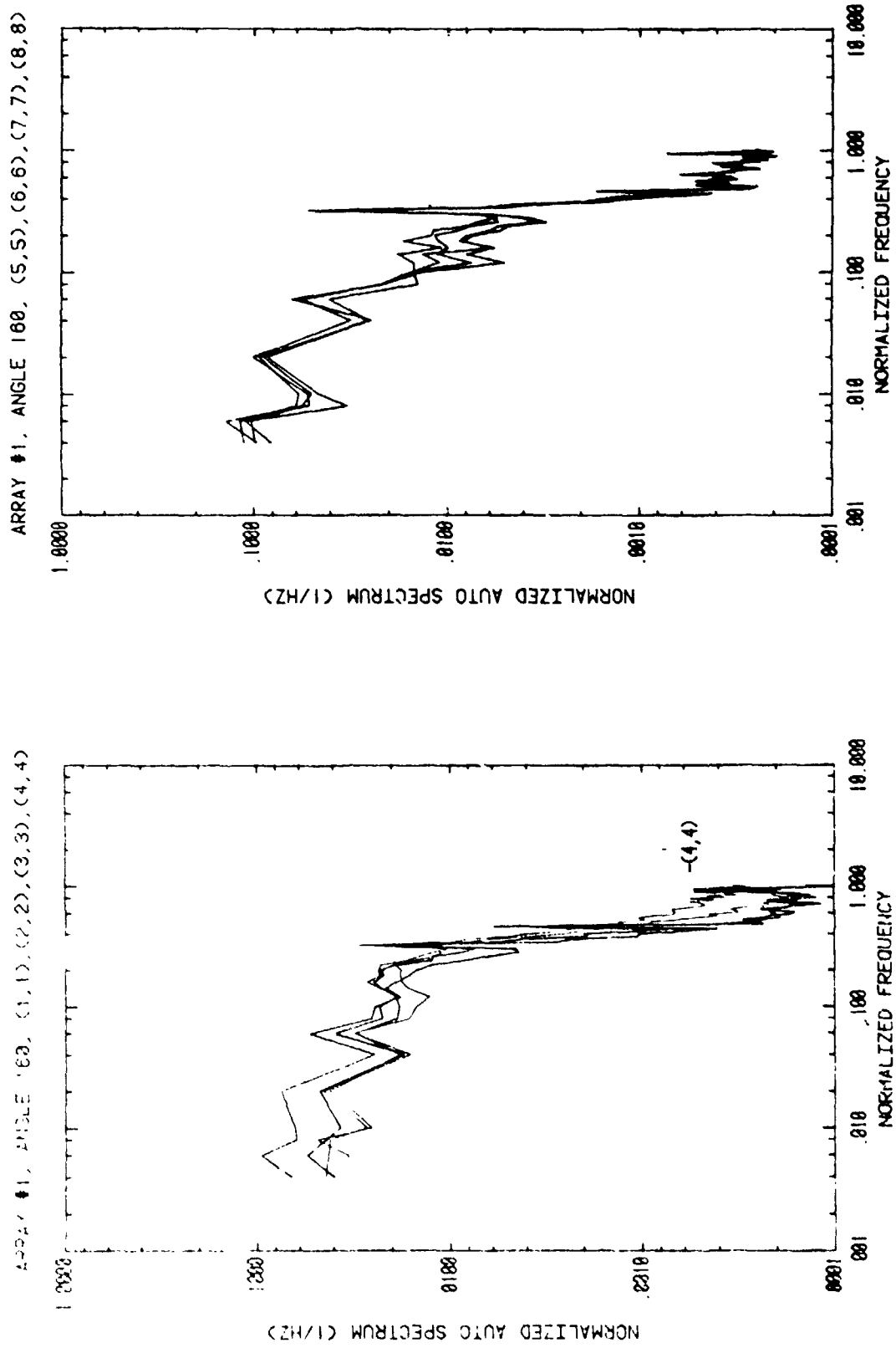

Figure 7. Auto-Spectra for First Array at $\alpha = 160°$, with Fence

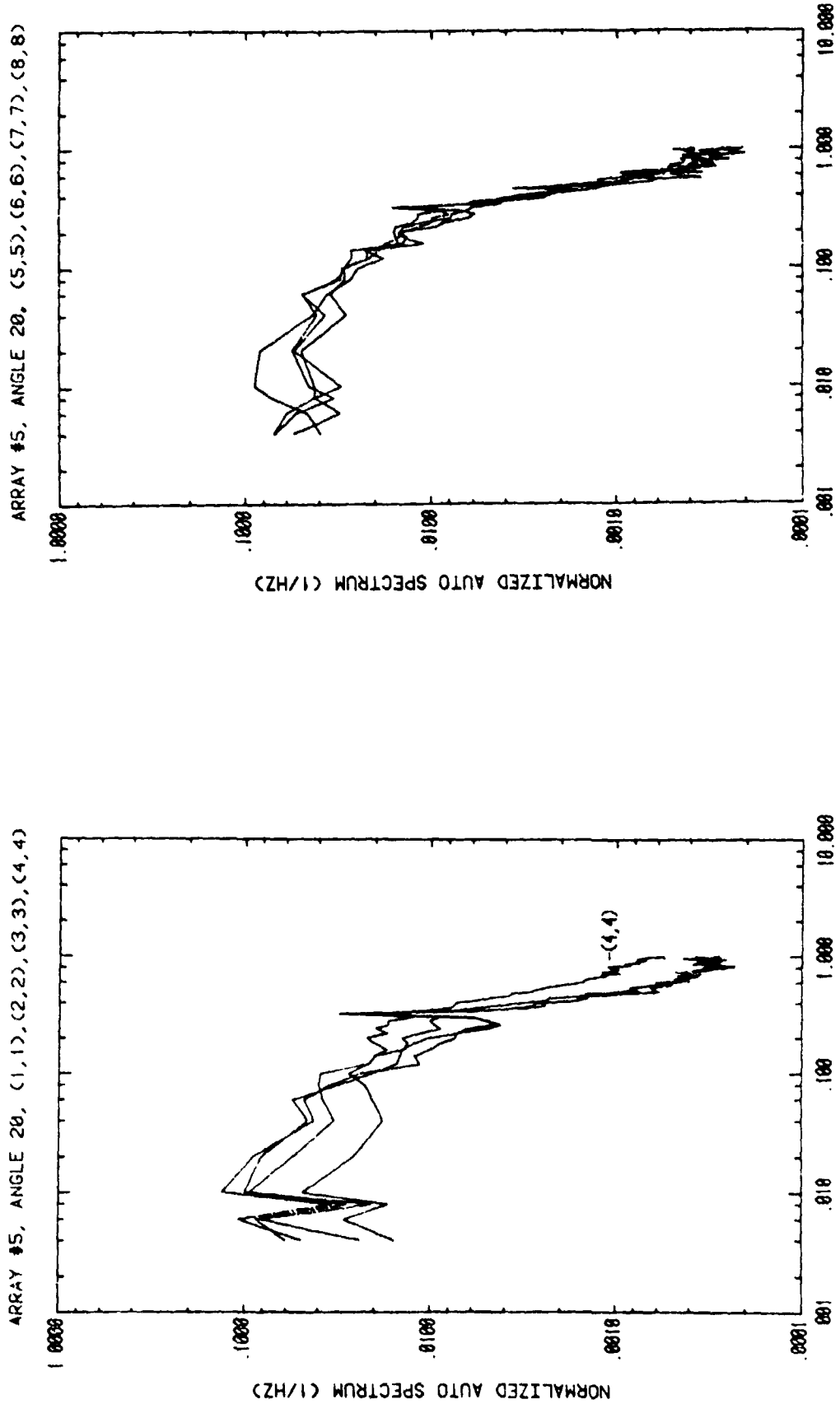

Figure 8. Auto-Spect a for Fifth Array at $\alpha = 20°$, without Fence

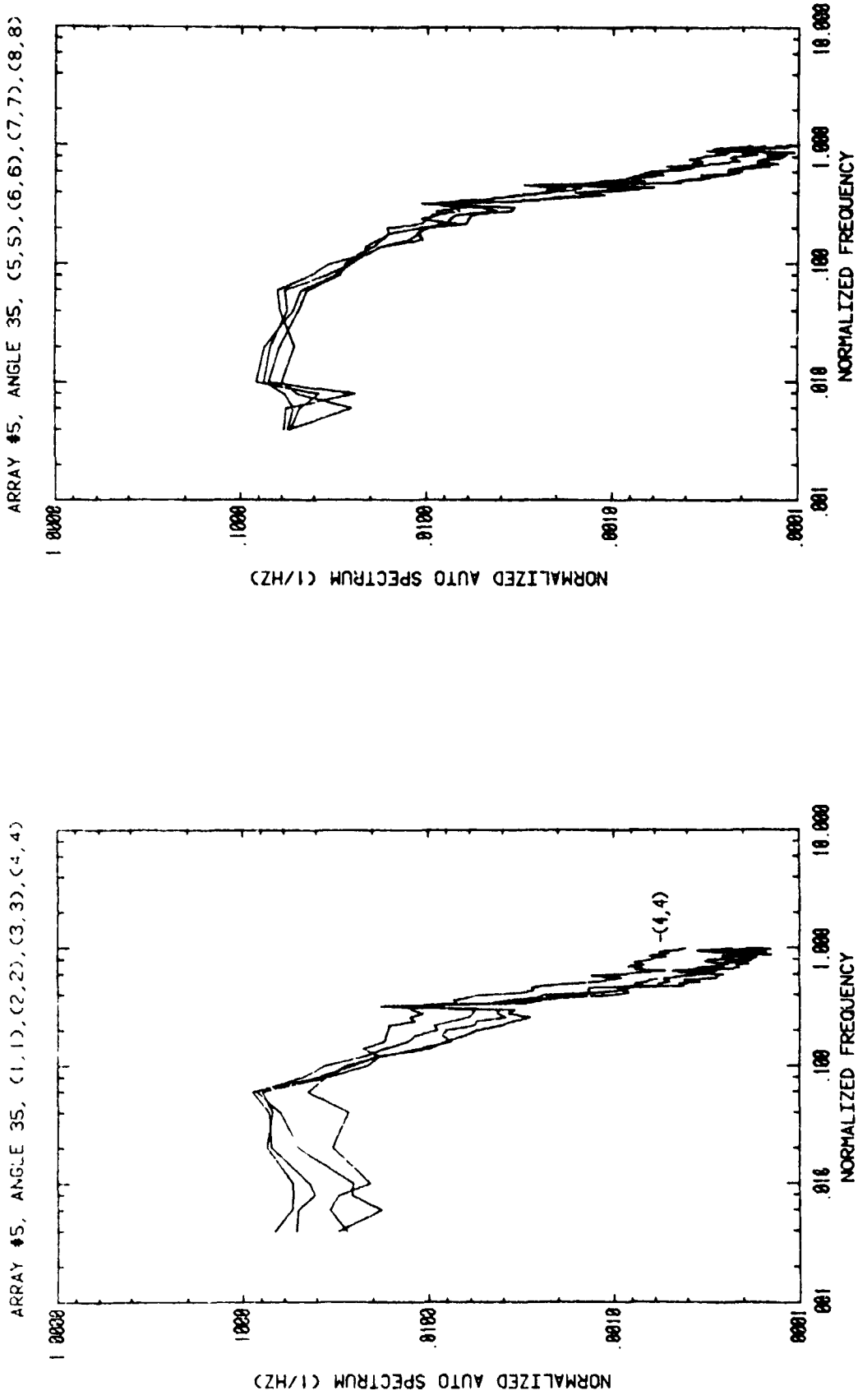

Figure 9. Auto-Spectra for Fifth Array at $\alpha = 35°$, without Fence

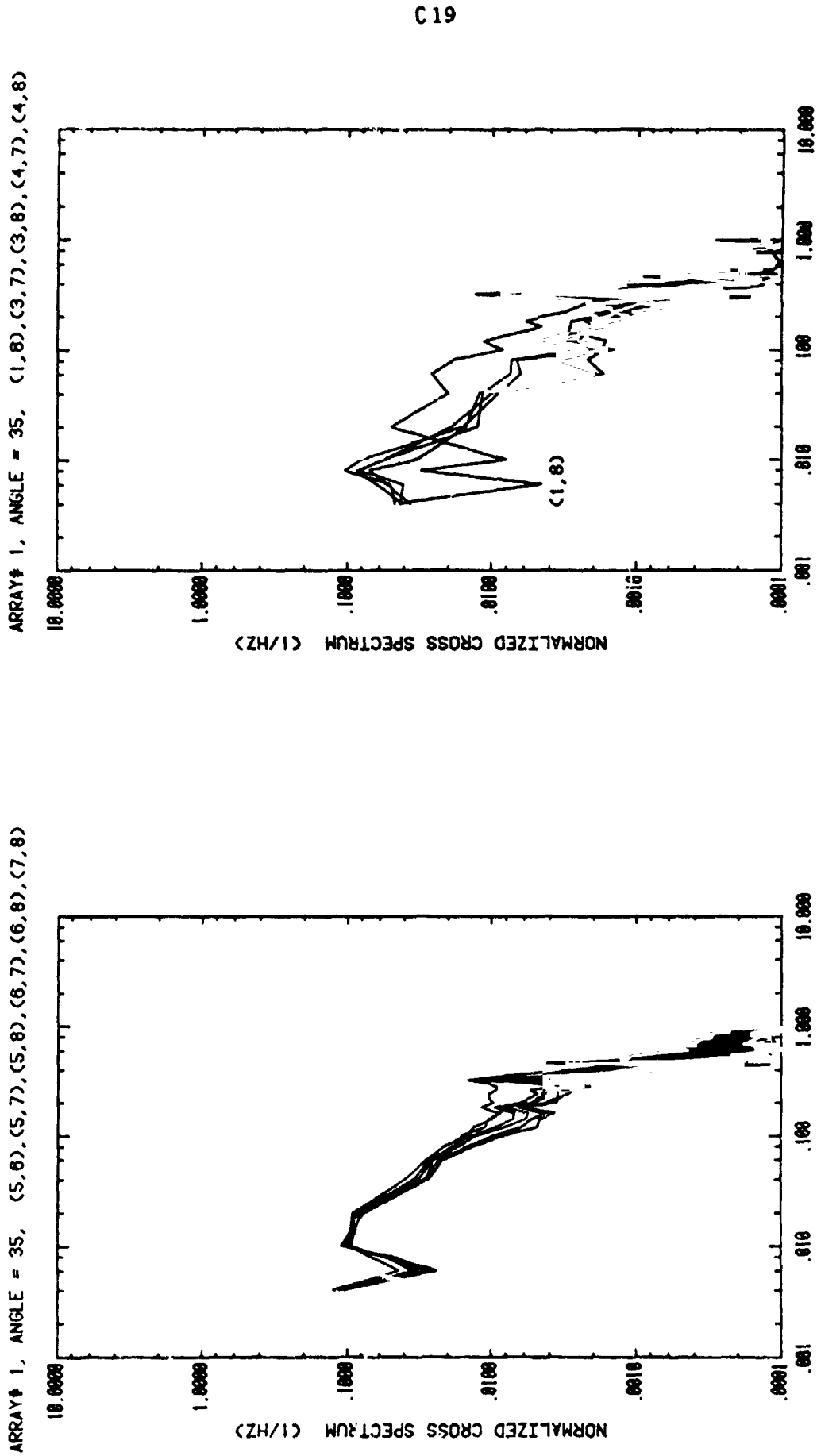

Figure 10. Cross-Spectra for First Array at $\alpha = 35°$, without Fence

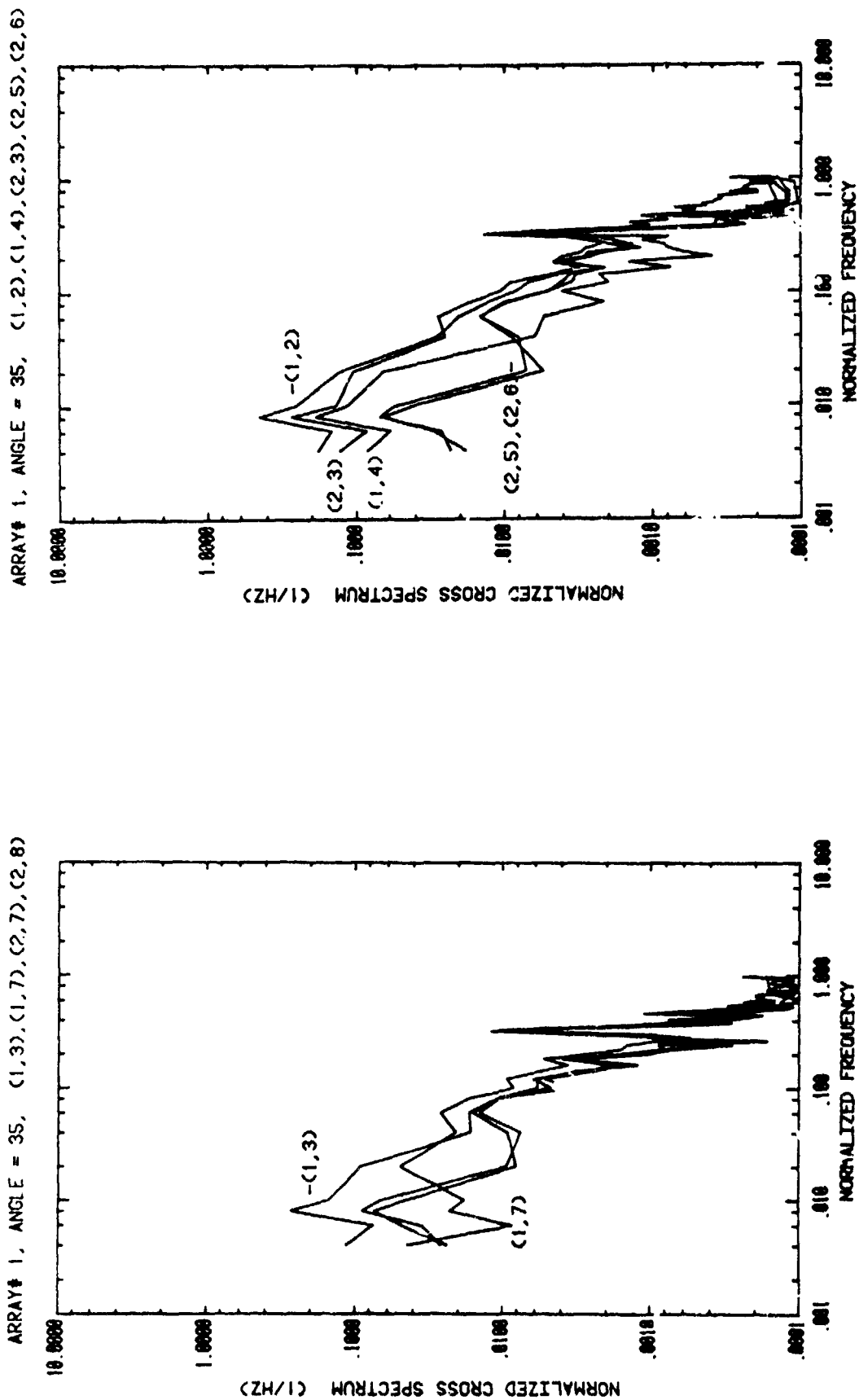

Figure 10. Cross-Spectra for First Array at $\alpha = 35°$, without Fence (continued)

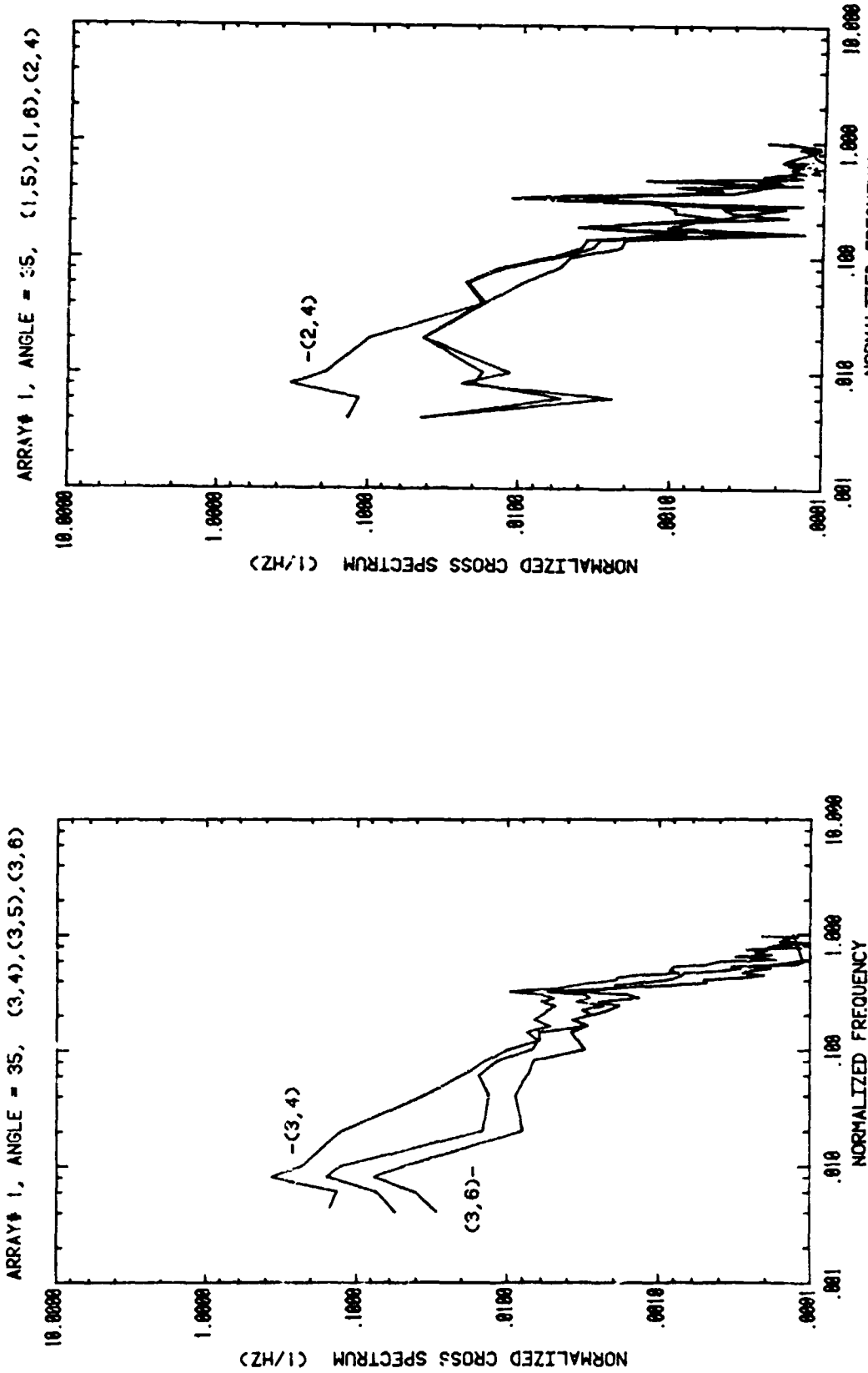

Figure 10. Cross-Spectra for First Array at $\alpha = 35°$, without Fence (continued)

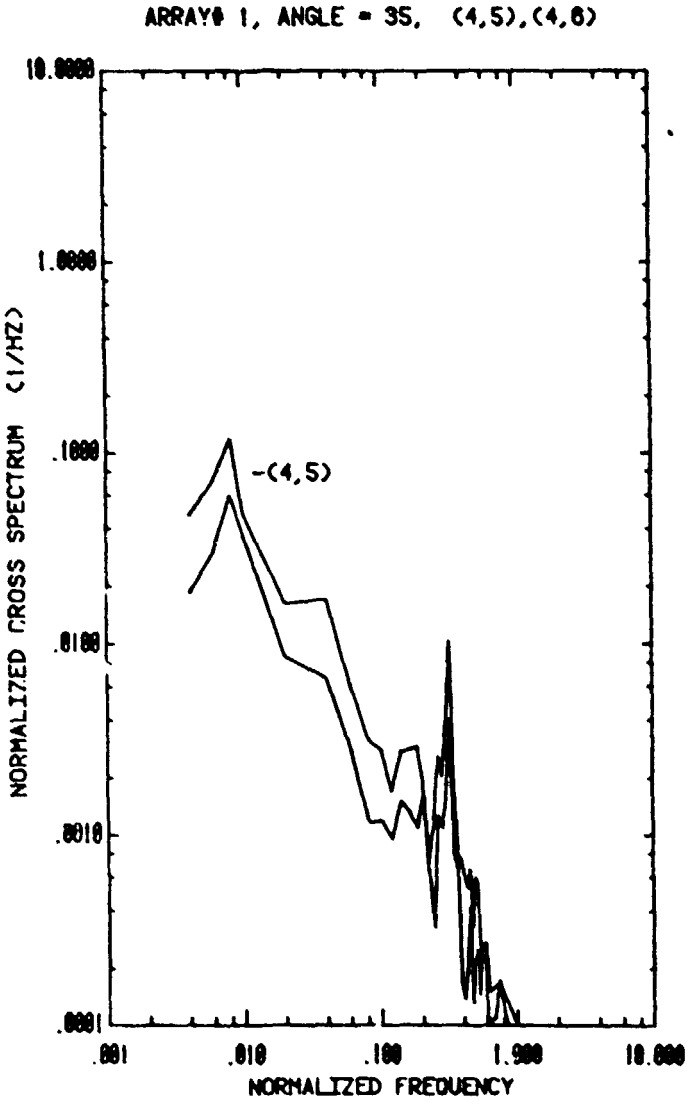

Figure 10. Cross-Spectra for First Array at $\alpha = 35°$, without Fence (concluded)

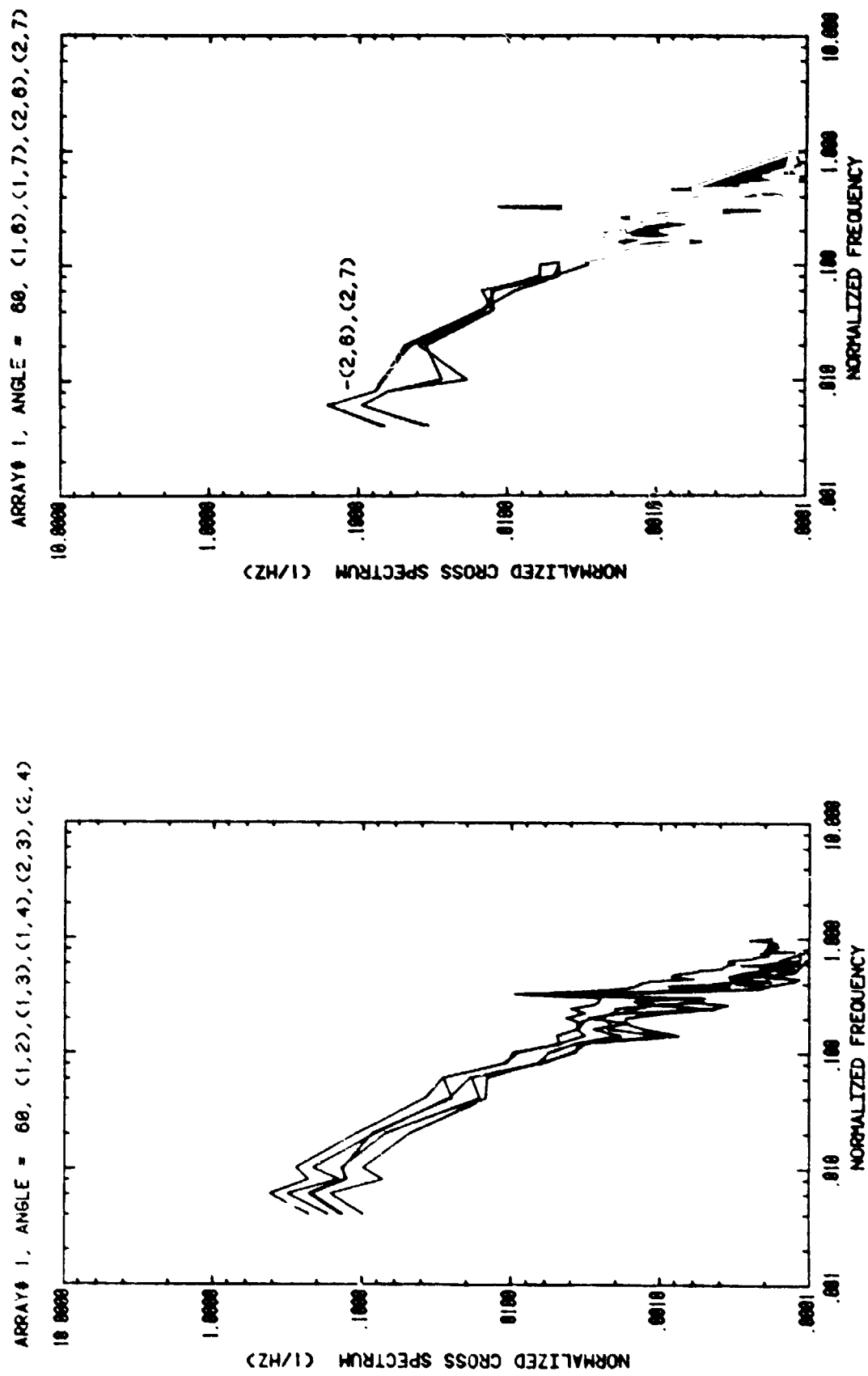

Figure 11. Cross-Spectra for First Array at γ = 60°, without Fence

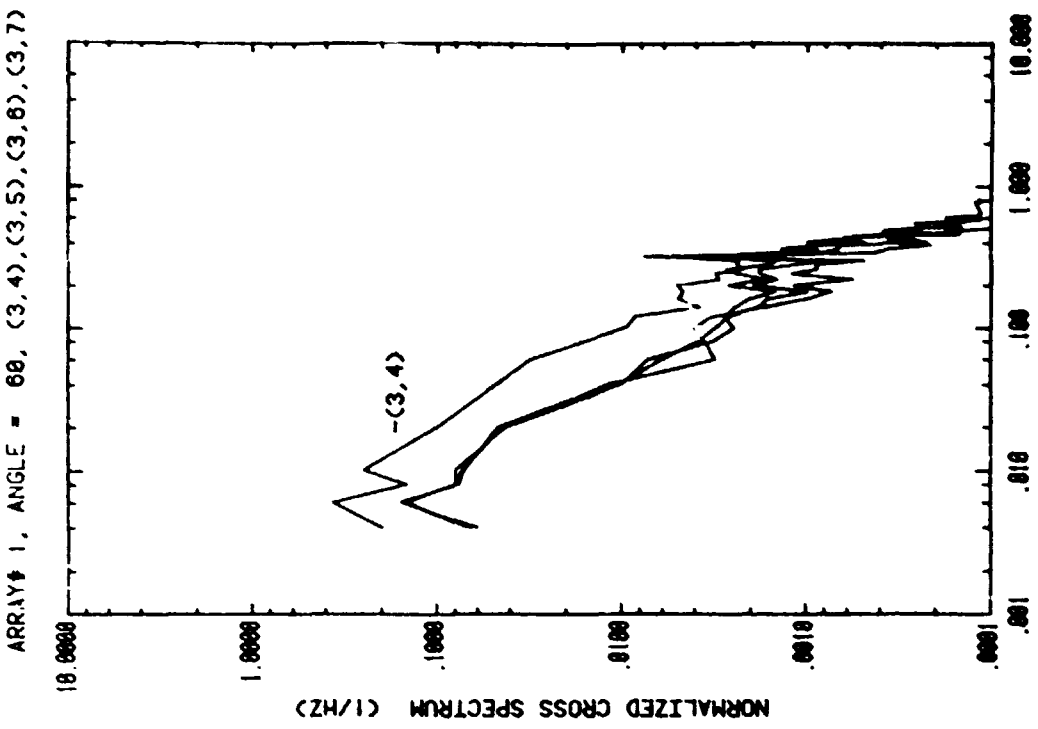

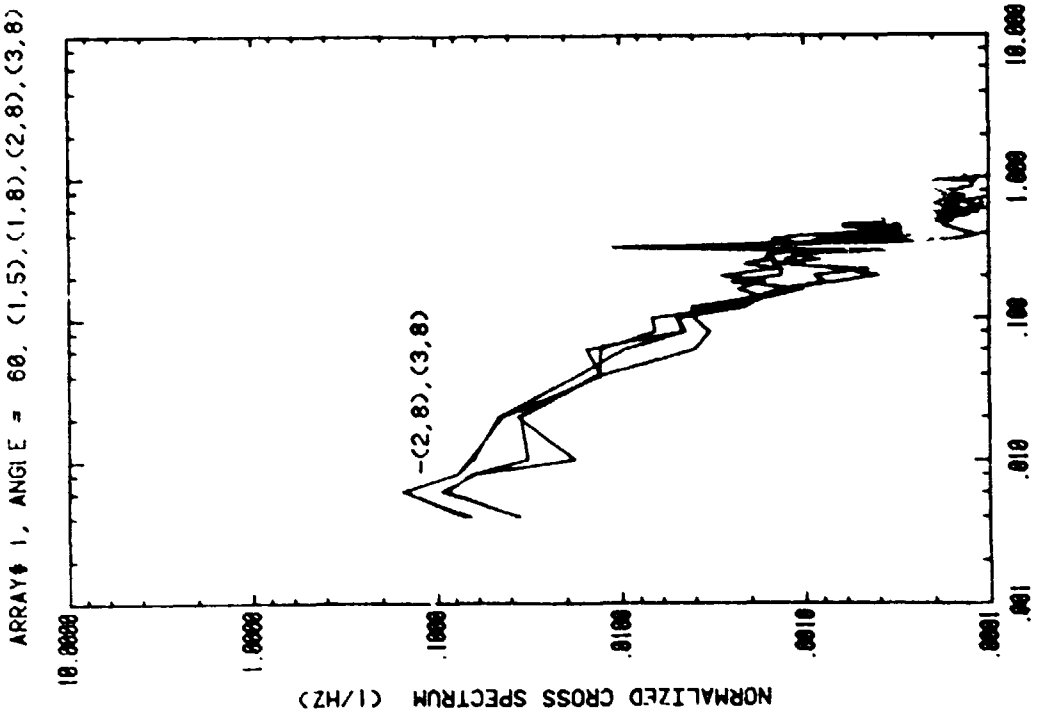

Figure 11. Cross-Spectra for First Array at $\alpha = 60°$, without Fence (continued)

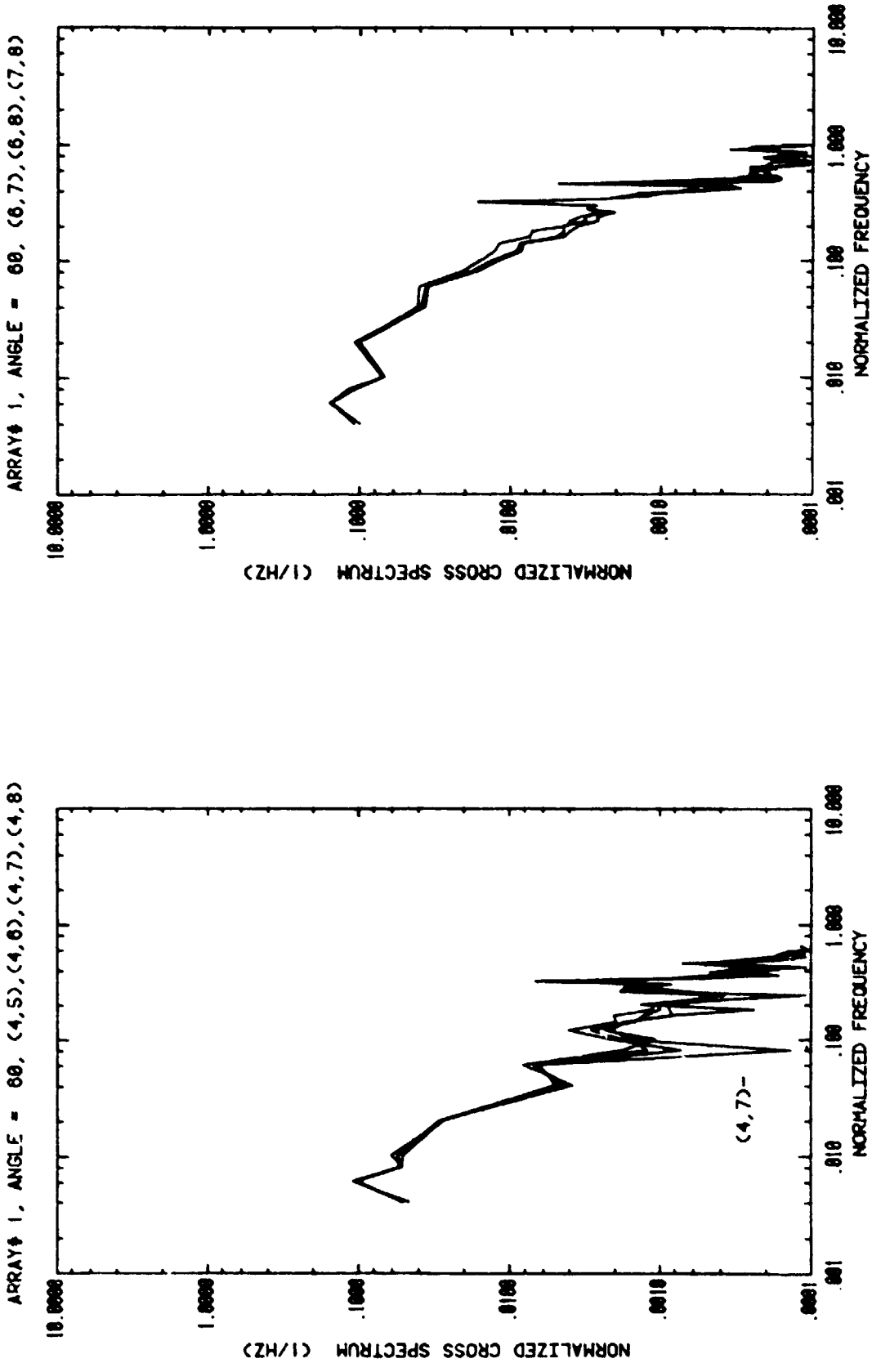

Figure 11. Cross-Spectra for First Array at $\alpha = 60°$, without Fence (continued)

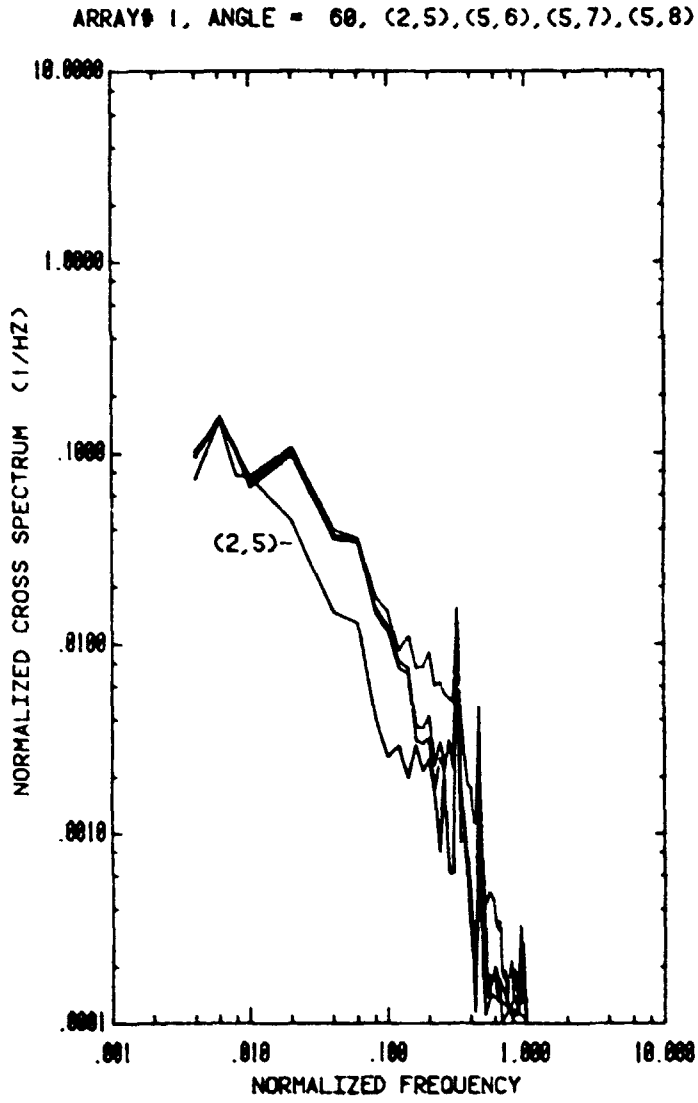

Figure 11. Cross-Spectra for First Array at $\alpha = 60°$, without Fence (concluded)

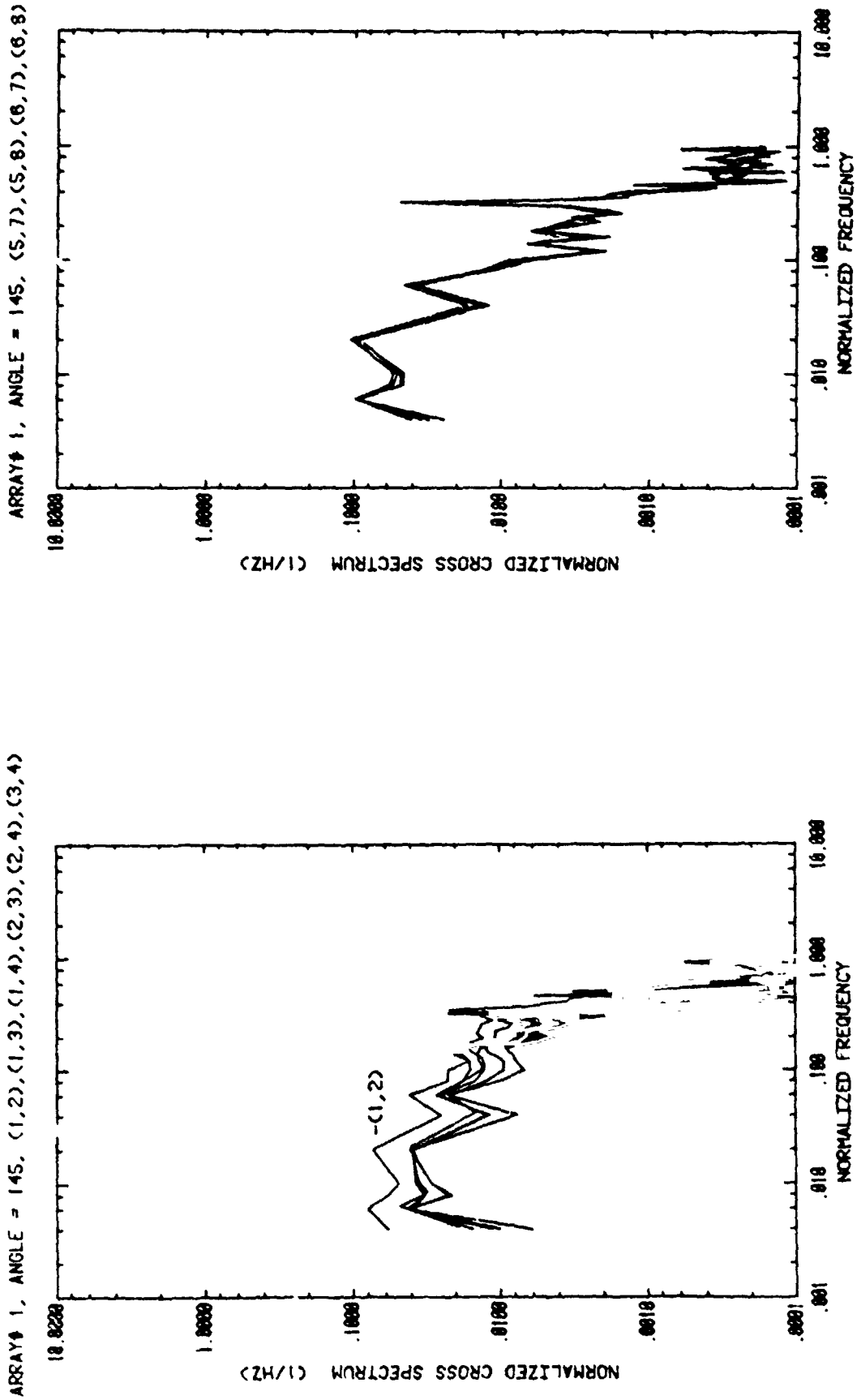

Figure 12. Cross-Spectra for First Array at $\alpha = 145°$, with Fence

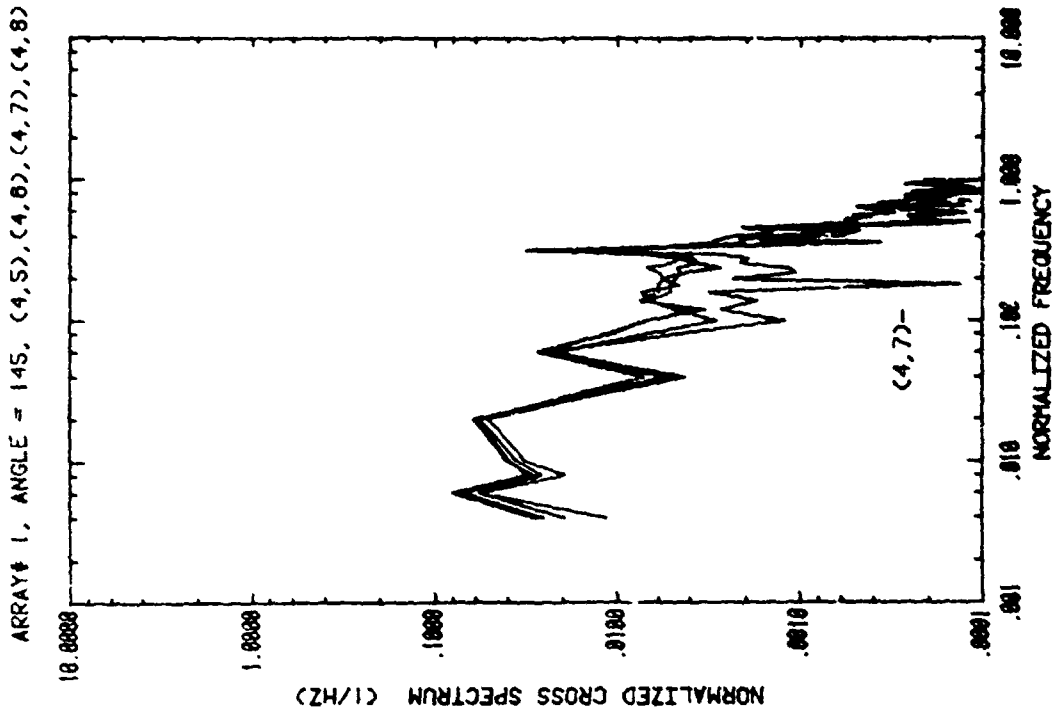

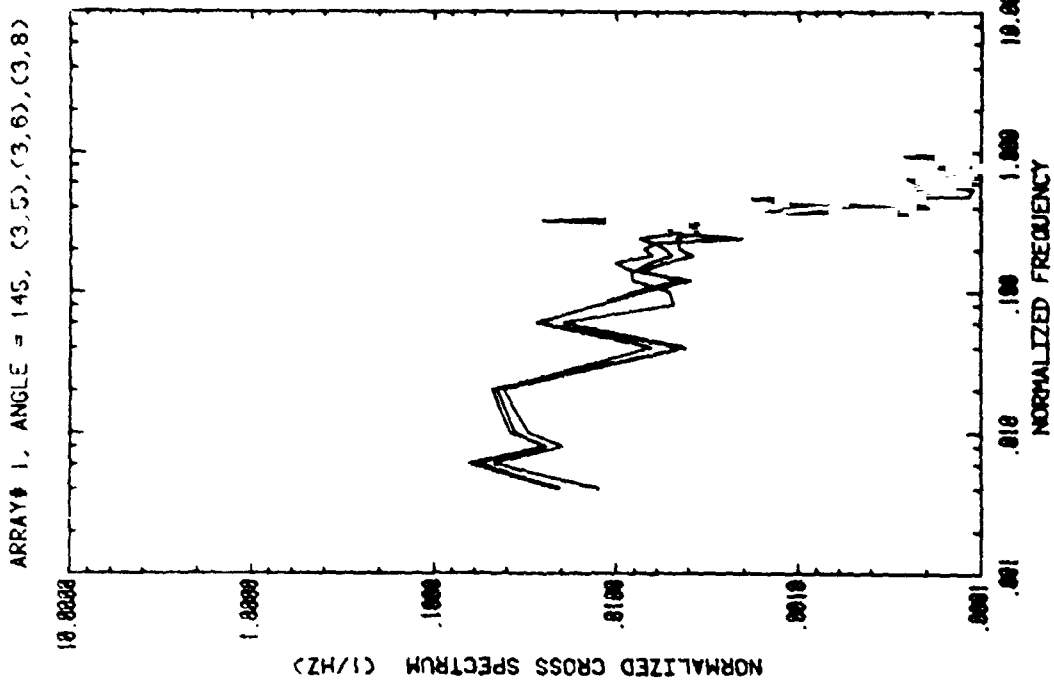

Figure 12. Cross-Spectra for First Array at α = 145°, with Fence (continued)

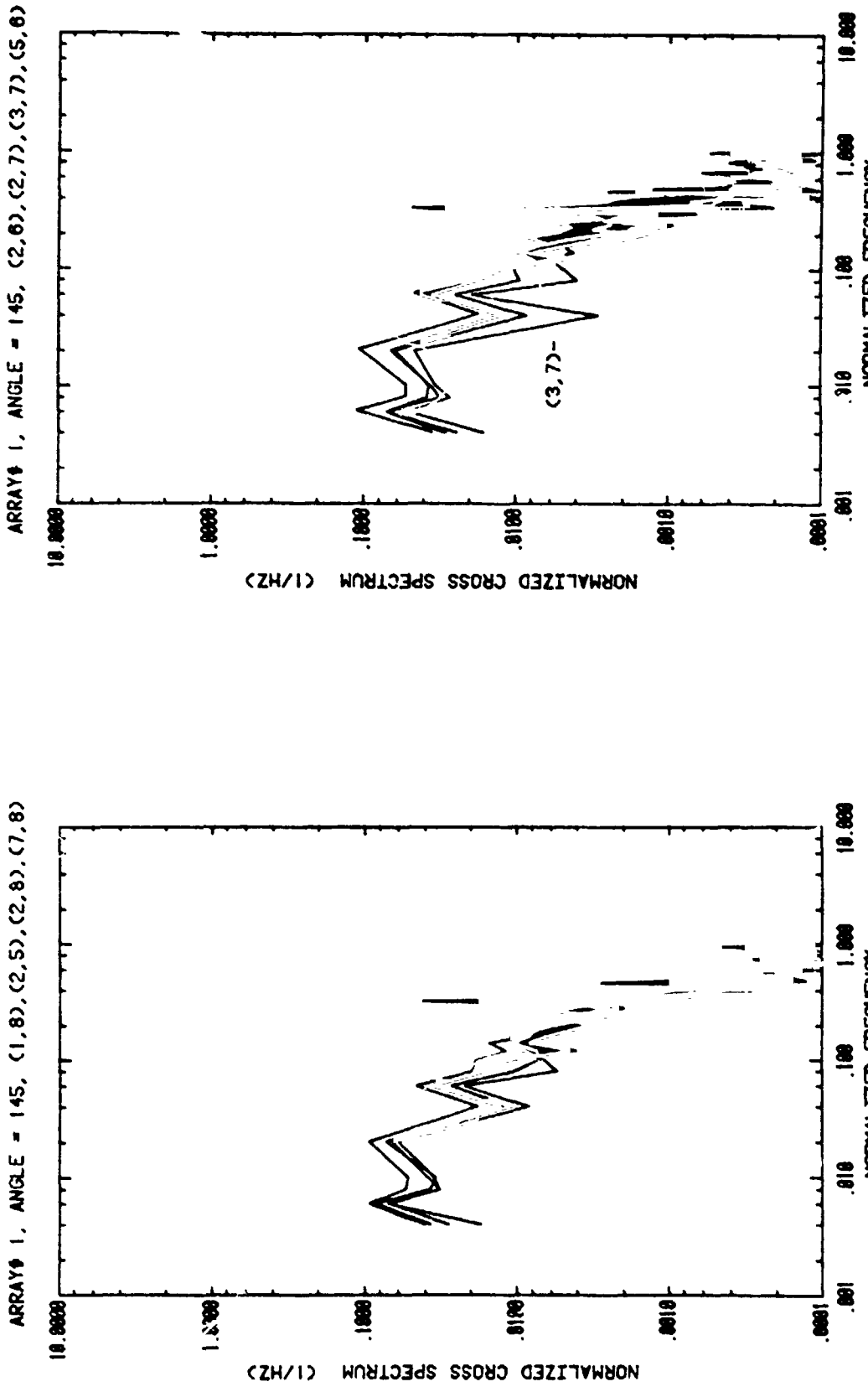

Figure 12. Cross-Spectra for First Array at α = 145°, with Fence (continued)

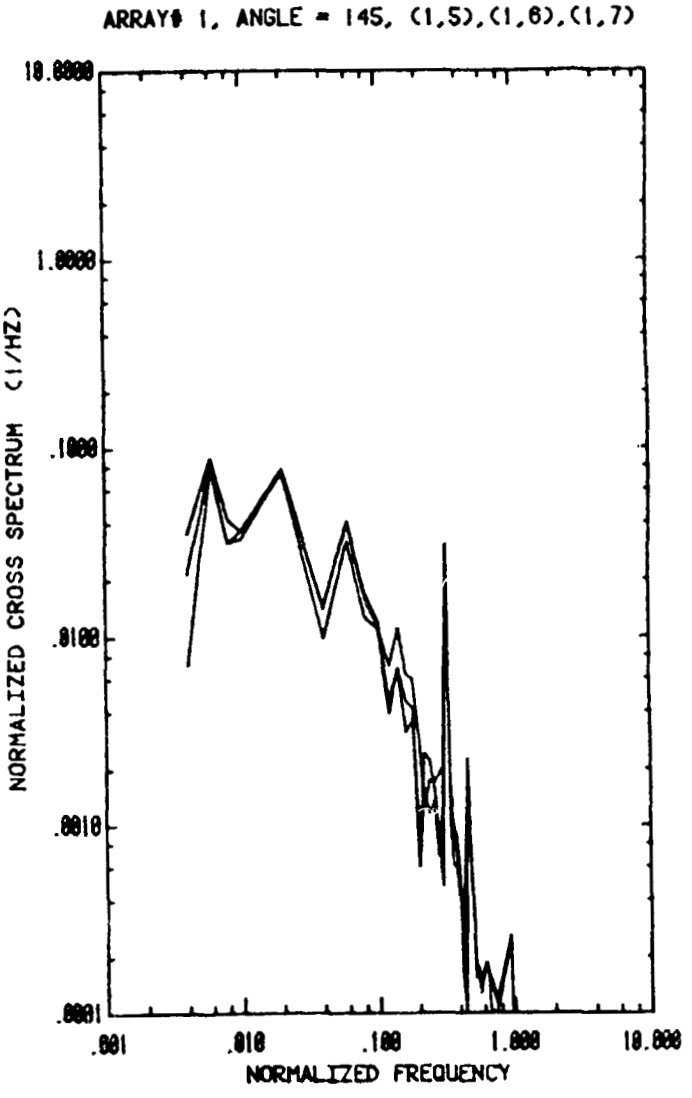

Figure 12. Cross-Spectra for First Array at $\alpha = 145°$, with Fence (concluded)

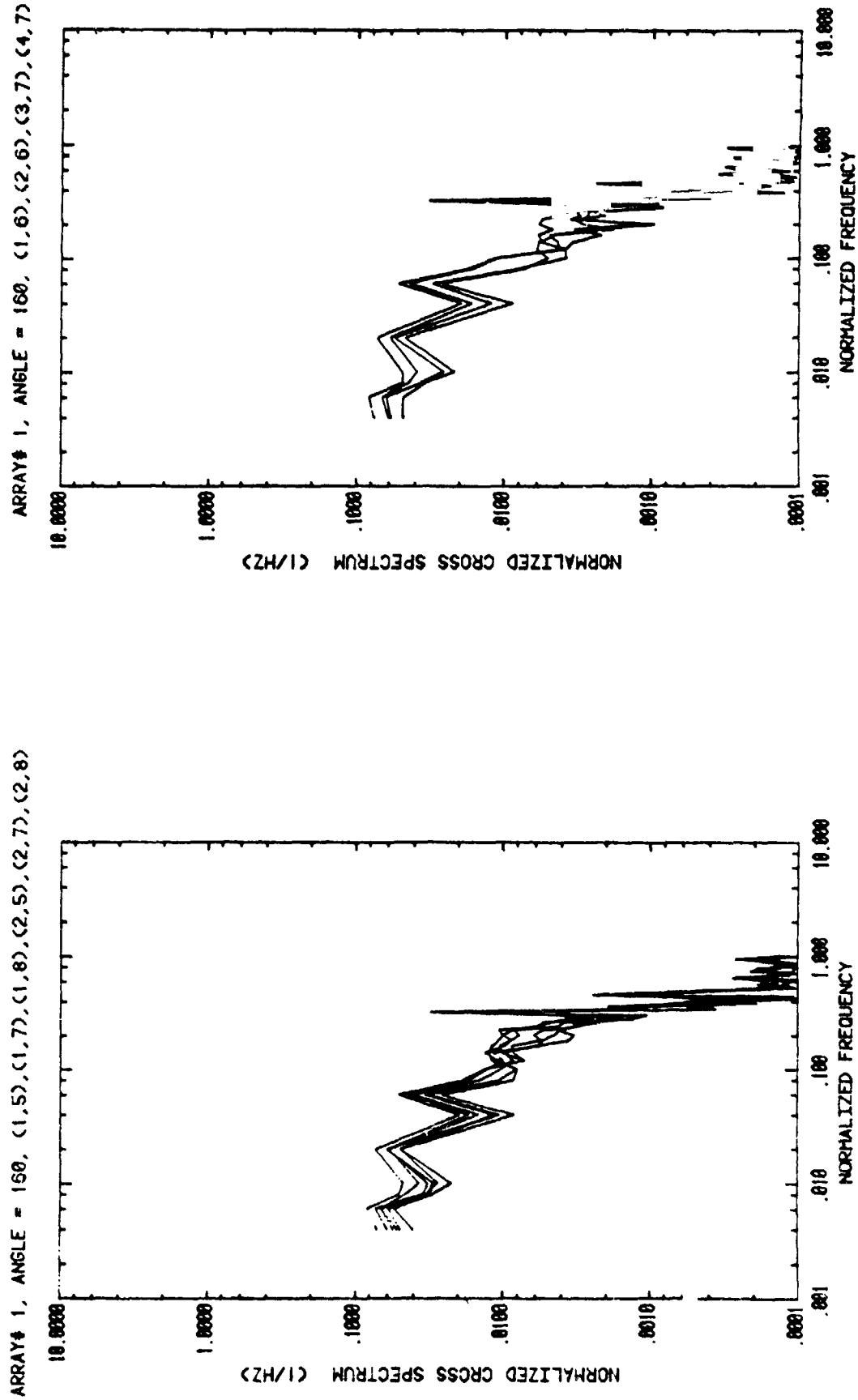

Figure 13. Cross-Spectra for First Array at $\alpha = 160°$, with Fence

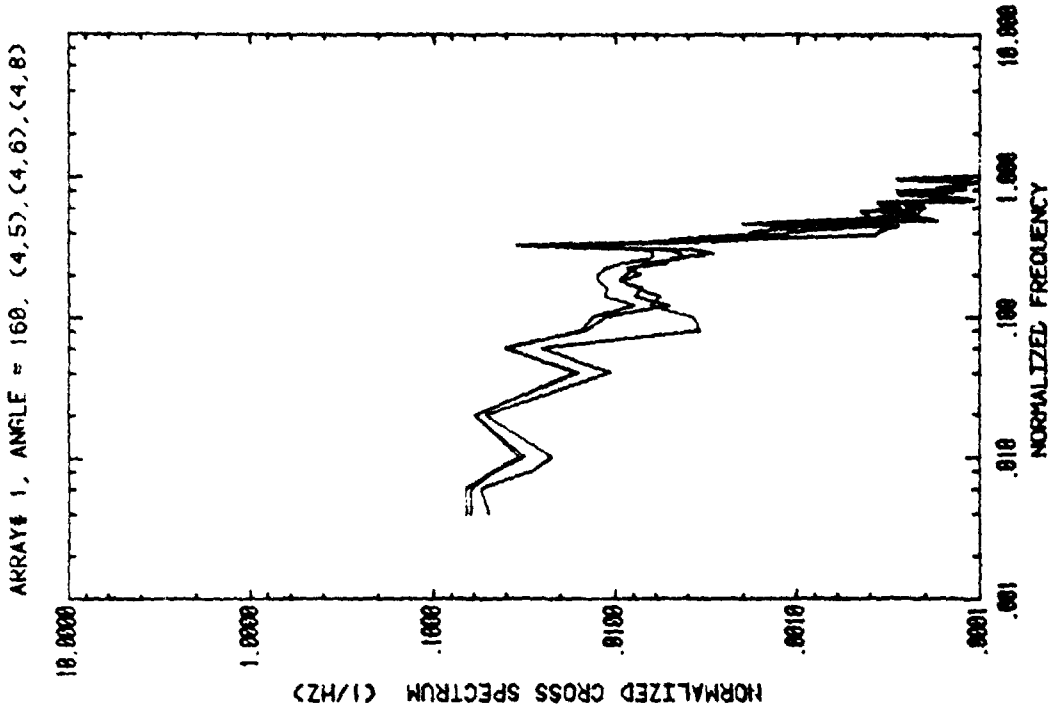

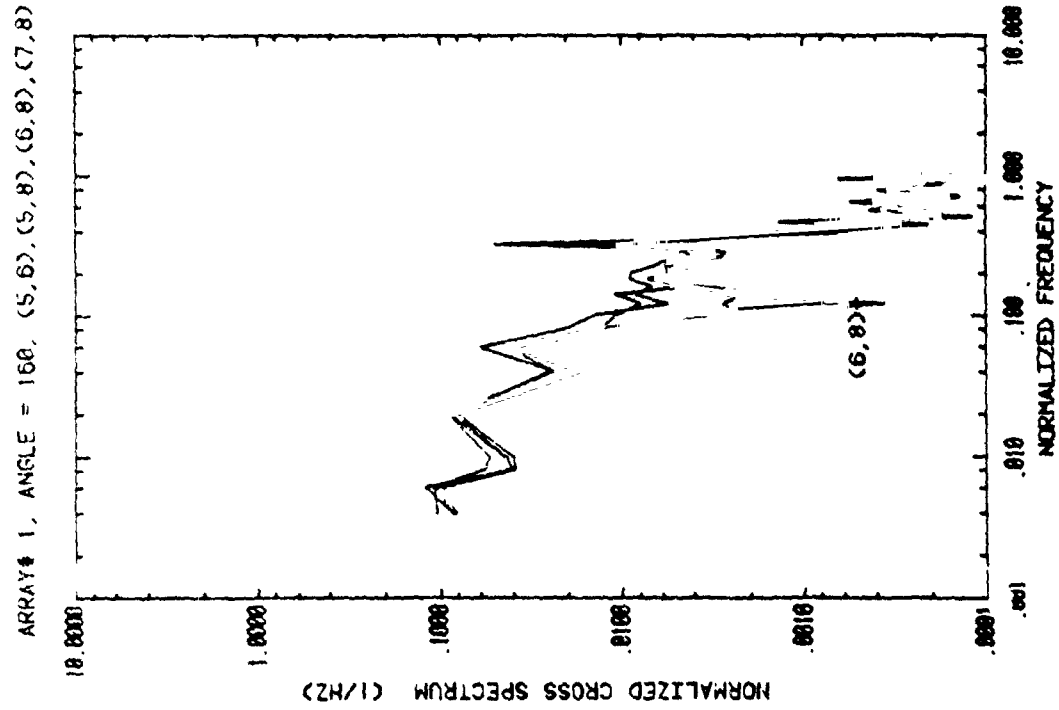

Figure 13. Cross-Spectra for First Array at $\alpha = 160°$, with Fence (continued)

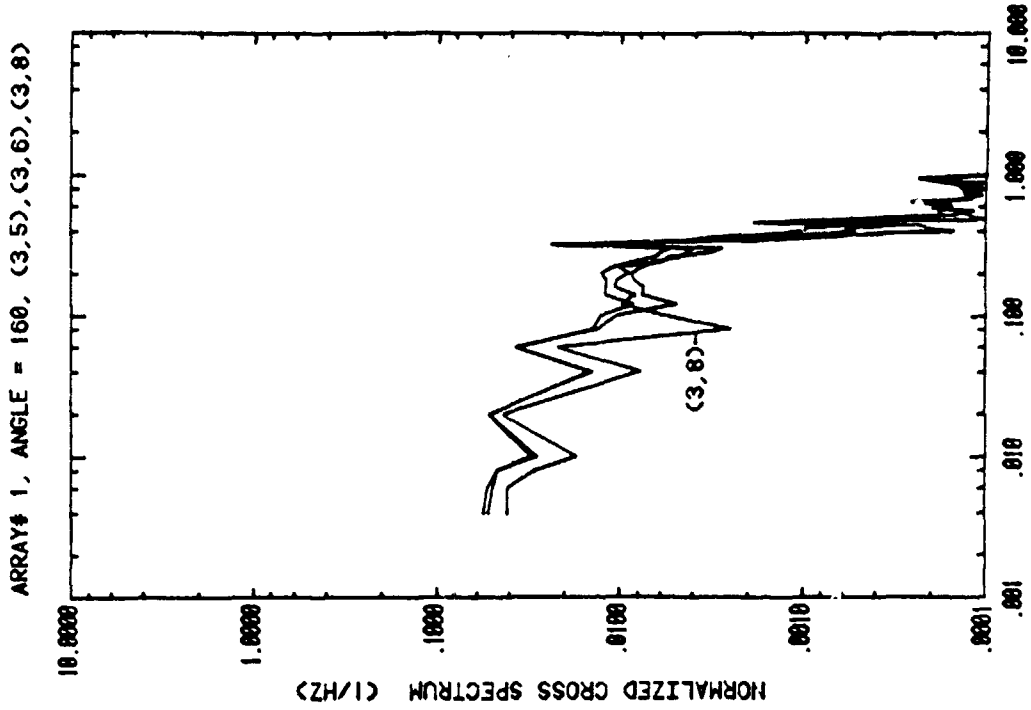

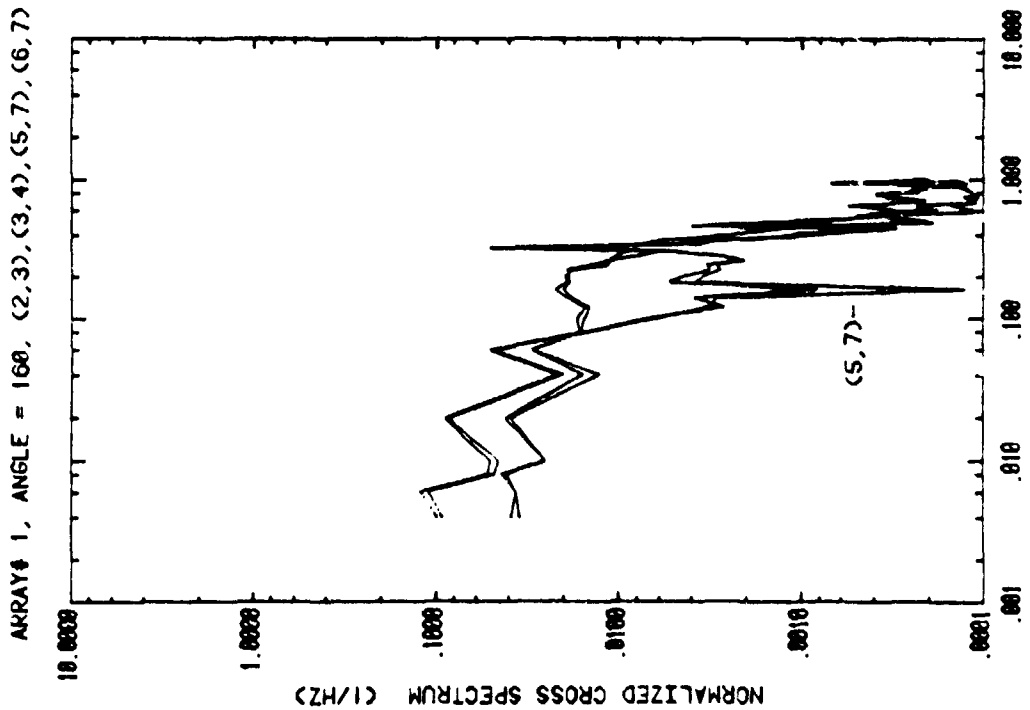

Figure 13. Cross-Spectra for First Array at $\alpha = 160°$, with Fence (continued)

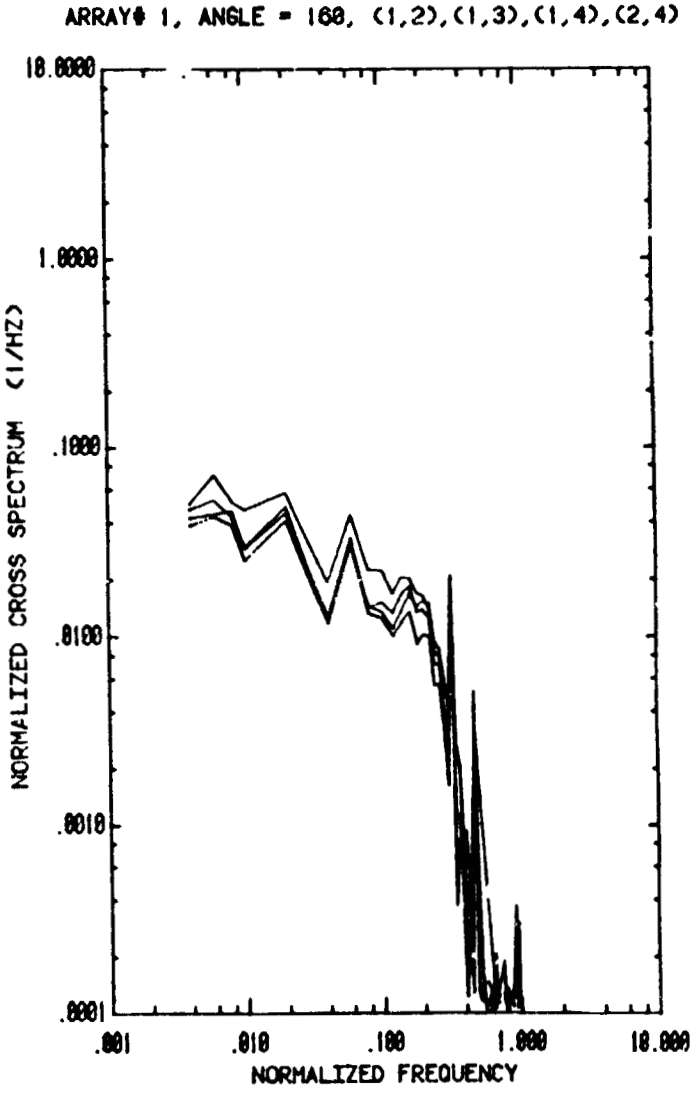

Figure 13. Cross-Spectra for First Array at $\alpha = 160°$, with Fence (concluded)

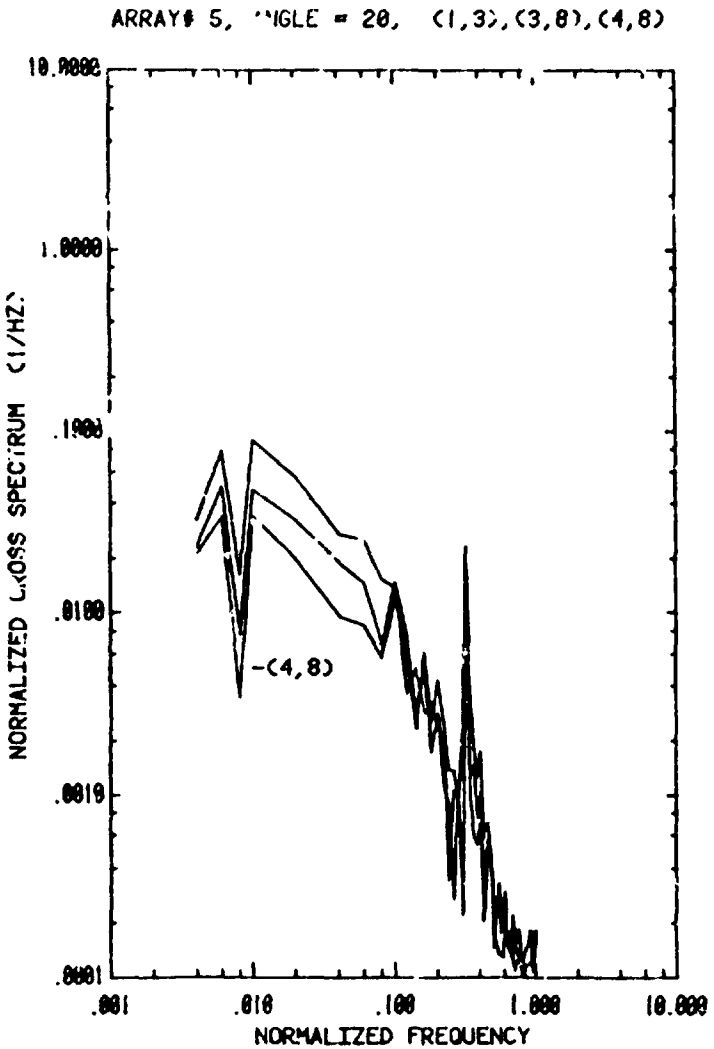

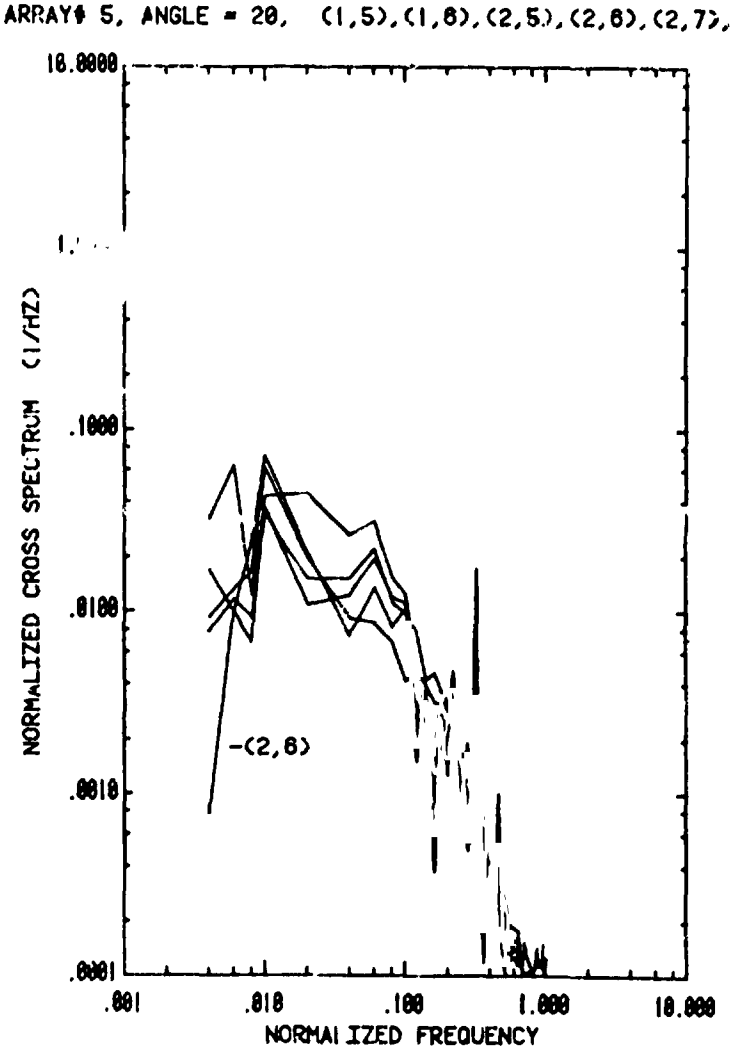

Figure 14. Cross-Spectra fo. ifth Array at α = 20°, without Fence

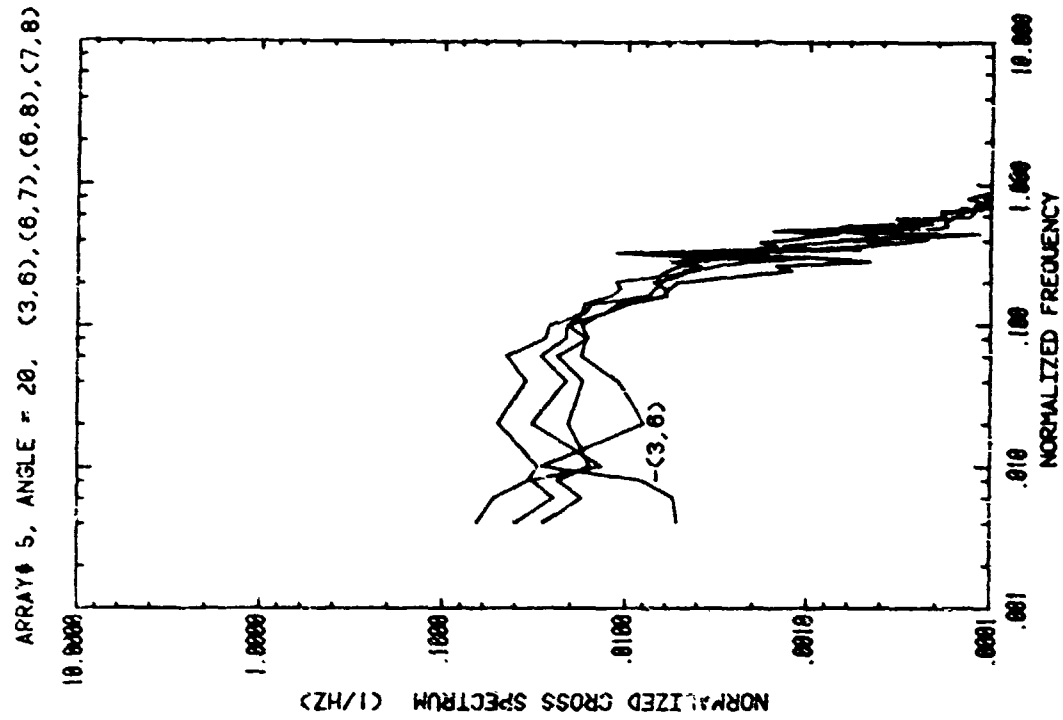

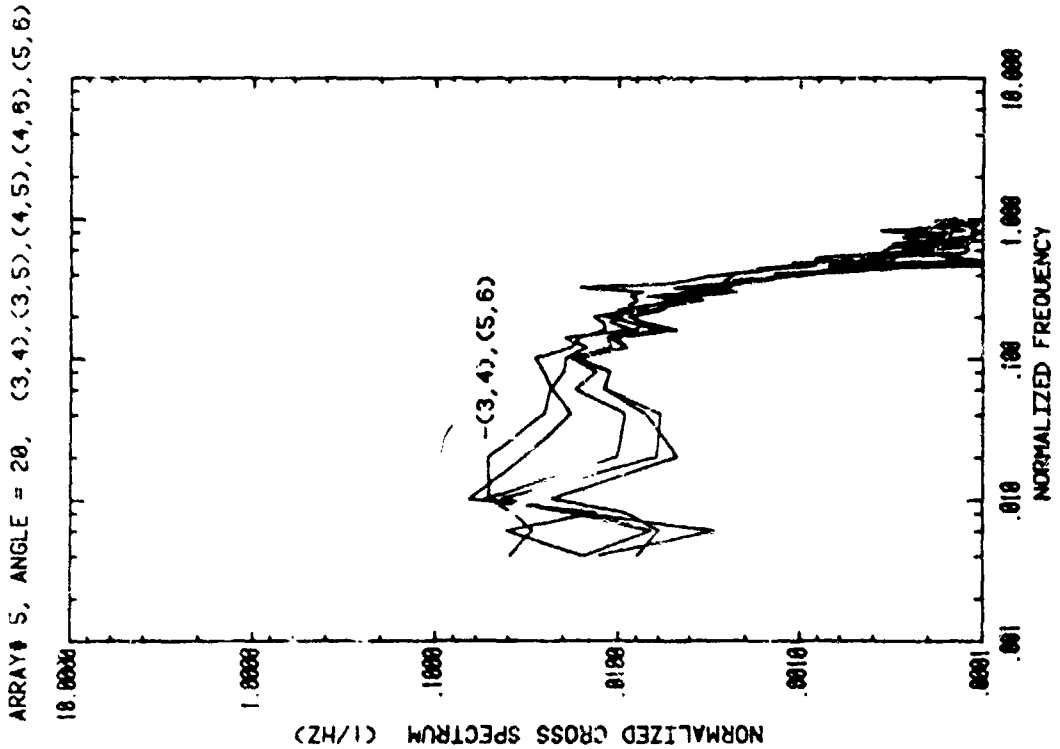

Figure 14. Cross-Spectra for Fifth Array at $\alpha = 20°$, without Fence (continued)

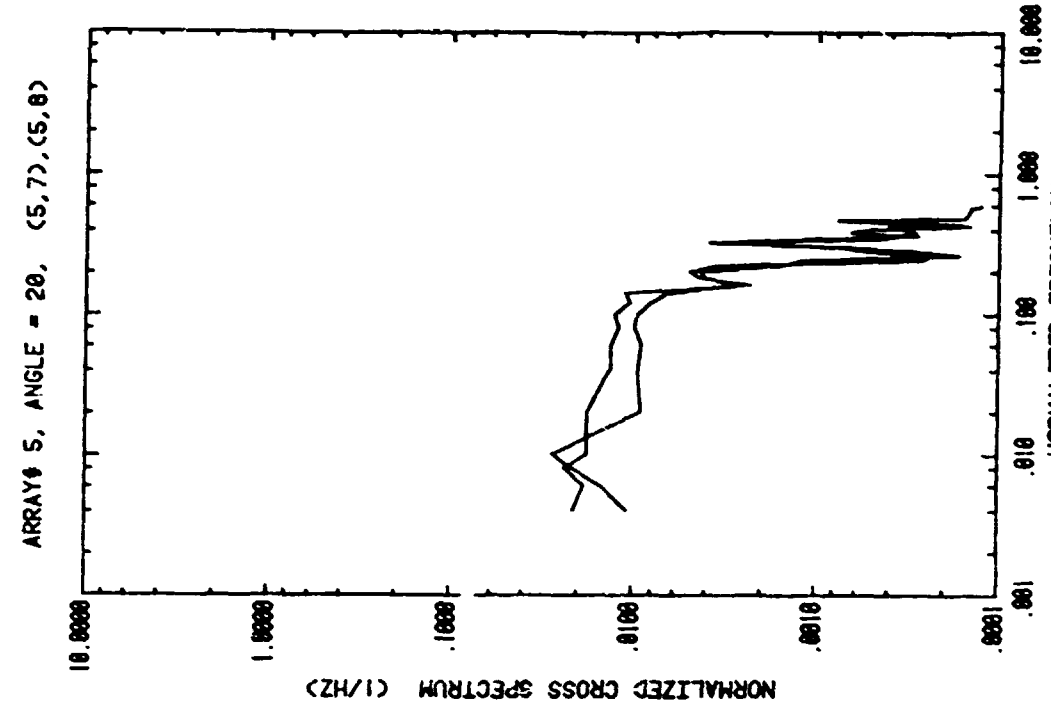

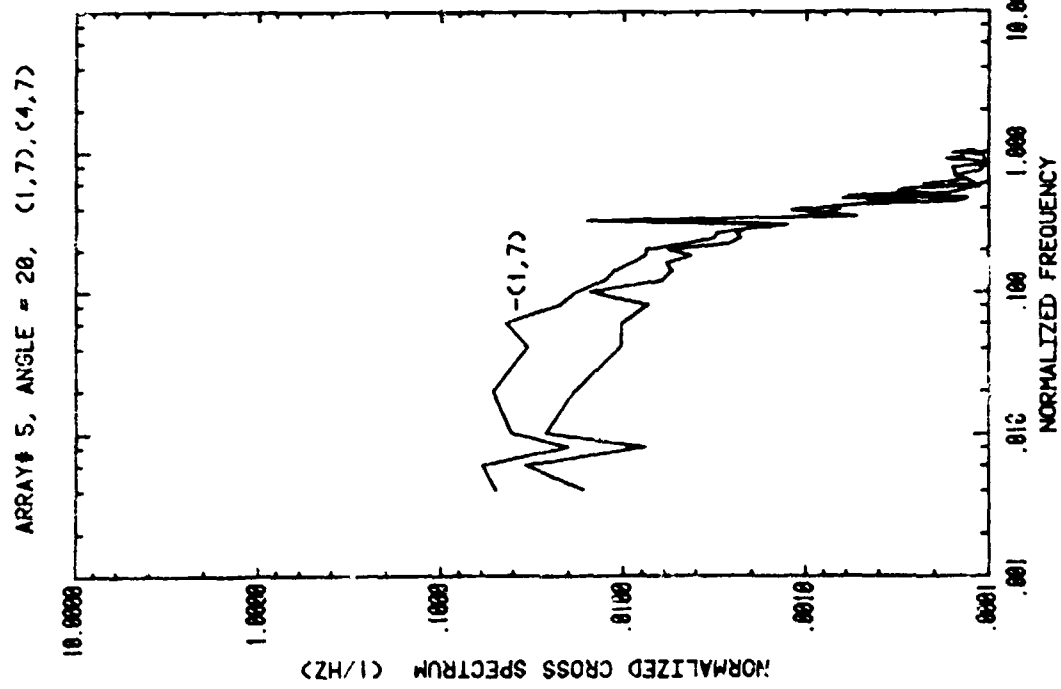

Figure 14. Cross-Spectra for Fifth Array at α = 20°, without Fence (continued)

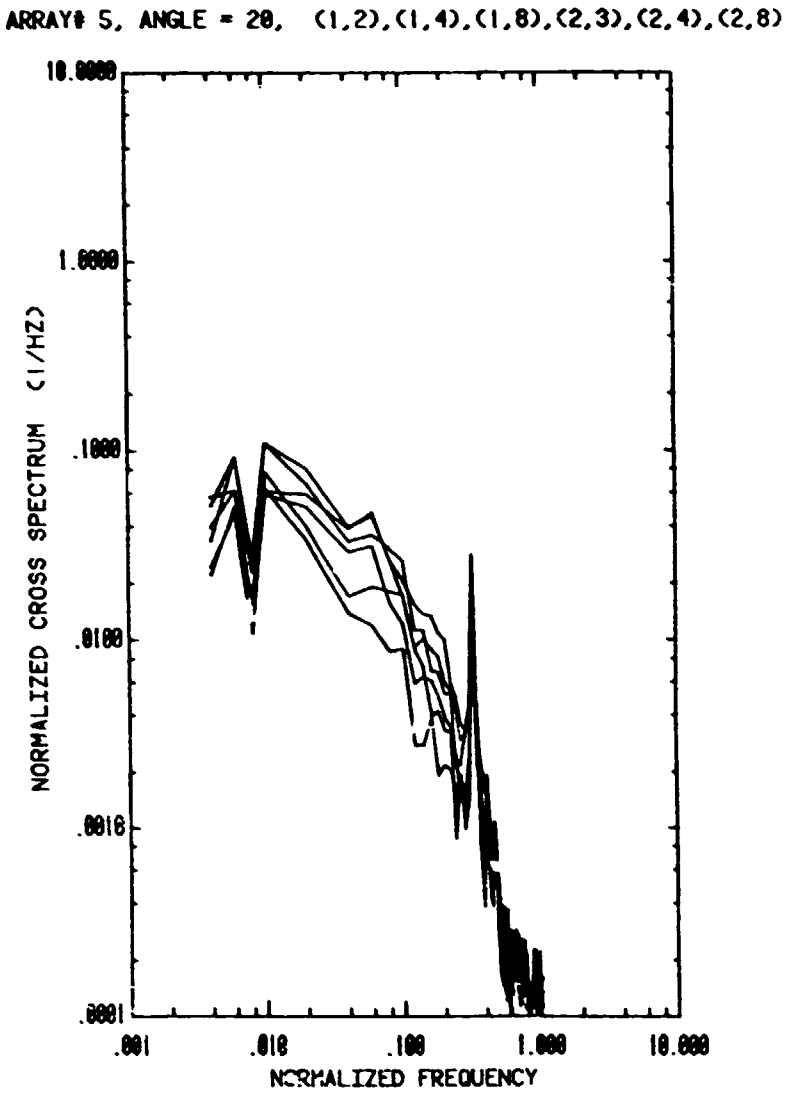

Figure 14. Cross-Spectra for Fifth Array at $\alpha = 20°$, without Fence (concluded)

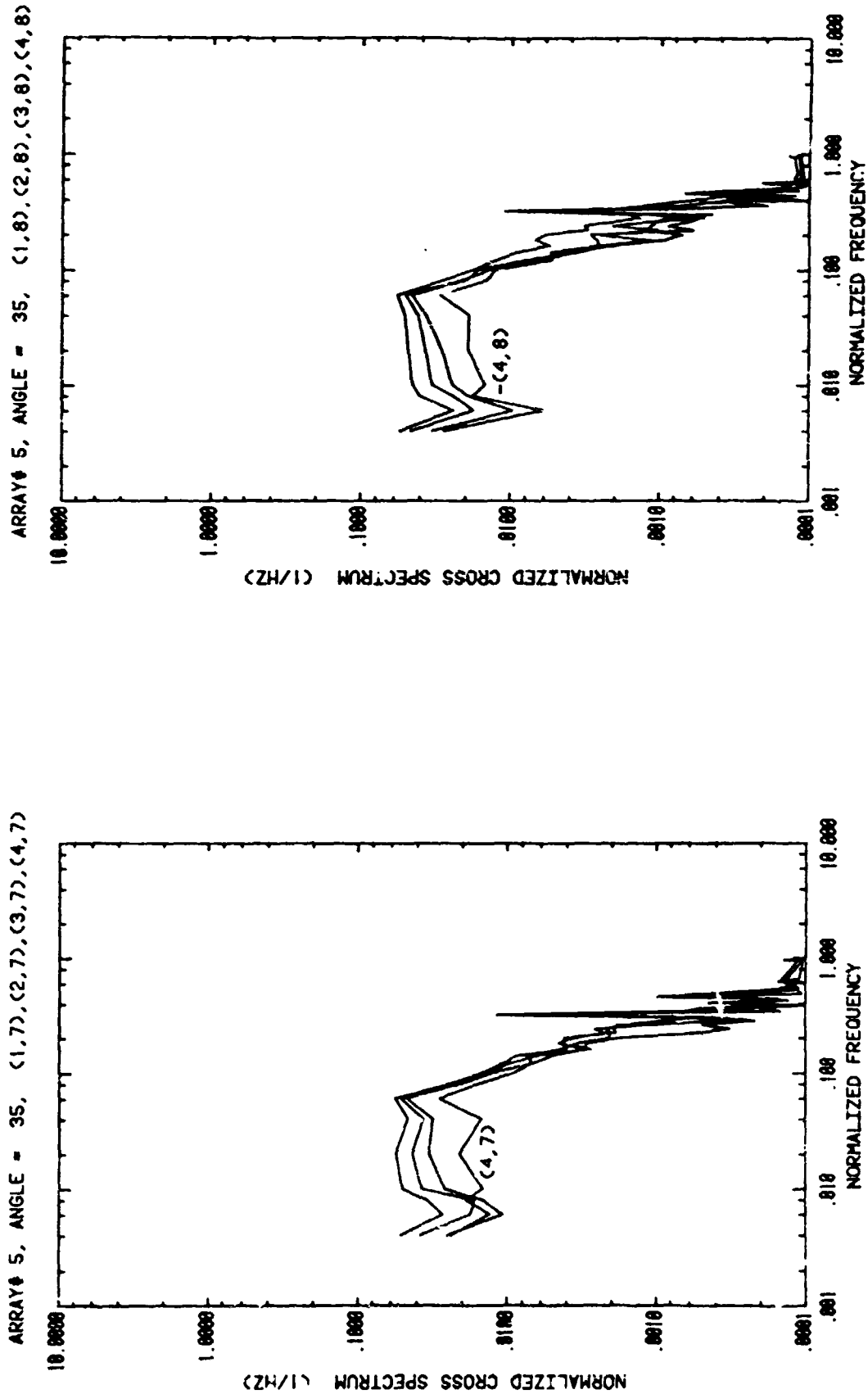

Figure 15. Cross-Spectra for Fifth Array at $\alpha = 35°$, without Fence

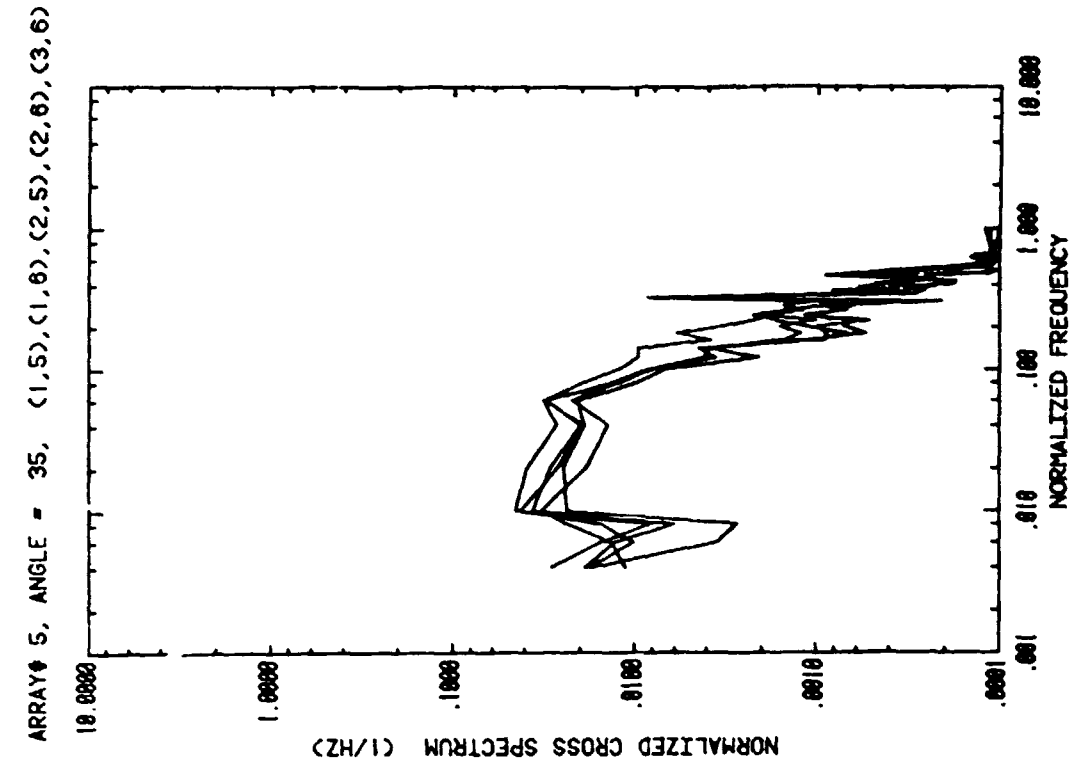

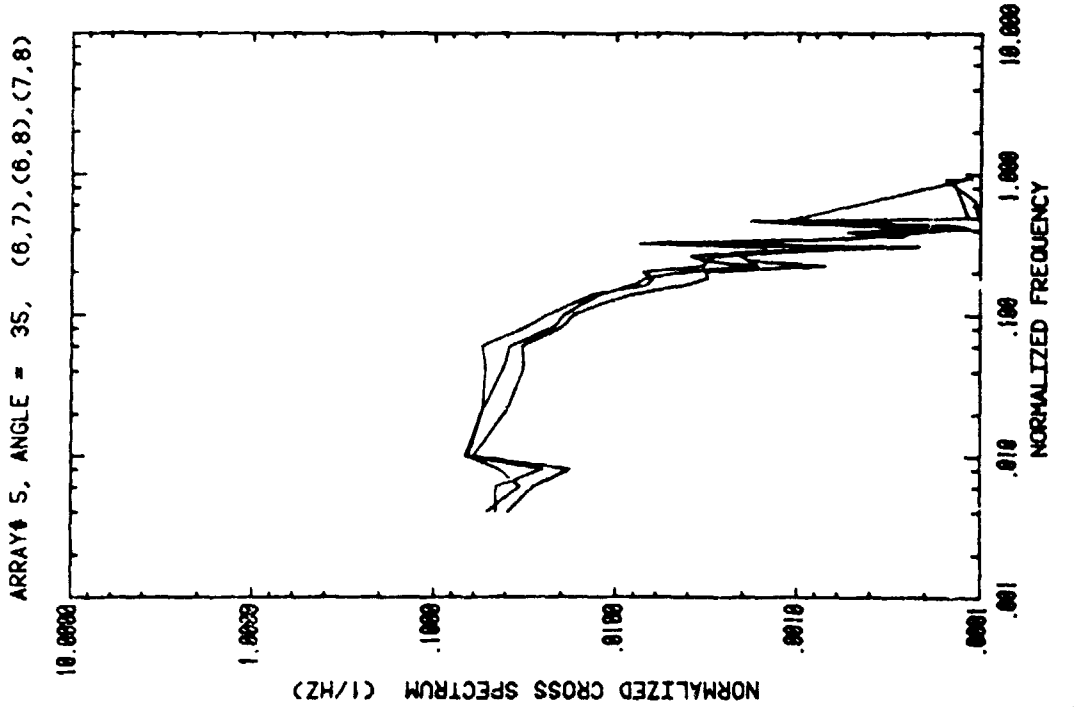

Figure 15. Cross-Spectra for Fifth Array at $\alpha = 35°$, without Fence (continued)

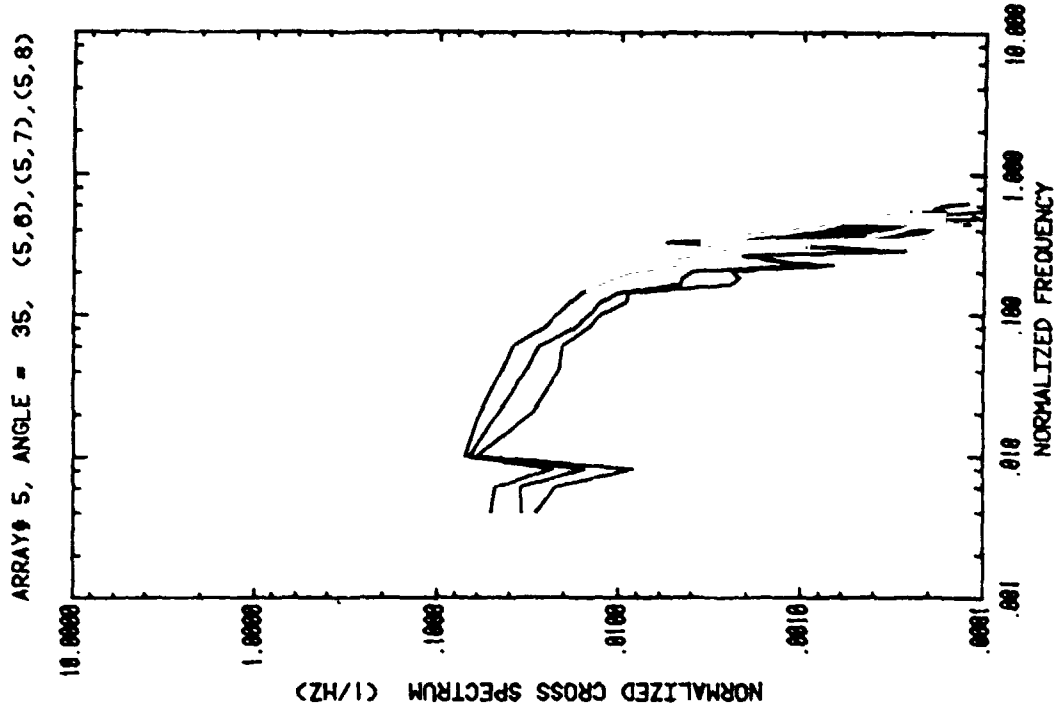

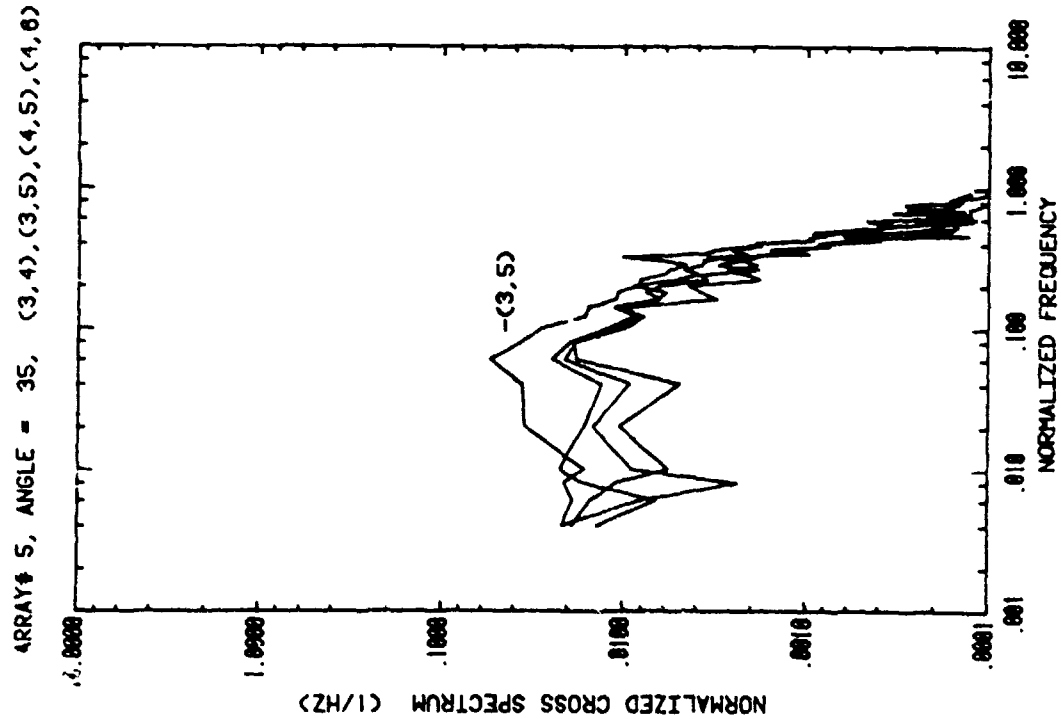

Figure 15. Cross-Spectra for Fifth Array at $\alpha = 35°$, without Fence (continued)

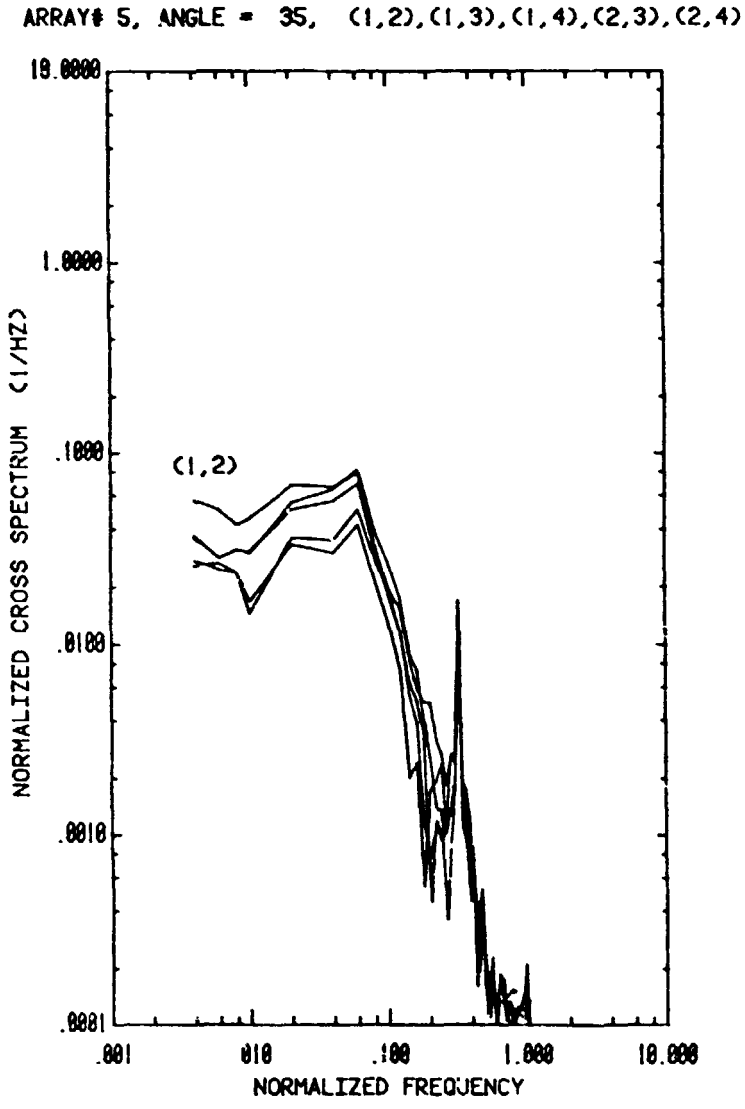

Figure 15. Cross-Spectra for Fifth Array at $\alpha = 35°$, without Fence (concluded)

TABLES

Table 1. List of Array Configurations Tested

Run	α	Array	Fence**		
			Height (H_f/c)	Distance (x_f/c)	Porosity (%)
21318	120	5	--	--	--
21321	120	1	--	--	--
21323	120	1	0.75	2.5	30
21325	145	5	--	--	--
21327	145	2	--	--	--
21329	145	1	--	--	--
21331	145	1	0.75	2.5	30
21338*	145	1	--	--	--
21340	160	5	--	--	--
21342	160	1	--	--	--
21344	160	1	0.75	2.5	30
21346	20	5	--	--	--
21348	20	1	--	--	--
21350	20	1	0.75	2.5	30
21352	35	5	--	--	--
21354	35	2	--	--	--
21356	35	1	--	--	--
21358	35	1	0.75	2.5	30
21364*	35	1	--	--	--
21366	60	5	--	--	--
21368	60	1	--	--	--
21370	60	1	0.75	2.5	30

*edge study (see Section 2.3 of the preceding report for the definition)
**see Figure 2 for definition of parameters

Table 2a. Time-Averaged Pressure Coefficients

	Run 21331*		Run 21344*		Run 21346	
	α	Array	α	Array	α	Array
	145	1	160	1	20	5
Tap (original)	$C_{p_{mean}}$	$C_{p_{rms}}$	$C_{p_{mean}}$	$C_{p_{rms}}$	$C_{p_{mean}}$	$C_{p_{rms}}$
1 (1)	-.083	.051	-.105	.052	.020	.051
2 (4)	-.068	.057	-.096	.061	.055	.050
3 (7)	-.088	.078	-.133	.072	.075	.069
4 (10)	-.107	.068	-.109	.060	.077	.113
5 (11)	-.134	.040	-.096	.040	-.196	.210
6 (14)	-.136	.039	-.096	.038	-.116	.121
7 (17)	-.153	.042	-.121	.042	-.103	.078
8 (20)	-.131	.044	-.107	.045	-.054	.072

*with fence

Table 2b. Time-Averaged Pressure Coefficients

	Run 21352		Run 21356		Run 21368	
	α	Array	α	Array	α	Array
	35	5	35	1	60	1
Tap (original)	$C_{P_{mean}}$	$C_{P_{rms}}$	$C_{P_{mean}}$	$C_{P_{rms}}$	$C_{P_{mean}}$	$C_{P_{rms}}$
1 (1)	-.013	.060	.087	.054	.223	.089
2 (4)	.001	.062	.292	.067	.376	.095
3 (7)	-.004	.081	.436	.107	.482	.148
4 (10)	-.002	.120	.451	.178	.279	.177
5 (11)	-.140	.147	-.300	.081	-.417	.066
6 (14)	-.104	.109	-.290	.073	-.398	.063
7 (17)	-.126	.089	-.346	.071	-.472	.063
8 (20)	-.092	.097	-.293	.072	-.417	.064

Table 3. Comparison of Integration of Auto-Spectra

array = 1, α = 35°, without fence	
pressure taps	$\int^{*} \Phi_{ii}(N)dN/C^2_{p_{rms_i}}$
(1, 1)	0.990
(2, 2)	1.069
(3, 3)	1.165
(4, 4)	1.059
(5, 5)	1.004
(6, 6)	0.971
(7, 7)	0.986
(8, 8)	0.963

array = 5, α = 35°, without fence	
(1, 1)	1.035
(2, 2)	1.016
(3, 3)	1.070
(4, 4)	0.986
(5, 5)	1.061
(6, 6)	1.061
(7, 7)	0.991
(8, 8)	0.972

*by theory, this quantity should be identically equal to 1 (see Equation 8)